

國立臺灣大學電機資訊學院電信工程學研究所

碩士論文

Graduate Institute of Communication Engineering

College of Electrical Engineering and Computer Science

National Taiwan University

Master Thesis

基於廣義概度比檢定和領導式通道估測的

正交分頻多工單輸入多輸出系統之解調性能分析

Performance Analysis of GLRT-Based OFDM SIMO
Demodulation System With Pilot-Aided Channel Estimation

廖芝青

Jy-Chin Liao

指導教授：鐘嘉德，陳維昌 博士

Advisor: Char-Dir Chung, Wei-Chang Chen Ph.D.

中華民國 110 年 6 月

June 2021

國立臺灣大學（碩）博士學位論文

口試委員會審定書

基於廣義概度比檢定和領導式通道估測的

單輸入多輸出正交分頻多工系統之解調性能分析

Performance Analysis of GLRT-Based SIMO-OFDM
Demodulation System With Pilot-Aided Channel Estimation

本論文係廖芝青君（R08942047）在國立臺灣大學電信工程學研究所完成之碩（博）士學位論文，於民國 110 年 6 月 25 日承下列考試委員審查通過及口試及格，特此證明

口試委員：

廖芝青

（簽名）

陳維昌（指導教授）

李穎

王育治

林茂和

所長

蔡火添

（簽名）

誌謝



今年因為疫情，原定所有畢業相關的活動都相繼被取消，導致畢業的氣氛減弱不少。但如今到了為自己的碩士論文收尾的階段，貌似不得不承認自己將要畢業的事實，心中有很多的感謝希望可以藉由接下來的這段文字加以記錄，也讓未來回憶起這段時光時有跡可循。

這篇碩士論文能夠順利完成，首先要感謝我的指導教授——鐘嘉德教授。這兩年來，鐘老師總是在第一時間回答我的疑問，並盡力給予我最完善的建議，在每次開會以及郵電討論的過程中，都能感受到老師的熱情以及用心，讓我十分敬佩。鐘老師淵博的學識、幽默風趣的談吐以及凡事力求完美的精神都對我造成深刻的影響，不論在學術或是人生方面，老師無疑都是位良好的典範。此外，還要感謝陳維昌教授，謝謝他願意在繁忙的教學過程中撥冗指導我的研究，奠定我許多通訊領域的基礎知識。

接著，我要謝謝 518 實驗室。謝謝這間實驗室讓我和何竹懿、馬笠瑜、周宗曄和鄒秉豐相遇，有了他們的陪伴，我的碩士生活每天都過得精彩且歡樂。當然也感謝所有的學長姐以及學弟蔡舜宇、王仲盡和盧長宏，不論是給予我學業上的幫助、或是分享彼此生活上的點滴，這間實驗室的每位成員都讓我的碩士變得更加完整。

謝謝我的父母和二姑姑，感謝他們提供我生活上所需的一切，有了他們的幫助，我才能夠專注於研究之中而無後顧之憂。當然也要謝謝我的男友和好朋友們，在我沮喪落寞的時候給予我最需要的陪伴。都是因為有了這些人的幫助，我才能夠順利完成我的碩士學位。

最後，謝謝兩年前的自己選擇在台灣就讀碩士。兩年的時間並不是太長，但已足以對我的未來造成一些不可逆的影響。當初的決定，不但讓我在疫情期間可以和家人作伴、使自己的感情更加穩定，也讓我得以遇到這些人、事、物，因而成就了今日的我，期望未來我也能對自己的所有決定感到驕傲。

謹以此向所有幫助我的人致上最深的謝意，並將這份成果呈獻給你們。

中文摘要



在現行的正交分頻多工 (OFDM) 系統中做數據解調時，領導信號 (pilot symbols) 經常穿插到均勻分布的子載波中以促進通道估測 (channel estimation)。當分段頻散通道的衰減程度加劇時，基於廣義概度比檢定 (GLRT) 的原理，由等間隔擺放的領導信號輔助的通道估測能夠實現在同一個正交分頻多工塊中逐個符號的數據解調。爲了進一步對抗更加衰減更加劇烈的分段頻散通道，採用單輸入多輸出 (SIMO) 天線分集系統可以增強基於廣義概度比檢定的解調性能。在本文中，對於所考慮的基於廣義概度比檢定的正交分頻多工單輸入多輸出系統解調，在固定和隨機分段頻散通道上採用各種二維的調變方式，分析推導出位元錯誤率 (bit error rate, BEP) 的上界和近似值，並通過模擬驗證其緊密性。數值分析顯示，當通道的衰減程度較小或單輸入多輸出系統的接收天線數足夠多時，位元錯誤率的上界表現出良好的緊密性，反之可以採用近似主導界線。透過推導出的界線，針對信號雜訊比、數據與領導信號功率比、天線分集、通道條件和領導信號長度等不同參數，分析且研究所考慮的基於廣義概度比檢定的正交分頻多工單輸入多輸出系統之錯誤性能特徵。

關鍵字: 正交分頻多工，領導式通道估測，廣義概度比檢定，單輸入多輸出，分段頻散通道

Abstract



Pilot symbols are commonly inserted into uniformly interleaved subcarriers to facilitate the channel estimation, thereby facilitating the data demodulation in practical orthogonal frequency-division multiplexing (OFDM) systems operating over block dispersive channels. When the block dispersive channel is fast time-varying, the channel estimation aided by the uniformly interleaved pilot symbols can enable symbol-by-symbol data demodulation within the same OFDM block, based on the principle of the generalized likelihood ratio test (GLRT). To further combat strong channel dispersion, a single-input multiple-output (SIMO) antenna diversity system is adopted and can enhance the GLRT-based demodulation performance. In this thesis, upper and approximate bounds to the bit error probability (BEP) are analytically derived for the considered GLRT-based OFDM SIMO demodulation, adopting various two-dimensional component modulation schemes, over both deterministic and random block dispersive channels, and verified by simulation for their tightness. Numerical results show that the BEP upper bounds exhibit tight performance measures when the channel dispersion is less fluctuated or when the SIMO diversity is sufficiently high, and that approximate dominant bounds can be used otherwise. Through the derived bounds, the error performance characteristics of the considered GLRT-based OFDM SIMO system are analytically studied with respect to data-to-noise power ratio, data-to-pilot power ratio, antenna diversity, channel condition, and pilot length.

Keywords: Orthogonal frequency division multiplexing, pilot-aided channel estimation, generalized likelihood ratio test, single-input multiple-output, block dispersive channel



Contents

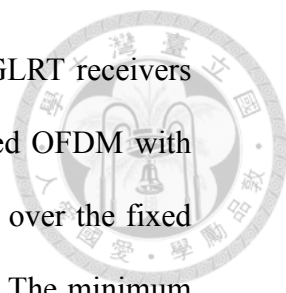
中文摘要	i
Abstract	ii
Contents	iii
List of Figures	v
List of Tables	xiii
1 Introduction	1
1.1 Review of OFDM Systems	1
1.2 Review of Channel Estimation	2
1.2.1 Review of Pilot Patterns	3
1.2.2 Reviews of Channel Estimation Methods	3
1.3 Thesis Motivation, Overview, and Contributions	4
1.4 Notations	6
2 Pilot-Aided OFDM System Model	7
2.1 Introduction	7
2.2 System Model	7
2.3 GLRT-based Decision Rule	10

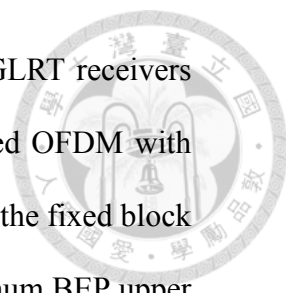
2.3.1	Decision Rule with Constant Amplitude Pilot Sequence	13
3	Performance Analysis	15
3.1	Introduction	15
3.2	Conditional BEP Upper Bound	15
3.2.1	Pairwise Error Probability for MPSK	17
3.3	Average BEP Upper Bound	18
4	Performance Results	23
4.1	Introduction	23
4.2	ZC Sequences	23
4.3	BEP Characteristics in Fixed Block Dispersive Channel	24
4.3.1	Fixed Block Dispersive Channel	24
4.3.2	Conditional BEP Upper Bound Performance	25
4.4	Average BEP Characteristics in Random Block Dispersive Channel	34
4.4.1	Random Block Dispersive Channel	34
4.4.2	Unconditional BEP Upper Bound Performance	36
5	Conclusion	50
	Bibliography	51
	Appendix A Derivation of (3.2)	56
	Appendix B Derivation of (3.10)	60



List of Figures

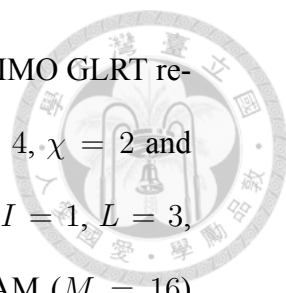
1.1	OFDM System	2
1.2	Pilot arrangement in OFDM systems	3
4.1	Fourier power spectrums of EDS channels with $D = 0.5, 1$ and 2 for the OFDM system with $i = 0, N = 64, \phi = 4$ and $L = 3$	25
4.2	Bit error probability characteristics of the SIMO GLRT receiver for the pilot-aided OFDM with $N = 64, \alpha = 1/4, \phi = 4, \varphi = 1, \chi = 2$, QPSK component modulation, and various I antenna paths over the fixed block dispersive channel with $L = 3$ and various D factors.	26
4.3	Bit error probability characteristics of the SIMO GLRT receivers for the pilot-aided OFDM with $N = 64, \alpha = 1/4, \phi = 4, \varphi = 1, \chi = 2$, 16-ary QAM component modulation, and various I antenna paths over the fixed block dispersive channel with $L = 3$ and various D factors.	26
4.4	Bit error probability versus φ characteristics of the SIMO GLRT receivers for QPSK ($M = 4$) and 16-ary QAM ($M = 16$) pilot-aided OFDM with $N = 64, \alpha = 1/4, \phi = 4, \chi = 2$ and various γ_{avg} values over the fixed block dispersive channel with $I = 1, L = 3$ and $D = 0.5$. The minimum BEP upper bound versus the corresponding φ for each γ_{avg} with respective component modulation is denoted by a broken line connecting dots.	27

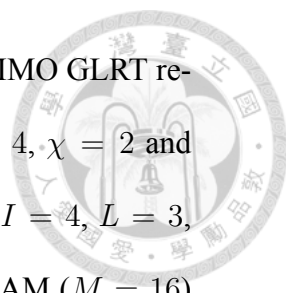
- 
- 4.5 Bit error probability versus φ characteristics of the SIMO GLRT receivers for QPSK ($M = 4$) and 16-ary QAM ($M = 16$) pilot-aided OFDM with $N = 64$, $\alpha = 1/4$, $\phi = 4$, $\chi = 2$ and various γ_{avg} values over the fixed block dispersive channel with $I = 4$, $L = 3$ and $D = 0.5$. The minimum BEP upper bound versus the corresponding φ for each γ_{avg} with respective component modulation is denoted by a broken line connecting dots. 28
- 4.6 Bit error probability versus φ characteristics of the SIMO GLRT receivers for QPSK ($M = 4$) and 16-ary QAM ($M = 16$) pilot-aided OFDM with $N = 64$, $\alpha = 1/4$, $\phi = 4$, $\chi = 2$ and various γ_{avg} values over the fixed block dispersive channel with $I = 1$, $L = 3$ and $D = 1$. The minimum BEP upper bound versus the corresponding φ for each γ_{avg} with respective component modulation is denoted by a broken line connecting dots. 29
- 4.7 Bit error probability versus φ characteristics of the SIMO GLRT receivers for QPSK ($M = 4$) and 16-ary QAM ($M = 16$) pilot-aided OFDM with $N = 64$, $\alpha = 1/4$, $\phi = 4$, $\chi = 2$ and various γ_{avg} values over the fixed block dispersive channel with $I = 4$, $L = 3$ and $D = 1$. The minimum BEP upper bound versus the corresponding φ for each γ_{avg} with respective component modulation is denoted by a broken line connecting dots. 29
- 4.8 Bit error probability versus φ characteristics of the SIMO GLRT receivers for QPSK ($M = 4$) and 16-ary QAM ($M = 16$) pilot-aided OFDM with $N = 64$, $\alpha = 1/4$, $\phi = 4$, $\chi = 2$ and various γ_{avg} values over the fixed block dispersive channel with $I = 1$, $L = 3$ and $D = 2$. The minimum BEP upper bound versus the corresponding φ for each γ_{avg} with respective component modulation is denoted by a broken line connecting dots. 30

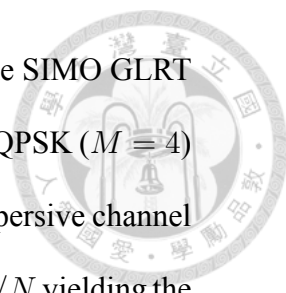
- 
- 4.9 Bit error probability versus φ characteristics of the SIMO GLRT receivers for QPSK ($M = 4$) and 16-ary QAM ($M = 16$) pilot-aided OFDM with $N = 64$, $\alpha = 1/4$, $\phi = 4$, $\chi = 2$ and various γ_{avg} values over the fixed block dispersive channel with $I = 4$, $L = 3$ and $D = 2$. The minimum BEP upper bound versus the corresponding φ for each γ_{avg} with respective component modulation is denoted by a broken line connecting dots. 30
- 4.10 Bit error probability versus φ/N characteristics of the SIMO GLRT receivers for QPSK ($M = 4$) pilot-aided OFDM with $\alpha = 1/4$, $\phi = 4$, $\chi = 2$ and $\gamma_{\text{avg}} = 8$ dB over the fixed block dispersive channel with $I = 1$, $L = 3$ and various D . The minimum BEP upper bound versus the corresponding φ/N with respective D and N is denoted by the dot. 31
- 4.11 Bit error probability versus φ/N characteristics of the SIMO GLRT receivers for QPSK ($M = 4$) pilot-aided OFDM with $\alpha = 1/4$, $\phi = 4$, $\chi = 2$ and $\gamma_{\text{avg}} = 8$ dB over the fixed block dispersive channel with $I = 4$, $L = 3$ and various D . The minimum BEP upper bound versus the corresponding φ/N with respective D and N is denoted by the dot. 31
- 4.12 Bit error probability versus φ/N characteristics of the SIMO GLRT receivers for 16-ary QAM ($M = 16$) pilot-aided OFDM with $\alpha = 1/4$, $\phi = 4$, $\chi = 2$ and $\gamma_{\text{avg}} = 14$ dB over the fixed block dispersive channel with $I = 1$, $L = 3$ and various D . The minimum BEP upper bound versus the corresponding φ/N with respective D and N is denoted by the dot. 32

4.13	Bit error probability versus φ/N characteristics of the SIMO GLRT receivers for 16-ary QAM ($M = 16$) pilot-aided OFDM with $\alpha = 1/4$, $\phi = 4$, $\chi = 2$ and $\gamma_{\text{avg}} = 14$ dB over the fixed block dispersive channel with $I = 4$, $L = 3$ and various D . The minimum BEP upper bound versus the corresponding φ/N with respective D and N is denoted by the dot.	32
4.14	Fourier power spectrums of multipath Rician fading channel realizations with $K = 0, 10$ dB and 20 dB and $D = 2$ for the OFDM system with $i = 0$, $N = 64$, $\phi = 4$ and $L = 3$	35
4.15	Average bit error probability characteristics of the SIMO GLRT receivers for the pilot-aided OFDM with $N = 64$, $\alpha = 1/4$, $\phi = 4$, $\varphi = 1$, and $\chi = 2$ over the i.n.i.d. random block dispersive channel with $L = 3$ and $D = 2$ under two considered cases. Both QPSK and 16-ary QAM component modulations are considered.	37
4.16	Average bit error probability versus φ characteristics of the SIMO GLRT receiver for pilot-aided OFDM with $N = 64$, $\alpha = 1/4$, $\phi = 4$, $\chi = 2$, QPSK component modulation, and various γ_{avg} values over the i.n.i.d. random block dispersive channel with $L = 3$ and $D = 2$ under two considered cases. The point φ yielding the minimum average BEP upper bound value for each SNR is denoted by a broken line connecting dots.	38
4.17	Average bit error probability versus φ characteristics of the SIMO GLRT receiver for pilot-aided OFDM with $N = 64$, $\alpha = 1/4$, $\phi = 4$, $\chi = 2$, 16-ary QAM component modulation, and various γ_{avg} values over the i.n.i.d. random block dispersive channel with $L = 3$ and $D = 2$ under two considered cases. The point φ yielding the minimum average BEP upper bound value for each SNR is denoted by a broken line connecting dots.	38

4.18	Average bit error probability versus φ/N characteristics of the SIMO GLRT receivers for pilot-aided OFDM with $\alpha = 1/4$, $\phi = 4$, $\chi = 2$, QPSK component modulation, and $\gamma_{\text{avg}} = 8$ dB over the i.n.i.d. random block dispersive channel with $L = 3$ and $D = 2$ under two considered cases. The point φ/N yielding the minimum average BEP upper bound value for respective case and N is denoted by dot.	39
4.19	Average bit error probability versus φ/N characteristics of the SIMO GLRT receivers for pilot-aided OFDM with $\alpha = 1/4$, $\phi = 4$, $\chi = 2$, 16-ary QAM component modulation, and $\gamma_{\text{avg}} = 14$ dB over the i.n.i.d. random block dispersive channel with $L = 3$ and $D = 2$ under two considered cases. The point φ/N yielding the minimum average BEP upper bound value for respective case and N is denoted by dot.	40
4.20	Average bit error probability characteristics of the SIMO GLRT receivers for the pilot-aided OFDM with $N = 64$, $\alpha = 1/4$, $\phi = 4$, $\varphi = 1$, $\chi = 2$, QPSK component modulation, and various I antenna paths over the random dispersive channel with $L = 3$, $D = 2$, and various K factors.	41
4.21	Average bit error probability characteristics of the SIMO GLRT receivers for the pilot-aided OFDM with $N = 64$, $\alpha = 1/4$, $\phi = 4$, $\varphi = 1$, $\chi = 2$, 16-ary QAM component modulation, and various I antenna paths over the random dispersive channel with $L = 3$, $D = 2$, and various K factors.	42

- 
- 4.22 Average bit error probability versus φ characteristics of the SIMO GLRT receiver for pilot-aided OFDM with $N = 64$, $\alpha = 1/4$, $\phi = 4$, $\chi = 2$ and various γ_{avg} values over the random dispersive channel with $I = 1$, $L = 3$, $D = 2$, and $K = 0$. Both QPSK ($M = 4$) and 16-ary QAM ($M = 16$) component modulations are demonstrated. For each component modulation, the point φ yielding the minimum average BEP upper bound value for each SNR is denoted by a broken line connecting dots. 44
- 4.23 Average bit error probability versus φ characteristics of the SIMO GLRT receiver for pilot-aided OFDM with $N = 64$, $\alpha = 1/4$, $\phi = 4$, $\chi = 2$ and various γ_{avg} values over the random dispersive channel with $I = 4$, $L = 3$, $D = 2$, and $K = 0$. Both QPSK ($M = 4$) and 16-ary QAM ($M = 16$) component modulations are demonstrated. For each component modulation, the point φ yielding the minimum average BEP upper bound value for each SNR is denoted by a broken line connecting dots. 44
- 4.24 Average bit error probability versus φ characteristics of the SIMO GLRT receiver for pilot-aided OFDM with $N = 64$, $\alpha = 1/4$, $\phi = 4$, $\chi = 2$ and various γ_{avg} values over the random dispersive channel with $I = 1$, $L = 3$, $D = 2$, and $K = 10$ dB. Both QPSK ($M = 4$) and 16-ary QAM ($M = 16$) component modulations are demonstrated. For each component modulation, the point φ yielding the minimum average BEP upper bound value for each SNR is denoted by a broken line connecting dots. 45

- 
- 4.25 Average bit error probability versus φ characteristics of the SIMO GLRT receiver for pilot-aided OFDM with $N = 64$, $\alpha = 1/4$, $\phi = 4$, $\chi = 2$ and various γ_{avg} values over the random dispersive channel with $I = 4$, $L = 3$, $D = 2$, and $K = 10$ dB. Both QPSK ($M = 4$) and 16-ary QAM ($M = 16$) component modulations are demonstrated. For each component modulation, the point φ yielding the minimum average BEP upper bound value for each SNR is denoted by a broken line connecting dots. 45
- 4.26 Average bit error probability versus φ characteristics of the SIMO GLRT receiver for pilot-aided OFDM with $N = 64$, $\alpha = 1/4$, $\phi = 4$, $\chi = 2$ and various γ_{avg} values over the random dispersive channel with $I = 1$, $L = 3$, $D = 2$, and $K = 20$ dB. Both QPSK ($M = 4$) and 16-ary QAM ($M = 16$) component modulations are demonstrated. For each component modulation, the point φ yielding the minimum average BEP upper bound value for each SNR is denoted by a broken line connecting dots. 46
- 4.27 Average bit error probability versus φ characteristics of the SIMO GLRT receiver for pilot-aided OFDM with $N = 64$, $\alpha = 1/4$, $\phi = 4$, $\chi = 2$ and various γ_{avg} values over the random dispersive channel with $I = 4$, $L = 3$, $D = 2$, and $K = 10$ dB. Both QPSK ($M = 4$) and 16-ary QAM ($M = 16$) component modulations are demonstrated. For each component modulation, the point φ yielding the minimum average BEP upper bound value for each SNR is denoted by a broken line connecting dots. 46

- 
- 4.28 Average bit error probability versus φ/N characteristics of the SIMO GLRT receivers for pilot-aided OFDM with $\alpha = 1/4$, $\phi = 4$, $\chi = 2$, QPSK ($M = 4$) component modulation, and $\gamma_{\text{avg}} = 7$ dB over the random dispersive channel with $I = 1$, $L = 3$, $D = 2$, and various K factors. The point φ/N yielding the minimum average BEP upper bound value for respective K and N is denoted by dot. 47
- 4.29 Average bit error probability versus φ/N characteristics of the SIMO GLRT receivers for pilot-aided OFDM with $\alpha = 1/4$, $\phi = 4$, $\chi = 2$, QPSK ($M = 4$) component modulation, and $\gamma_{\text{avg}} = 7$ dB over the random dispersive channel with $I = 4$, $L = 3$, $D = 2$, and various K factors. The point φ/N yielding the minimum average BEP upper bound value for respective K and N is denoted by dot. 47
- 4.30 Average bit error probability versus φ/N characteristics of the SIMO GLRT receivers for pilot-aided OFDM with $\alpha = 1/4$, $\phi = 4$, $\chi = 2$, 16-ary QAM ($M = 16$) component modulation, and $\gamma_{\text{avg}} = 14$ dB over the random dispersive channel with $I = 1$, $L = 3$, $D = 2$, and various K factors. The point φ/N yielding the minimum average BEP upper bound value for respective K and N is denoted by dot. 48
- 4.31 Average bit error probability versus φ/N characteristics of the SIMO GLRT receivers for pilot-aided OFDM with $\alpha = 1/4$, $\phi = 4$, $\chi = 2$, 16-ary QAM ($M = 16$) component modulation, and $\gamma_{\text{avg}} = 14$ dB over the random dispersive channel with $I = 4$, $L = 3$, $D = 2$, and various K factors. The point φ/N yielding the minimum average BEP upper bound value for respective K and N is denoted by dot. 48



List of Tables

4.1	Polynomial functions for $\varphi^{(\text{opt})}(\gamma_{\text{avg}})$ of the SIMO GLRT receivers for the pilot-aided OFDM with $N = 64$, $\alpha = 1/4$, $\phi = 4$, $\chi = 2$, various component modulations, and various I antenna paths over the fixed dispersive channel with $L = 3$ and $D = 0.5$	33
4.2	Polynomial functions for $\varphi^{(\text{opt})}(\gamma_{\text{avg}})$ of the SIMO GLRT receivers for the pilot-aided OFDM with $N = 64$, $\alpha = 1/4$, $\phi = 4$, $\chi = 2$, various component modulations, and various I antenna paths over the fixed dispersive channel with $L = 3$ and $D = 1$	33
4.3	Polynomial functions for $\varphi^{(\text{opt})}(\gamma_{\text{avg}})$ of the SIMO GLRT receivers for the pilot-aided OFDM with $N = 64$, $\alpha = 1/4$, $\phi = 4$, $\chi = 2$, various component modulations, and various I antenna paths over the fixed dispersive channel with $L = 3$ and $D = 2$	34
4.4	Polynomial functions for $\varphi^{(\text{opt})}(\gamma_{\text{avg}})$ of the SIMO GLRT receivers for the pilot-aided OFDM with $N = 64$, $\alpha = 1/4$, $\phi = 4$, $\chi = 2$, various component modulations over i.n.i.d. random block dispersive channel with $L = 3$ and $D = 2$ under two considered cases.	40

4.5	Polynomial functions for $\varphi^{(\text{opt})}(\gamma_{\text{avg}})$ of the SIMO GLRT receivers for the pilot-aided OFDM with $N = 64$, $\alpha = 1/4$, $\phi = 4$, $\chi = 2$, various component modulations, and various I antenna paths over random dispersive channel with $L = 3$, $D = 2$ and $K = 0$	49
4.6	Polynomial functions for $\varphi^{(\text{opt})}(\gamma_{\text{avg}})$ of the SIMO GLRT receivers for the pilot-aided OFDM with $N = 64$, $\alpha = 1/4$, $\phi = 4$, $\chi = 2$, various component modulations, and various I antenna paths over random dispersive channel with $L = 3$, $D = 2$ and $K = 10$ dB.	49
4.7	Polynomial functions for $\varphi^{(\text{opt})}(\gamma_{\text{avg}})$ of the SIMO GLRT receivers for the pilot-aided OFDM with $N = 64$, $\alpha = 1/4$, $\phi = 4$, $\chi = 2$, various component modulations, and various I antenna paths over random dispersive channel with $L = 3$, $D = 2$ and $K = 20$ dB.	49



Chapter 1

Introduction

This chapter will give a brief introduction to the orthogonal frequency-division multiplexing (OFDM) system. In the following, channel estimation techniques are reviewed, including two typical pilot patterns and several channel estimation methods. In addition, the motivation, contributions, and overview of the thesis are mentioned.

1.1 Review of OFDM Systems

Orthogonal frequency division multiplexing (OFDM) is a well-known digital multicarrier technique that uses a large number of orthogonal subcarriers to transmit data in parallel [1]-[3]. Due to the orthogonality, the OFDM system offers high spectrum efficiency even if the subcarriers suffer from overlapping. In addition, the OFDM system is more resistant to frequency selective fading channels than single carrier systems and has the advantage of using a simple equalization for linear time-invariant (LTI) frequency-selective channels. By adopting the concept of cyclic prefix (CP) in the front of an OFDM block, intersymbol interference (ISI) and intercarrier interference (ICI) can be eliminated successfully. An OFDM modulator is shown in Fig. 1.1. The N parallel signal flows in the frequency-domain are first converted to

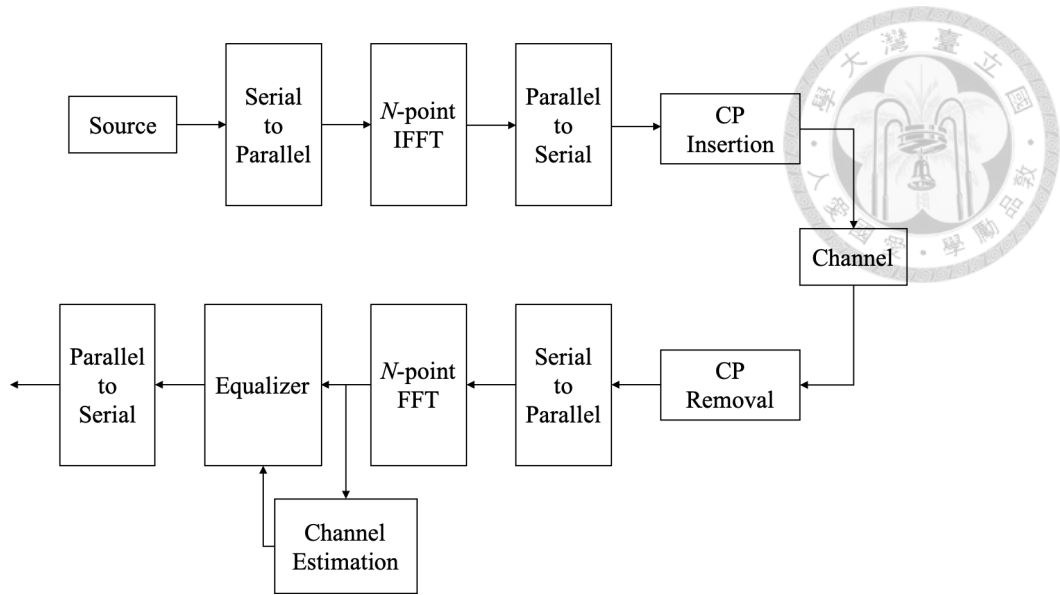


Figure 1.1: OFDM System

the time-domain through inverse fast Fourier transform (IFFT) and then followed by inserting the cyclic prefix in the guard intervals. After passing through the channels, the signal will be truncated block by block at the receiver and the receiver deletes the CP to avoid interblock interference (IBI). Next, by implementing the channel estimation, the channel state information (CSI) can be achieved and several equalization methods can be adopted to eliminate the channel effects.

1.2 Review of Channel Estimation

In practical systems, channel estimation plays a vital role because the channel is time-variant, and the channel state information (CSI) is hard to obtain. Generally, there are two types of methods to perform channel estimation. The first type, known as blind channel estimation, is based on unknown received signal only and extract channel statistics by focusing on the deterministic or stochastic properties of the systems [4]-[5]. However, the technique needs longer data records and therefore entails high complexity, making it less practical. The second type of channel estimation can be performed by inserting several pilot symbols into either the

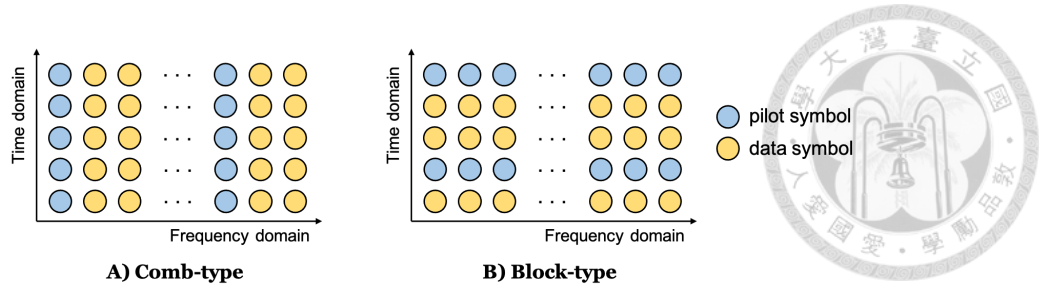


Figure 1.2: Pilot arrangement in OFDM systems

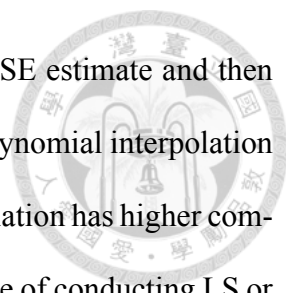
time-domain or the frequency domain [6]-[13]. Based on these known symbols, the receiver can acquire channel response with low complexity.

1.2.1 Review of Pilot Patterns

The channel estimation can be realized by either inserting the pilot symbols into each OFDM block or inserting pilot symbols into all the subcarriers in OFDM symbols, and these two types of patterns are shown in Fig. 1.2. The first one is the comb-type, which is equally spaced in the frequency domain and is often applied in fast fading channels. The second type, block-type, is uniformly aligned in the time domain and is usually used in frequency selective channels. In this thesis, the time-variant block dispersive channel is assumed, and therefore, the comb-type pattern is applied.

1.2.2 Reviews of Channel Estimation Methods

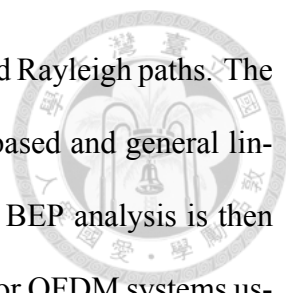
The comb-type pilot channel estimation consists of algorithms to estimate the channel frequency response (CFR) at pilot subcarriers and interpolate within these pilot symbols to obtain CFR at data subcarriers. Usually, the receiver will first estimate the channel response at pilot positions with either least-square (LS) estimation or linear minimum mean square error (LMMSE) estimation. Then, based on this information, obtain CFR at data subcarriers through different interpolation techniques such as linear interpolation [8], polynomial interpolation [8], and sinc interpolation[9]. Another stream to present channel estimation is to obtain



channel impulse response (CIR) by either direct LS estimate or LMMSE estimate and then receive estimate CFR by conducting DFT. It is shown in [8] that the polynomial interpolation has better performance than linear interpolation, but polynomial interpolation has higher complexity which is harder to implement. Moreover, in [13] the performance of conducting LS or LMMSE estimation on both pilot and data positions outperforms other interpolation schemes, and the LMMSE estimator performs better than LS estimator at low SNR. However, such LS estimator is more practical when the channel statistic is available.

1.3 Thesis Motivation, Overview, and Contributions

When the dispersive channel is time-variant in a way that it is fixed only within one OFDM block but may vary over different OFDM blocks, pilot-aided channel estimation is still achievable. And it becomes even more attractive because the temporary block-wise CSI can be accurately tracked when sufficient power is allocated to uniformly interleaved pilot symbols in each OFDM block [7]-[13]. In the literature, researches on pilot-aided OFDM systems focus on the design of channel estimators and the analysis of channel estimation performance over block dispersive channels [6]-[16], but relatively less attention is paid on the analysis of data decision performance in the presence of channel estimation error [20]-[24]. A tight lower bound on channel capacity is derived and the optimum data-to-pilot ratio is given in [20] under the assumption that the block dispersive channel consists of independent and identically distributed (i.i.d.) Rayleigh paths. And a linear minimum mean square error (LMMSE) channel estimator is used at the receiver. The other part of the studies concentrate on the average symbol error probability (SEP) and average bit error probability (BEP) characteristics for various pilot-aided OFDM systems under different system setups and channel models in [21]-[24]. The average BEP is first derived in [21] for pilot-aided OFDM systems with square quadrature amplitude modulation (QAM) component modulations over block disper-



sive channels over independent but not necessarily identically distributed Rayleigh paths. The BEP analysis is carried out for the receiver using polynomial, model-based and general linear interpolation channel estimator at the data positions. The average BEP analysis is then extended to dispersive channels with correlated Rayleigh paths in [22] for OFDM systems using QPSK and linear interpolation channel estimator. The minimum number of pilot symbols required to achieve a target BEP at a given signal-to-noise power ratio (SNR) is numerically found in [22] under the condition that all pilot and data symbols are equipowered. To further combat strong channel dispersion, pilot-aided OFDM systems are incorporated with a single-input multiple-output (SIMO) antenna diversity system in [23]-[24] and maximum ratio combining (MRC) is employed at the receiver to yield decision statistic. The dispersive channels associated with different receive antenna elements are assumed to be independent, consist of independent Rayleigh [23]-[24] or Rician [24] paths, and have identical power delay profile. In [23], the average SEP is derived using M -ary PSK component modulation and adopting LS and MMSE estimators at the receiver. On the other hand, the average BEP is given in [24] using 16-ary QAM component modulation and sinc interpolation channel estimator. However, to simplify the pilot-aided data decision performance analysis, all results aforementioned have some restrictions on block dispersive channel and component modulation scheme due to analytical difficulty.

In this thesis, I relax the restriction on block dispersive channels and component modulation scheme. And a more general analysis on the BEP performance is provided for the OFDM SIMO system in the presence of channel estimation error. Specifically, my pilot-aided OFDM SIMO system can adopt arbitrary two-dimensional component modulation scheme, and the random block dispersive channel is generally modeled to have independent but not necessarily identically distributed random antenna paths. I also apply pilot-aided LS estimator, which is also implemented in [23], instead of LMMSE estimator because of the absence of channel

response statistic. Moreover, a symbol decision scheme based on the generalized likelihood ratio test (GLRT) principle [34] is considered at the receiver [23]-[24].

The block dispersive channel adopted in Section IV can be further categorized into fixed block dispersive channel and random block dispersive channel. The former decays identically in each OFDM block, but only a few OFDM blocks have been received at the receiver. In second channel, the coherence time is relatively short but not shorter than one OFDM block. Therefore, assuming these two types of block dispersive channels can only perform channel estimation and entail data decisions within one OFDM block, the BEP characteristics have been thoroughly verified under the assumption of time-variant block dispersive channel.

After numerical study and simulation, upper and approximate bounds to the BEP are analytically derived for the considered GLRT-based SIMO OFDM system and verified by simulation for their tightness. The derived bounds are useful for characterizing the error performance characteristics of the considered GLRT-based SIMO OFDM system with different system configurations.

1.4 Notations

Boldface lower-case and upper-case letters denote column vectors and matrices, respectively. Superscripts t , $*$, and h denote transpose, complex conjugate, and conjugate transpose, respectively. \mathcal{Z}_K and \mathcal{Z}_K^+ are respectively the sets $\{0, 1, \dots, K-1\}$ and $\{1, 2, \dots, K\}$. I also use $[x_k; k \in \mathcal{Z}_K]$ to represent a $K \times 1$ vector with x_k being the k -th entry, $[x_{m,n}; m \in \mathcal{Z}_M, n \in \mathcal{Z}_N]$ an $M \times N$ matrix with $x_{m,n}$ being the (m, n) -th entry, $\text{diag}([x_k; k \in \mathcal{Z}_K])$ a $K \times K$ diagonal matrix with x_k being the k -th diagonal entry, \mathbf{I}_K a $K \times K$ identity matrix, $\mathbf{O}_{K,K}$ a $K \times K$ all-zero matrix, $\mathbf{0}_K$ a $K \times 1$ all-zero vector, $n \bmod N$ the modulo- N value of n , $\|\mathbf{x}\|$ the Frobenius norm of vector \mathbf{x} , and $\text{Re}\{x\}$ the real part of complex x . $\text{tr}(\mathbf{X})$ and \mathbf{X}^{-1} are the trace and the inverse, respectively, of matrix \mathbf{X} . I let $\omega_K \triangleq \exp\{-j\frac{2\pi}{K}\}$ and $j \triangleq \sqrt{-1}$.



Chapter 2

Pilot-Aided OFDM System Model

2.1 Introduction

In this chapter, the pilot-added OFDM SIMO system model is defined, and the GLRT-based decision rule assisted by the channel estimation is given. The uniformly interleaved pilot pattern mentioned in the introduction is adopted to achieve the optimum channel estimation while the channel state information is unknown to the receivers.

2.2 System Model

Consider the OFDM block transmission with $N\phi$ subcarriers, among which $N(\phi - 1)$ subcarriers are used to convey useful data symbols and N subcarriers are used to transmit pilot symbols and facilitate channel estimation at the receiver. In practical OFDM systems, pilot subcarriers are uniformly interleaved among data subcarriers with interleaving length ϕ and pilot subcarrier positions may vary periodically among different OFDM blocks to facilitate accurate channel estimation on frequency selective channels [14]-[19]. At the receiver, I received antennas followed by respective I OFDM demodulators are adopted to extract channel

information with the aid of known pilot symbols and then assist data decision. Antenna elements are placed sufficiently apart in a way that I received signals suffer independent channel effects.

In a nominal OFDM block of length T , I denote $\rho_k^{1/2} d_k[n]$ as the complex-valued symbol modulated on the $(n\phi + k)$ -th subcarrier for $k \in \mathcal{Z}_\phi$ and $n \in \mathcal{Z}_N$, ρ_k as the average (data or pilot) symbol power, and $\mathbf{d}_k \triangleq [d_k[n]; n \in \mathcal{Z}_N]$ as the normalized symbol vector modulated on N uniformly interleaved subcarriers with initial subcarrier index k and interleaving length ϕ . Specifically, $d_k[n]$ is set to a fixed pilot symbol $p[n]$ with average transmitted pilot power $\rho_k = \rho^{(p)}$ under the normalization $\frac{1}{N} \sum_{n \in \mathcal{Z}_N} |p[n]|^2 = 1$ when the initial subcarrier index is $k = \chi$, and it represents a transmitted M -ary (MPSK or QAM) data symbol with average (transmitted) data power $\rho_k = \rho^{(d)}$ under the normalization $E\{|d_k[n]|^2\} = 1$ otherwise. Thus, $\mathbf{d}_\chi = \mathbf{p}$ and $\mathbf{p} \triangleq [p[n]; n \in \mathcal{Z}_N]$ with $\|\mathbf{p}\|^2 = N$ is the pilot vector transmitted for aiding channel estimation. The baseband output from the (normalized) inverse discrete Fourier transform (DFT) carries $d_k[n]$'s and after the insertion of $\alpha\phi N$ cyclic-prefix guard symbols yields

$$s[m] = \sum_{k \in \mathcal{Z}_\phi} \sum_{n \in \mathcal{Z}_N} \sqrt{\frac{\rho_k}{N\phi}} d_k[n] \omega_{\phi N}^{-m(n\phi+k)} \quad (2.1)$$

for $m \in \{-\alpha\phi N, -\alpha\phi N + 1, \dots, -1, 0, 1, \dots, \phi N - 1\}$, where α is the ratio of the number of guard symbols to the number of useful (data plus pilot) symbols per block and $\alpha\phi N$ is assumed throughout to be an integer.

In this thesis, I consider the time-selective multipath fading channel in a SIMO system with I received antennas, which has short coherence time T_c not shorter than but close to block time T . In the analytical framework, the channel is modeled to exhibit fixed CIR within a block but may vary over blocks. In baseband discrete-time representation, the multipath channel within a block time on the i -th antenna for $i \in \mathcal{Z}_I$ can be characterized by the CIR vector $\mathbf{h}^{(i)} = [h^{(i)}[l]; l \in \mathcal{Z}_L]$ where $L \leq \alpha\phi N$ is restricted so that interblock interference can

be completely rejected by removing the guard portions of the received cyclic-prefix OFDM signal at the receiver. Under block fading modeling, each CIR vector $\mathbf{h}^{(i)}$ is thus fixed in each OFDM block interval but may vary over blocks in a way that channel estimation is possible based on pilot symbols within a block but not feasibly over several consecutive blocks. The receiver frontend consists of I receive antenna paths. When the i -th receive antenna path is aligned perfectly in time and frequency to the received signal, the guard portions can be deleted at the receiver and the received baseband signal carrying \mathbf{d}_k 's in the nominal block can be modeled as

$$r^{(i)}[m] = \sum_{l=0}^{L-1} h^{(i)}[l] s[m - l \bmod \phi N] + u^{(i)}[m] \quad (2.2)$$

for $m \in \mathcal{Z}_{\phi N}$ and $i \in \mathcal{Z}_I$. Here, $u^{(i)}[m]$'s are independent and identically distributed (i.i.d.) circularly symmetric complex Gaussian (CSCG) noise samples on the i -th received antenna, each having mean zero and variance $E\{|u^{(i)}[m]|^2\} = \sigma^2$. For analytical convenience, I ignore the propagation loss so that $\rho^{(d)} \|\mathbf{h}^{(i)}\|^2$ and $\rho^{(p)} \|\mathbf{h}^{(i)}\|^2$ represent the average received data and pilot symbol powers, respectively. After taking the (normalized) DFT of $r^{(i)}[m]$'s for each receive antenna path, the frequency-domain received samples at the i -th antenna path are given by

$$\tilde{r}^{(i)}[n\phi + k] = \rho_k^{\frac{1}{2}} \tilde{h}^{(i)}[n\phi + k] d_k[n] + \tilde{u}^{(i)}[n\phi + k] \quad (2.3)$$

for $n \in \mathcal{Z}_N$, $k \in \mathcal{Z}_\phi$, and $i \in \mathcal{Z}_I$. Here, $\tilde{u}^{(i)}[n\phi + k]$'s are the normalized DFT of $u^{(i)}[m]$'s and still i.i.d. CSCG samples, each having mean zero and variance σ^2 . $\tilde{h}^{(i)}[n\phi + k]$'s are the channel frequency response (CFR) corresponding to $\mathbf{h}^{(i)}$'s as

$$\tilde{h}^{(i)}[n\phi + k] = \sum_{l=0}^{L-1} h^{(i)}[l] \omega_{\phi N}^{l(n\phi + k)}. \quad (2.4)$$

These $\tilde{\mathbf{r}}^{(i)}[n\phi + k]$'s can be conveniently grouped in vector form as

$$\tilde{\mathbf{r}}_k^{(i)} = \rho_k^{\frac{1}{2}} \mathbf{D}_k \mathbf{W}_L \mathbf{\Omega}_k \mathbf{h}^{(i)} + \tilde{\mathbf{u}}_k^{(i)}, k \in \mathcal{Z}_\phi \text{ and } i \in \mathcal{Z}_I \quad (2.5)$$



where I have defined $\tilde{\mathbf{u}}_k^{(i)} \triangleq [\tilde{u}^{(i)}[n\phi + k]; n \in \mathcal{Z}_N]$, $\mathbf{D}_k \triangleq \text{diag}([d_k[n]; n \in \mathcal{Z}_N])$, $\mathbf{W}_L \triangleq [\omega_N^{nl}; n \in \mathcal{Z}_N, l \in \mathcal{Z}_L]$, and $\mathbf{\Omega}_k \triangleq \text{diag}([\omega_{\phi N}^{kl}; l \in \mathcal{Z}_L])$. Notably, \mathbf{D}_k carries the data vector \mathbf{d}_k for $k \neq \chi$ and the pilot vector \mathbf{p} otherwise.

2.3 GLRT-based Decision Rule

Given $\mathbf{h}^{(i)}$'s and \mathbf{D}_k 's, $\tilde{\mathbf{r}}_k^{(i)}$'s are independent complex Gaussian random vectors with mean vectors $\rho_k^{1/2} \mathbf{D}_k \mathbf{W}_L \mathbf{\Omega}_k \mathbf{h}^{(i)}$ for $k \in \mathcal{Z}_\phi$ and $i \in \mathcal{Z}_I$ and identical covariance matrix $\sigma^2 \mathbf{I}_N$. Obviously, all $\tilde{\mathbf{r}}_k^{(i)}$'s for the i -th antenna path are affected by the CIR vector $\mathbf{h}^{(i)}$, but $\tilde{\mathbf{r}}_k^{(i)}$'s for the k -th subchannel carry the data vector \mathbf{d}_k for $k \neq \chi$ and the pilot vector \mathbf{p} otherwise. Based on the observables $\tilde{\mathbf{r}}_k^{(i)}$'s, there are two different approaches of deciding \mathbf{d}_k 's for $k \neq \chi$ with the aid of known pilot vector \mathbf{p} . Based on all observables $\tilde{\mathbf{r}}_k^{(i)}$'s, the first approach is to decide \mathbf{d}_k 's for $k \neq \chi$ and estimate $\mathbf{h}^{(i)}$'s jointly in the maximum-likelihood (ML), or least-square, sense. By maximizing the conditional joint density of $\tilde{\mathbf{r}}_k^{(i)}$'s given $\mathbf{h}^{(i)}$'s and \mathbf{D}_k 's, this approach yields the decision rule

$$\begin{aligned} \{\hat{\mathbf{d}}_k\} &= \arg \min_{\{\mathbf{d}_k\}} \min_{\{\mathbf{h}^{(i)}\}} \left\{ \sum_{i \in \mathcal{Z}_I} \sum_{k \in \mathcal{Z}_\phi} \|\tilde{\mathbf{r}}_k^{(i)} - \rho_k^{\frac{1}{2}} \mathbf{D}_k \mathbf{W}_L \mathbf{\Omega}_k \mathbf{h}^{(i)}\|^2 \right\} \\ &= \arg \min_{\{\mathbf{d}_k\}} \left\{ \sum_{i \in \mathcal{Z}_I} \sum_{k \in \mathcal{Z}_\phi} \|\tilde{\mathbf{r}}_k^{(i)} - \rho_k^{\frac{1}{2}} \mathbf{D}_k \mathbf{W}_L \mathbf{\Omega}_k \hat{\mathbf{h}}_1^{(i)}(\{\mathbf{d}_k\}, \{\tilde{\mathbf{r}}_k^{(i)}\})\|^2 \right\} \end{aligned} \quad (2.6)$$

where $\{\mathbf{d}_k\}$ represents the collection of all data vectors except \mathbf{p} , and

$$\begin{aligned} \widehat{\mathbf{h}}_1^{(i)}(\{\mathbf{d}_k\}, \{\widetilde{\mathbf{r}}_k^{(i)}\}) &= \left[\sum_{k \in \mathcal{Z}_\phi} \rho_k ((\mathbf{D}_k \mathbf{W}_L \boldsymbol{\Omega}_k)^h \mathbf{D}_k \mathbf{W}_L \boldsymbol{\Omega}_k)^{-1} \right. \\ &\quad \times \left. \left[\sum_{k \in \mathcal{Z}_\phi} \rho_k^{\frac{1}{2}} (\mathbf{D}_k \mathbf{W}_L \boldsymbol{\Omega}_k)^h \widetilde{\mathbf{r}}_k^{(i)} \right] \right] \end{aligned} \quad (2.7)$$



is the embedded CIR estimate for any given $\{\mathbf{d}_k\}$.

When a correct $\{\mathbf{d}_k\}$ is used, $\widehat{\mathbf{h}}_1^{(i)}(\{\mathbf{d}_k\}, \{\widetilde{\mathbf{r}}_k^{(i)}\})$'s are expected to yield accurate estimates of $\mathbf{h}^{(i)}$'s since the CIR information is extracted from all $\widetilde{\mathbf{r}}_k^{(i)}$'s and this highly facilitate the decision of $\{\mathbf{d}_k\}$. However, this rule decides the whole data block $\{\mathbf{d}_k\}$ jointly and is complicated to realize when ϕN is large. Instead, I consider the second approach which decides $d_k[n]$'s symbol by symbol with the aid of the CIR estimate based on $\widetilde{\mathbf{r}}_\chi^{(i)}$'s only, as follows.

Given $\mathbf{h}^{(i)}$ and $d_k[n]$, $\widetilde{\mathbf{r}}^{(i)}[n\phi+k]$'s are CSCG distributed with mean $\rho_k^{1/2} d_k[n] \mathbf{1}_n^t \mathbf{W}_L \boldsymbol{\Omega}_k \mathbf{h}^{(i)}$ and variance σ^2 for $i \in \mathcal{Z}_I$, $n \in \mathcal{Z}_N$ and $k \in \mathcal{Z}_\phi$, where $\mathbf{1}_n$ represents the $N \times 1$ vector in which the n -th entry is one and all the other are zero. Moreover, when $\mathbf{h}^{(i)}$'s and $d_k[n]$'s are given, all $\widetilde{\mathbf{r}}^{(i)}[n\phi+k]$'s are independent. As such, $\widetilde{\mathbf{r}}^{(0)}[n\phi+k]$, $\widetilde{\mathbf{r}}^{(1)}[n\phi+k]$, ..., $\widetilde{\mathbf{r}}^{(I-1)}[n\phi+k]$ suffice to make decision on $d_k[n]$ when $\mathbf{h}^{(i)}$'s are given. This enables the decision on $d_k[n]$'s symbol by symbol if $\mathbf{h}^{(i)}$'s can be estimated respectively and in advance. Although not sufficient for CIR estimation, $\widetilde{\mathbf{r}}_\chi^{(i)}$'s carry known pilot \mathbf{p} only and can be used to estimate the CIR $\mathbf{h}^{(i)}$'s without interference from data. Such estimates can naturally serve to enable the symbol-by-symbol decision, as follows. First, I note that $\widetilde{\mathbf{r}}_\chi^{(i)}$'s are independent CSCG vectors with means $(\rho^{(p)})^{1/2} \mathbf{D}_\chi \mathbf{W}_L \boldsymbol{\Omega}_\chi \mathbf{h}^{(i)}$ for $i \in \mathcal{Z}_I$ and covariance matrix $\sigma^2 \mathbf{I}_N$ when $\mathbf{h}^{(i)}$'s and \mathbf{p} are given. Also, $\mathbf{h}^{(i)}$'s are mutually irrelevant since antenna elements are spaced sufficiently apart. Thus, based on $\widetilde{\mathbf{r}}_\chi^{(i)}$, the ML estimate of $\mathbf{h}^{(i)}$ can be obtained respectively by maximizing the

likelihood density of $\tilde{\mathbf{r}}_\chi^{(i)}$ given $\mathbf{h}^{(i)}$, as

$$\begin{aligned}\hat{\mathbf{h}}_2^{(i)}(\tilde{\mathbf{r}}_\chi^{(i)}) &= \arg \min_{\mathbf{h}^{(i)}} \{ \|\tilde{\mathbf{r}}_\chi^{(i)} - (\rho^{(p)})^{\frac{1}{2}} \mathbf{D}_\chi \mathbf{W}_L \boldsymbol{\Omega}_\chi \mathbf{h}^{(i)}\|^2 \} \\ &= \frac{1}{\sqrt{\rho^{(p)}}} ((\mathbf{D}_\chi \mathbf{W}_L \boldsymbol{\Omega}_\chi)^h \mathbf{D}_\chi \mathbf{W}_L \boldsymbol{\Omega}_\chi)^{-1} (\mathbf{D}_\chi \mathbf{W}_L \boldsymbol{\Omega}_\chi)^h \tilde{\mathbf{r}}_\chi^{(i)}.\end{aligned}\quad (2.8)$$

Notably, $\hat{\mathbf{h}}_2^{(i)}(\tilde{\mathbf{r}}_\chi^{(i)})$ is unbiased with $E\{\hat{\mathbf{h}}_2^{(i)}(\tilde{\mathbf{r}}_\chi^{(i)})\} = \mathbf{h}^{(i)}$ and yields the mean-square error variance (MSE)

$$E\{\|\hat{\mathbf{h}}_2^{(i)}(\tilde{\mathbf{r}}_\chi^{(i)}) - \mathbf{h}^{(i)}\|^2\} = \gamma_p^{-1} \text{tr}\{((\mathbf{D}_\chi \mathbf{W}_L \boldsymbol{\Omega}_\chi)^h \mathbf{D}_\chi \mathbf{W}_L \boldsymbol{\Omega}_\chi)^{-1}\} \quad (2.9)$$

where $\|\mathbf{h}^{(i)}\|^2 \gamma_p$ is the ratio of average received pilot symbol power to noise power (PNR) on the i -th antenna path, with $\gamma_p \triangleq \rho^{(p)} / \sigma^2$. Under the restriction $\|\mathbf{p}\|^2 = N$, the minimum MSE is given by $\frac{L}{N\gamma_p}$, which can be achieved by restricting $|p[n]| = 1$ for all $n \in \mathcal{Z}_N$ [14]-[16].

Next, using the CIR estimates $\hat{\mathbf{h}}_2^{(i)}(\tilde{\mathbf{r}}_\chi^{(i)})$'s for all I antenna paths, $d_k[n]$ for $k \neq \chi$ can be decided through the generalized likelihood ratio test (GLRT) [34, Appendix A, eqs. (A-3-4) and (A-3-5)] based on the observables $\tilde{r}^{(0)}[n\phi+k]$, $\tilde{r}^{(1)}[n\phi+k]$, ..., $\tilde{r}^{(I-1)}[n\phi+k]$, which maximizes the product of the conditional densities for I observables given $d_k[n]$ and $\mathbf{h}^{(i)} = \hat{\mathbf{h}}_2^{(i)}(\tilde{\mathbf{r}}_\chi^{(i)})$ for all $i \in \mathcal{Z}_I$, as

$$\begin{aligned}\hat{d}_k[n] &= \arg \min_d \left\{ \sum_{i \in \mathcal{Z}_I} |\tilde{r}^{(i)}[n\phi+k] - (\rho^{(d)})^{\frac{1}{2}} d \mathbf{1}_n^t \mathbf{W}_L \boldsymbol{\Omega}_k \hat{\mathbf{h}}_2^{(i)}(\tilde{\mathbf{r}}_\chi^{(i)})|^2 \right\} \\ &= \arg \min_d \sum_{i \in \mathcal{Z}_I} F_{k,n}^{(i)}(d)\end{aligned}\quad (2.10)$$

$$= \arg \max_d \left[2 \sum_{i \in \mathcal{Z}_I} \text{Re}\{\tilde{r}^{(i)}[n\phi+k] (\mathbf{1}_n^t \mathbf{V}_k \tilde{\mathbf{r}}_\chi^{(i)})^* d^*\} - \varphi^{\frac{1}{2}} |d \mathbf{1}_n^t \mathbf{V}_k \tilde{\mathbf{r}}_\chi^{(i)}|^2 \right] \quad (2.11)$$

for each $n \in \mathcal{Z}_N$ and $k \in \mathcal{Z}_\phi - \{\chi\}$, where I have conveniently defined

$$\mathbf{V}_k \triangleq \mathbf{W}_L \mathbf{\Omega}_k ((\mathbf{D}_\chi \mathbf{W}_L \mathbf{\Omega}_\chi)^h \mathbf{D}_\chi \mathbf{W}_L \mathbf{\Omega}_\chi)^{-1} (\mathbf{D}_\chi \mathbf{W}_L \mathbf{\Omega}_\chi)^h \quad (2.12)$$

$$F_{k,n}^{(i)}(d) \triangleq |\tilde{r}^{(i)}[n\phi + k] - \varphi^{\frac{1}{2}} d \mathbf{1}_n^t \mathbf{V}_k \tilde{\mathbf{r}}_\chi^{(i)}|^2 \quad (2.13)$$

and $\varphi \triangleq \rho^{(d)}/\rho^{(p)}$ represents the ratio of average transmitted data symbol power to average transmitted pilot symbol power (DPR). Rules (2.10) and (2.11) are equivalent. Rule (2.10) is the considered GLRT-based decision rule in the following.

Note that, the GLRT rule in (2.11) can be rewritten as

$$\hat{d}_k[n] = \arg \min_d \left| \frac{\sum_{i \in \mathcal{Z}_I} \tilde{r}^{(i)}[n\phi + k] (\hat{h}_k^{(i)}[n])^*}{\sum_{i \in \mathcal{Z}_I} |\hat{h}_k^{(i)}[n]|^2} - (\rho^{(d)})^{\frac{1}{2}} d \right|^2. \quad (2.14)$$

In (2.14), $\sum_{i \in \mathcal{Z}_I} \tilde{r}^{(i)}[n\phi + k] (\hat{h}_k^{(i)}[n])^* / \sum_{i \in \mathcal{Z}_I} |\hat{h}_k^{(i)}[n]|^2$ is exactly the test statistic adopted by the MRC-based SIMO-OFDM system in [23]-[24]. Thus, the GLRT rule (2.10) is equivalent to and thus performs the same as the MRC decision rule in [23]-[24].

2.3.1 Decision Rule with Constant Amplitude Pilot Sequence

Constant-amplitude (CA) pilot sequences are commonly modulated on uniformly interleaved subcarriers to compose training waveforms in OFDM systems and facilitate channel estimation at the receiver [14]-[19]. Due to symbol amplitude constancy, CA pilot sequences can achieve the minimum CRB $CRB_{\min} = \frac{L}{N\gamma_p}$ by using the LS estimate $\hat{\mathbf{h}}_2^{(i)}(\tilde{\mathbf{r}}_\chi^{(i)})$ and enable high estimation accuracy for pilot-aided channel estimation on block dispersive channels [14]-[19]. Thus, CA pilot sequence \mathbf{p} with $|p[n]| = 1$ for all $n \in \mathcal{Z}_N$ is considered throughout the paper to enable such unbiased and efficient CIR estimate $\hat{\mathbf{h}}_2^{(i)}(\tilde{\mathbf{r}}_\chi^{(i)})$ and thereby unbiased and effi-

cient direct CFR estimates $\hat{h}_k^{(i)}[n]$'s [34]. In this case, $\mathbf{D}_\chi^h \mathbf{D}_\chi = \mathbf{I}_N$ and this simplifies \mathbf{V}_k in (2.12) to

$$\mathbf{V}_k|_{\text{CA pilot}} = N^{-1} \mathbf{W}_L \mathbf{\Omega}_k \mathbf{\Omega}_\chi^h \mathbf{W}_L^h \mathbf{D}_\chi^h \quad (2.15)$$

and thus $\mathbf{V}_k|_{\text{CA pilot}} \mathbf{V}_k^h|_{\text{CA pilot}} = N^{-1} \mathbf{W}_L \mathbf{W}_L^h$ is the same for all $k \in \mathcal{Z}_\phi$. Moreover, when γ_p approaches to the infinity, $\hat{\mathbf{h}}_2^{(i)}(\tilde{\mathbf{r}}_\chi^{(i)})$ approaches to true CIR $\mathbf{h}^{(i)}$ in the mean square sense and thereby the considered GLRT decision rule approaches to the coherent ML decision rule asymptotically in the sense that the SEP is minimized for an infinitely large γ_p . Specifically, the decision rule in (2.10) approaches to the limiting rule

$$\hat{d}_k[n] = \arg \min_d \left\{ \sum_{i \in \mathcal{Z}_I} |\tilde{r}^{(i)}[n\phi + k] - (\rho^{(d)})^{\frac{1}{2}} d \mathbf{1}_n^t \mathbf{W}_L \mathbf{\Omega}_k \mathbf{h}^{(i)}|^2 \right\}. \quad (2.16)$$

which is a minimum Euclidean-distance rule and exactly the optimum coherent decision rule on $d_k[n]$ based on I independently received signals $\tilde{r}^{(0)}[n\phi + k], \tilde{r}^{(1)}[n\phi + k], \dots, \tilde{r}^{(I-1)}[n\phi + k]$ in the additive white Gaussian noise (AWGN) channel. Thus, when γ_p is sufficiently large, the proposed GLRT rule in (2.10) is expected to provide an error performance close to the optimum coherent performance in the I -diversity AWGN channel with the received signal-to-noise power ratios per symbol (symbol SNRs) $\|\mathbf{h}^{(0)}\|^2 \rho^{(d)} / \sigma^2, \|\mathbf{h}^{(1)}\|^2 \rho^{(d)} / \sigma^2, \dots, \|\mathbf{h}^{(I-1)}\|^2 \rho^{(d)} / \sigma^2$ [28].



Chapter 3

Performance Analysis

3.1 Introduction

The exact bit error probability (BEP) of rule (2.10) is difficult, if not impossible, to analyze. Instead, an upper bound to BEP is derived in this chapter. In the following analysis, I consider that a CA pilot sequence \mathbf{p} is used to enable an efficient ML estimate $\hat{\mathbf{h}}_2^{(i)}(\tilde{\mathbf{r}}_\chi)$. and also that $d_k[n]$'s are generated independently and equally likely from the identical symbol source \mathcal{S} with size M and further that $d_k[n]$'s are encoded respectively by use of the identical code mapping of bits to symbols.

3.2 Conditional BEP Upper Bound

Conditional BEP upper bound is derived here for given CIRs $\{\mathbf{h}^{(i)}\}$. Using the union bound argument [33], the BEP of rule (2.10) is bounded for given $\{\mathbf{h}^{(i)}\}$ by

$$\begin{aligned}
 P_b(\{\mathbf{h}^{(i)}\}) &\leq \frac{1}{N(\phi-1)} \sum_{k \in \mathcal{Z}_\phi} \sum_{n \in \mathcal{Z}_N} \sum_{\substack{d_k[n], \hat{d}_k[n] \in \mathcal{S} \\ \hat{d}_k[n] \neq d_k[n]}} \frac{D_H(d_k[n], \hat{d}_k[n])}{M \log_2 M} \\
 &\times \Pr\left\{ \sum_{i \in \mathcal{Z}_I} F_{k,n}^{(i)}(\hat{d}_k[n]) < \sum_{i \in \mathcal{Z}_I} F_{k,n}^{(i)}(d_k[n]) \mid d_k[n], \{\mathbf{h}^{(i)}\} \right\}. \quad (3.1)
 \end{aligned}$$

Here, $D_H(d_k[n], \hat{d}_k[n])$ is the Hamming distance between the binary representations of symbols $d_k[n]$ and $\hat{d}_k[n]$. $\Pr\{\sum_{i=0}^{I-1} F_{k,n}^{(i)}(\hat{d}_k[n]) < \sum_{i=0}^{I-1} F_{k,n}^{(i)}(d_k[n]) | d_k[n], \{\mathbf{h}^{(i)}\}\}$ is the pairwise error probability that $\sum_{i=0}^{I-1} F_{k,n}^{(i)}(\hat{d}_k[n])$ is smaller than $\sum_{i=0}^{I-1} F_{k,n}^{(i)}(d_k[n])$ when $d_k[n]$ was indeed transmitted and the CIRs $\mathbf{h}^{(i)}$'s are fixed. Given $\mathbf{h}^{(i)}$'s, $\sum_{i=0}^{I-1} F_{k,n}^{(i)}(d_k[n])$ and $\sum_{i=0}^{I-1} F_{k,n}^{(i)}(\hat{d}_k[n])$ are correlated noncentral chi-square random variables with $2I$ degrees of freedom and the probability of the event $\{\sum_{i=0}^{I-1} F_{k,n}^{(i)}(\hat{d}_k[n]) < \sum_{i=0}^{I-1} F_{k,n}^{(i)}(d_k[n])\}$ has been derived in [31, Appendix B], [29, eqs. (60)] and is quoted in *Appendix A*, where $d_k[n] = d$ and $\hat{d}_k[n] = \hat{d}$ are denoted for notational simplicity, as

$$\begin{aligned}
& \Pr\left\{\sum_{i \in \mathcal{Z}_I} F_{k,n}^{(i)}(\hat{d}) < \sum_{i \in \mathcal{Z}_I} F_{k,n}^{(i)}(d) \middle| d, \{\mathbf{h}^{(i)}\}\right\} \\
&= [1 - Q_1(\beta^{1/2}\varepsilon_2, \beta^{1/2}\varepsilon_1)] \left[1 - \frac{\sum_{a=0}^{I-1} \binom{2I-1}{a} \left(\frac{\nu_2}{\nu_1}\right)^a}{(1 + \nu_2/\nu_1)^{2I-1}}\right] \\
&+ Q_1(\beta^{1/2}\varepsilon_1, \beta^{1/2}\varepsilon_2) \frac{\sum_{a=0}^{I-1} \binom{2I-1}{a} \left(\frac{\nu_2}{\nu_1}\right)^a}{(1 + \nu_2/\nu_1)^{2I-1}} \\
&+ \frac{\sum_{a=2}^I \binom{2I-1}{I-a} \left(\frac{\nu_2}{\nu_1}\right)^{I-a}}{(1 + \nu_2/\nu_1)^{2I-1}} \times [Q_a(\beta^{1/2}\varepsilon_1, \beta^{1/2}\varepsilon_2) - Q_1(\beta^{1/2}\varepsilon_1, \beta^{1/2}\varepsilon_2)] \\
&- \frac{\sum_{a=2}^I \binom{2I-1}{I-a} \left(\frac{\nu_2}{\nu_1}\right)^{I-1+a}}{(1 + \nu_2/\nu_1)^{2I-1}} \times [Q_a(\beta^{1/2}\varepsilon_2, \beta^{1/2}\varepsilon_1) - Q_1(\beta^{1/2}\varepsilon_2, \beta^{1/2}\varepsilon_1)] \quad (3.2)
\end{aligned}$$

where $Q_a(x, y)$ is the generalized Marcum Q -function of order a [31, eqs. (2.3-36)] and specifically $Q_1(x, y)$ is the first-order Marcum function [31, eqs. (2.3-37) and (2.3-38)]. In

(3.2), I have defined the following parameters

$$\varepsilon_1 \triangleq \left[\frac{1-\lambda^2}{2} \gamma_d |d - \hat{d}|^2 (\vartheta \zeta - \nu_1) \right]^{\frac{1}{2}} \quad (3.3)$$

$$\varepsilon_2 \triangleq \left[\frac{1-\lambda^2}{2} \gamma_d |d - \hat{d}|^2 (\vartheta \zeta + \nu_2) \right]^{\frac{1}{2}} \quad (3.4)$$

$$\beta \triangleq \sum_{i \in \mathcal{Z}_I} |\mathbf{1}_n^t \mathbf{W}_L \mathbf{\Omega}_k \mathbf{h}^{(i)}|^2 \quad (3.5)$$

$$\nu_1 = (\xi^2 + \zeta)^{\frac{1}{2}} - \xi \quad (3.6)$$

$$\nu_2 = (\xi^2 + \zeta)^{\frac{1}{2}} + \xi \quad (3.7)$$

$$\xi = \frac{|\hat{d}|^2 - |d|^2}{2|\hat{d} - d|^2} \quad (3.8)$$

where ζ , λ , and ϑ are defined as in (A.21), (A.22), and (A.23), respectively. Here, $\|\mathbf{h}^{(i)}\|^2 \gamma_d$ is the ratio of average received data symbol power to noise power (DNR) on the i -th antenna path, with $\gamma_d \triangleq \rho^{(d)} / \sigma^2$. Notably, β depends on CIRs $\{\mathbf{h}^{(i)}\}$, while the other parameters ε_1 , ε_2 , ν_1 , and ν_2 do not.

3.2.1 Pairwise Error Probability for MPSK

The pairwise error probability in (3.2) holds for MPSK and QAM data symbols, and can be further simplified for MPSK data symbols. For MPSK data, $|d_k[n]| = 1$ for all $n \in \mathcal{Z}_N$ and $k \in \mathcal{Z}_\phi - \{\chi\}$ are restricted. In this case, $\mathbf{D}_k^h \mathbf{D}_k = \mathbf{I}_N$ for all $k \in \mathcal{Z}_\phi - \{\chi\}$ and both ξ in (3.8) and λ in (A.22) reduce to zeros. Thus, the parameters ν_1 , ν_2 , ε_1 and η_2 in (A.9)-(A.10) reduce to $\nu_1 = \nu_2 = \zeta^{1/2}$, $\varepsilon_1 = [\frac{1}{2}(\vartheta \zeta - \zeta^{1/2})]^{1/2}$, and $\varepsilon_2 = [\frac{1}{2}(\vartheta \zeta + \zeta^{1/2})]^{1/2}$ with $\zeta = \frac{N}{L\varphi} |\hat{d} - d|^{-2}$ and $\vartheta = 1 + \frac{L\varphi}{N}$, which simplifies (3.2) to

$$\begin{aligned} \Pr\left\{ \sum_{i \in \mathcal{Z}_I} F_{k,n}^{(i)}(\hat{d}) < \sum_{i \in \mathcal{Z}_I} F_{k,n}^{(i)}(d) | d, \{\mathbf{h}^{(i)}\} \right\} &= \frac{1}{2} \\ &+ \frac{1}{2^{2I-1}} \sum_{a=1}^I \binom{2I-1}{I-a} [Q_a(\beta^{1/2} \varepsilon_1, \beta^{1/2} \varepsilon_2) - Q_a(\beta^{1/2} \varepsilon_2, \beta^{1/2} \varepsilon_1)]. \end{aligned} \quad (3.9)$$



3.3 Average BEP Upper Bound

Here, the conditional BEP upper bound (3.1) using (3.2) is averaged over the joint density of CIRs $\{\mathbf{h}^{(i)}\}$ to yield the upper bound to the average BEP $E\{P_b(\{\mathbf{h}^{(i)}\})\}$. Since only β in the arguments of $Q_a(\beta^{1/2}\varepsilon_1, \beta^{1/2}\varepsilon_2)$ and $Q_a(\beta^{1/2}\varepsilon_2, \beta^{1/2}\varepsilon_1)$ for all $a \in \mathcal{Z}_I^+$ in (3.2) depends on $\{\mathbf{h}^{(i)}\}$, the average BEP upper bound can be equivalently derived by averaging (3.1) over the density of β . In the latter approach, it is convenient to adopt the integral representation of the generalized Marcum Q -function proposed in [29] and then achieve a single integral representation of the upper bound to $E\{P_b(\{\mathbf{h}^{(i)}\})\}$ in terms of the moment generating function (MGF) of β , $\Phi_\beta(s) \triangleq E\{\exp\{s\beta\}\}$, as follows.

In terms of the single-integral representations of the generalized Marcum Q -function in [29, eq. (61)], the pairwise error probability in (3.2) is rewritten in *Appendix B* as

$$\begin{aligned} & \Pr\left\{\sum_{i \in \mathcal{Z}_I} F_{k,n}^{(i)}(\hat{d}) < \sum_{i \in \mathcal{Z}_I} F_{k,n}^{(i)}(d) \mid d, \{\mathbf{h}^{(i)}\}\right\} \\ &= \frac{\varrho^I}{2\pi(1+\varrho)^{2I-1}} \int_{-\pi}^{\pi} \frac{\Psi(\theta; I, \tau, \varrho)}{1+2\tau \sin \theta + \tau^2} \\ & \quad \times \exp\left\{-\frac{\beta \varepsilon_2^2}{2}(1+2\tau \sin \theta + \tau^2)\right\} d\theta \end{aligned} \quad (3.10)$$

where I have defined $\tau \triangleq \varepsilon_1/\varepsilon_2$ and $\varrho \triangleq \nu_2/\nu_1$ with $0 \leq \tau < 1$ and

$$\begin{aligned} \Psi(\theta; I, \tau, \varrho) &= (\tau^2 + \tau \sin \theta) \left\{ -\frac{(1+\varrho)^{2I-1}}{\varrho^I} + \sum_{a=1}^I \binom{2I-1}{I-a} [\varrho^{-a} + \varrho^{a-1}] \right\} \\ &+ \sum_{a=1}^I \binom{2I-1}{I-a} \{ \cos((a-1)(\theta + \pi/2)) \times [\varrho^{-a}\tau^{-a+1} - \varrho^{a-1}\tau^{a+1}] \\ &- \cos(a(\theta + \pi/2)) \times [\varrho^{-a}\tau^{-a+2} - \varrho^{a-1}\tau^a] \}. \end{aligned} \quad (3.11)$$

As shown, (3.10) is a single integral with an integrand in which the sole channel-dependent parameter β resides only in a single exponential function $\exp\{-\frac{\beta \varepsilon_2^2}{2}(1+2\tau \sin \theta + \tau^2)\}$. This

facilitates the process of averaging the pairwise error probability over the density of β and the result can be represented in terms of the MGF $\Phi_\beta(s)$. Explicitly, averaging (3.1) using (3.10) over the density of β yields

$$\begin{aligned}
 E\{P_b(\{\mathbf{h}^{(i)}\})\} \leq & \frac{1}{N(\phi-1)} \sum_{k \in \mathcal{Z}_\phi} \sum_{n \in \mathcal{Z}_N} \sum_{\substack{d_k[n], \hat{d}_k[n] \in \mathcal{S} \\ \hat{d}_k[n] \neq d_k[n]}} \\
 & \frac{D_H(d_k[n], \hat{d}_k[n])}{M \log_2 M} \times \frac{\varrho^I}{2\pi(1+\varrho)^{2I-1}} \\
 & \times \int_{-\pi}^{\pi} \frac{\Psi(\theta; I, \tau, \varrho) \Phi_\beta(-\frac{\varepsilon_2^2}{2}(1+2\tau \sin \theta + \tau^2))}{1+2\tau \sin \theta + \tau^2} d\theta.
 \end{aligned} \tag{3.12}$$

where the parameters ϱ , τ , and ε_2 in the summation are computed with the aid of (3.3)-(3.7) with $d \rightarrow d_k[n]$ and $\hat{d} \rightarrow \hat{d}_k[n]$.

The average BEP upper bound holds for arbitrary statistic of $\{\mathbf{h}^{(i)}\}$ as long as $\Phi_\beta(s)$ can be explicitly obtained. In what follows, I consider a particular SIMO block multipath fading model where the CIRs $\{\mathbf{h}^{(i)}\}$ are independent over different antenna paths and each $\mathbf{h}^{(i)}$ is fixed in one OFDM block but varies randomly over blocks according to several multipath fading channel model.

Similar to the multipath Rician fading in [35], the CIR $\mathbf{h}^{(i)}$ on the i -th antenna path is modeled to exhibit a direct path with random response $h^{(i)}[0]$, which is a complex Gaussian random variable having mean $E\{h^{(i)}[0]\} = \sigma_{\text{direct}}^{(i)} \exp\{j\theta^{(i)}\}$ and correlations $E\{(h^{(i)}[0] - E\{h^{(i)}[0]\})^2\} = 0$ and $E\{|h^{(i)}[0] - E\{h^{(i)}[0]\}|^2\} = (\sigma_{\text{diffuse}}^{(i)}[0])^2$ where the phase $\theta^{(i)}$ is arbitrary, $(\sigma_{\text{direct}}^{(i)})^2$ is the direct power, and $(\sigma_{\text{diffuse}}^{(i)}[0])^2$ represents the diffuse power on the zeroth path, and $L-1$ diffuse paths with random responses $h^{(i)}[1], h^{(i)}[2], \dots, h^{(i)}[L-1]$ which are independent CSCGs with common mean zero and respective diffuse path power $E\{|h^{(i)}[l]|^2\} = (\sigma_{\text{diffuse}}^{(i)}[l])^2$ for $l \in \mathcal{Z}_{L-1}^+$. The direct path response is also independent of all diffuse path responses.

In order to describe the density of β , I first rewrite β as

$$\beta \triangleq \sum_{i=0}^{I-1} |\beta^{(i)}|^2 \quad (3.13)$$



where

$$\beta^{(i)} \triangleq \mathbf{1}_n^t \mathbf{W}_L \mathbf{\Omega}_k \mathbf{h}^{(i)}. \quad (3.14)$$

Because the zeroth entry of each tuple in the row vector $\mathbf{1}_n^t \mathbf{W}_L \mathbf{\Omega}_k = [\omega_{\phi N}^{kl} \omega_N^{nl}; l \in \mathcal{Z}_L]^t$ is equal to one and all entries have unit magnitude, it can be immediately shown that each $\beta^{(i)}$ is the sum of constant mean $\sigma_{\text{direct}}^{(i)} \exp\{j\theta^{(i)}\}$ and a CSCG random variable with mean zero and variance $\sum_{l \in \mathcal{Z}_L} (\sigma_{\text{diffuse}}^{(i)}[l])^2$, for $i \in \mathcal{Z}_I$. Moreover, since $\mathbf{h}^{(i)}$'s are mutually independent over different antenna paths, $\beta^{(i)}$'s are independent complex-valued Gaussian random variables with

$$E\{\beta^{(i)}\} = \sigma_{\text{direct}}^{(i)} \exp\{j\theta^{(i)}\} \quad (3.15)$$

$$E\{(\beta^{(i)} - E\{\beta^{(i)}\})^2\} = 0 \quad (3.16)$$

$$E\{|\beta^{(i)} - E\{\beta^{(i)}\}|^2\} = \sum_{l \in \mathcal{Z}_L} (\sigma_{\text{diffuse}}^{(i)}[l])^2 \quad (3.17)$$

for $i \in \mathcal{Z}_I$. Within such statistic, $|\beta^{(i)}|^2$ follows a noncentral chi-square distribution with two degrees of freedom, noncentrality parameter $(\sigma_{\text{direct}}^{(i)})^2$, and variance $\sum_{l \in \mathcal{Z}_L} (\sigma_{\text{diffuse}}^{(i)}[l])^2$. When the direct power is zero (i.e., there is no line of sight), the distribution of $|\beta^{(i)}|^2$ reduces to a central chi-square distribution. Given the MGF function of a noncentral chi-square random variable with two degrees of freedom in [36] and the mutual independence among $|\beta^{(i)}|^2$'s,

the quadratic sum random variable $\beta = \sum_{i=0}^{I-1} |\beta^{(i)}|^2$ has the MGF

$$\begin{aligned}\Phi_{\beta}(s) &= \prod_{i=0}^{I-1} \Phi_{|\beta^{(i)}|^2}(s) \\ &= \prod_{i=0}^{I-1} (1 - s \sum_{l \in \mathcal{Z}_L} (\sigma_{\text{diffuse}}^{(i)}[l])^2)^{-1} \exp\left\{ \frac{(\sigma_{\text{direct}}^{(i)})^2 s}{1 - s \sum_{l \in \mathcal{Z}_L} (\sigma_{\text{diffuse}}^{(i)}[l])^2} \right\}. \quad (3.18)\end{aligned}$$



By substituting (3.18) into (3.12), the average BEP upper bound can be evaluated numerically.

In the uplink DAS application [37]-[38], multiple receive antennas are located in several remote antenna ports and the CIR vectors $\mathbf{h}^{(i)}$'s can be plausibly modeled to follow i.n.i.d. statistic. Consider the special SIMO DAS where there are Q distributed antenna ports located in different geographic locations and the q -th port consists of I_q antennas experiencing a group of independent CIRs $\mathcal{H}^{(q)} = \{\mathbf{h}^{(\tilde{I}_q)}, \mathbf{h}^{(\tilde{I}_q+1)}, \dots, \mathbf{h}^{(\tilde{I}_q+I_q-1)}\}$ with $\tilde{I}_q \triangleq \sum_{n=0}^{q-1} I_n$ and $\tilde{I}_Q = I$. Because Q ports are geographically apart, the CIR group $\mathcal{H}^{(q)}$ may have different statistic from another group $\mathcal{H}^{(p)}$ with $p \neq q$. Also, we consider the special but somehow practical scenario that the receive antenna elements in the same port are compactly placed with antenna spacing much smaller than the distances in direct path and all diffuse paths. Under this scenario, the l -th paths $h^{(\tilde{I}_q)}[l], h^{(\tilde{I}_q+1)}[l], \dots, h^{(\tilde{I}_q+I_q-1)}[l]$ in all CIR vectors in $\mathcal{H}^{(q)}$ can be modeled as identically distributed, and thus $\mathcal{H}^{(q)}$ exhibits identical power on all l -th channel paths, i.e., all $h^{(i)}[l]$'s in $\mathcal{H}^{(q)}$ have the same power for each l (with $\sigma_{\text{direct}}^{(i)} = \sigma_{q,\text{direct}}$ and $\sigma_{\text{diffuse}}^{(i)}[l] = \sigma_{q,\text{diffuse}}[l]$ for all $l \in \mathcal{Z}_L$). Under this special DAS model, the MGF $\Phi_{\beta}(s)$ in (3.18) reduces to

$$\Phi_{\beta}(s) = \prod_{q=0}^{Q-1} \exp\left\{ \frac{I_q s \sigma_{q,\text{direct}}^2}{1 - s \sum_{l \in \mathcal{Z}_L} \sigma_{q,\text{diffuse}}^2[l]} \right\} (1 - s \sum_{l \in \mathcal{Z}_L} \sigma_{q,\text{diffuse}}^2[l])^{-I_q}. \quad (3.19)$$

When all antenna elements are collocated in the same port (i.e., $Q = 1$ and $I_0 = I$), all l -th channel paths have the identical power distribution with $\sigma_{\text{direct}}^{(i)} = \sigma_{\text{direct}}$ and $\sigma_{\text{diffuse}}^{(i)}[l] =$

$\sigma_{\text{diffuse}}[l]$ for $l \in \mathcal{Z}_L$. In this case, the MGF $\Phi_\beta(s)$ in (3.18) simplifies to

$$\Phi_\beta(s) = \exp\left\{\frac{Is\sigma_{\text{direct}}^2}{1 - s \sum_{l \in \mathcal{Z}_L} \sigma_{\text{diffuse}}^2[l]}\right\} \left(1 - s \sum_{l \in \mathcal{Z}_L} \sigma_{\text{diffuse}}^2[l]\right)^{-I}. \quad (3.20)$$





Chapter 4

Performance Results

4.1 Introduction

This chapter illustrates the BEP characteristics and average BEP characteristics of the proposed GLRT-based pilot-aided OFDM SIMO system over both fixed and random block dispersive channels. For demonstration simplicity, I consider the special but somehow practical scenario that the receive antenna elements are compactly placed with antenna spacing much smaller than the distances in direct path and all diffuse paths. Under this scenario, I SIMO channels can be plausibly modeled to exhibit identical power on all antenna paths for each channel path, i.e., $h^{(i)}[l]$ for all $i \in \mathcal{Z}_I$ have the same power for each l .

4.2 ZC Sequences

The ZC sequences adopted for pilot-aided channel estimation in LTE [25] and 5G NR [27] are considered as pilot sequences in the following demonstration. Specifically, ZC sequence is defined by $p^{(ZC)}[n] = \exp\{-j\frac{\pi v n^2}{N}\}$ when N is even and $p^{(ZC)}[n] = \exp\{-j\frac{\pi v n(n+1)}{N}\}$ when N is odd for $n \in \mathcal{Z}_N$, where v is a positive integer relatively prime to N . All ZC sequences

$\mathbf{p}^{(ZC)}$ consist of constant-amplitude symbols and thus provide optimum pilot-based channel estimation performance achieving the Cramér-Rao bound for the fixed dispersive channel [17]-[18].



4.3 BEP Characteristics in Fixed Block Dispersive Channel

4.3.1 Fixed Block Dispersive Channel

For the fixed dispersive channel, CIRs $\{\mathbf{h}^{(i)}\}$ are fixed over consecutive OFDM blocks and modeled as the exponential delay spread (EDS) channel [39] characterized by

$$h^{(i)}[l] = C_h \exp\{j\theta_l^{(i)}\} \exp\{-l/D\} \quad (4.1)$$

for $l \in \mathcal{Z}_L$ and $i \in \mathcal{Z}_I$, where the constant coefficient D represents the ratio of sampling time $[(1 + \alpha)N\phi]^{-1}T$ to root-mean-square delay spread value, the constant amplitude C_h is chosen to normalize $\|\mathbf{h}^{(i)}\| = 1$ and $\theta_l^{(i)}$'s are arbitrary phase values over $[0, 2\pi)$. Under the normalization $\|\mathbf{h}^{(i)}\| = 1$, γ_d , γ_p , φ , and γ_{avg} represent the average received symbol DNR, the average received symbol PNR, the received DPR, and the average received symbol SNR (i.e., $(1 - \frac{1}{\phi})\gamma_d + \frac{1}{\phi}\gamma_p$), respectively. In this case, the BEP characteristic $P_b(\{\mathbf{h}^{(i)}\})$ for given CIRs $\{\mathbf{h}^{(i)}\}$ is demonstrated versus the average received bit DNR $\gamma_d/\log_2 M$. With CFR $H^{(i)}[k] = \sum_{l=0}^{L-1} h^{(i)}[l] \exp\{-j2\pi lk/(N\phi)\}$, the Fourier power spectrum density for antenna path i is given by $|H^{(i)}[k]|^2$. In order to demonstrate the effect of D on CFR, the power spectrum densities of three different EDS channels with $D = 0.5, 1$, and 2 are illustrated in Fig. 4.1, where $i = 0$, $N = 64$, $\phi = 4$ and $L = 3$ are fixed. As shown, the fluctuation in CFR varies slower with subcarrier index when D is smaller, and *vice versa*.

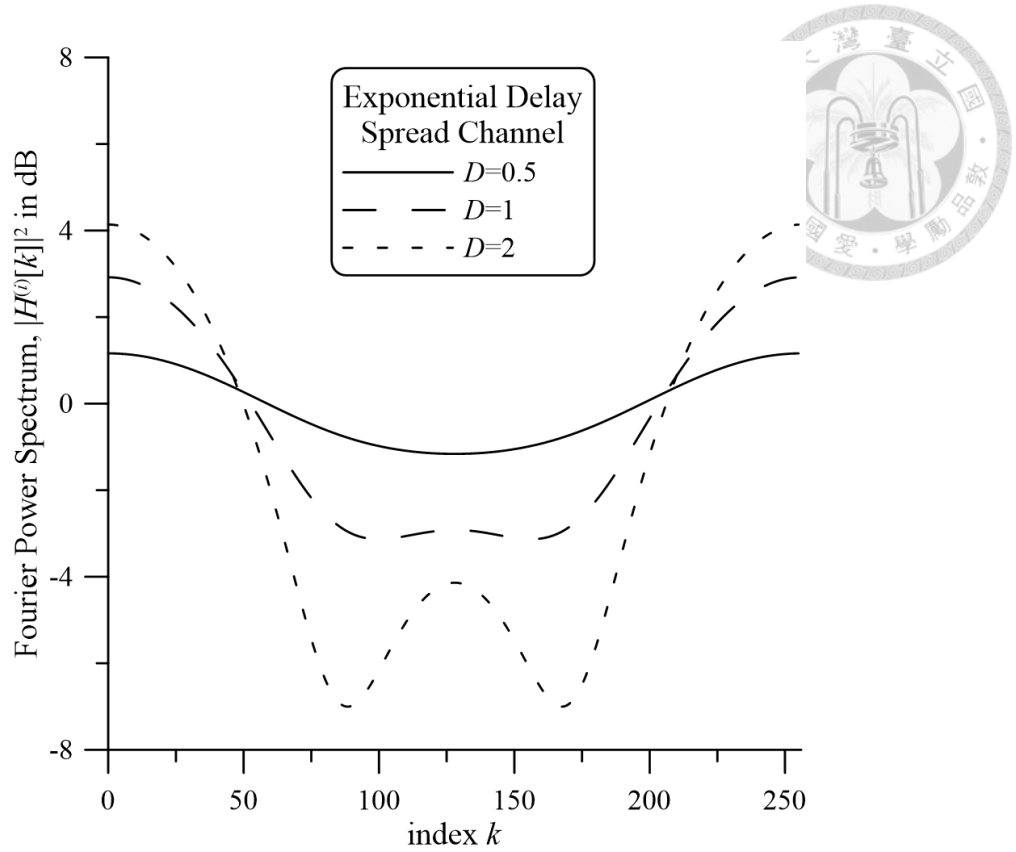


Figure 4.1: Fourier power spectra of EDS channels with $D = 0.5, 1$ and 2 for the OFDM system with $i = 0, N = 64, \phi = 4$ and $L = 3$.

4.3.2 Conditional BEP Upper Bound Performance

The BEP results for the SIMO GLRT reception over the fixed EDS channel are evaluated by using the conditional BEP upper bound in (3.1) with exact PEP (3.2) and verified for tightness by Monte Carlo simulation. Illustrated in Figs. 4.2 and 4.3 are the characteristics of BEP versus the received bit DNR for QPSK (with $M = 4$) and 16-ary QAM (with $M = 16$) component modulations, respectively. In both figures, φ is fixed to one to ensure sufficiently accurate pilot-aided channel estimation and various values for D and I are tested to show the robustness of SIMO GLRT reception over fixed channel dispersion. As shown, BEP upper bound in (3.1) agrees with simulation when the BEP is below 10^{-2} for fixed dispersive channels. Moreover, the BEP performance improves when more antenna paths are adopted (i.e., a larger I is adopted) and when the channel is less fluctuated (i.e., D is smaller).

The BEP characteristic of the SIMO GLRT receiver depends strongly on the power al-

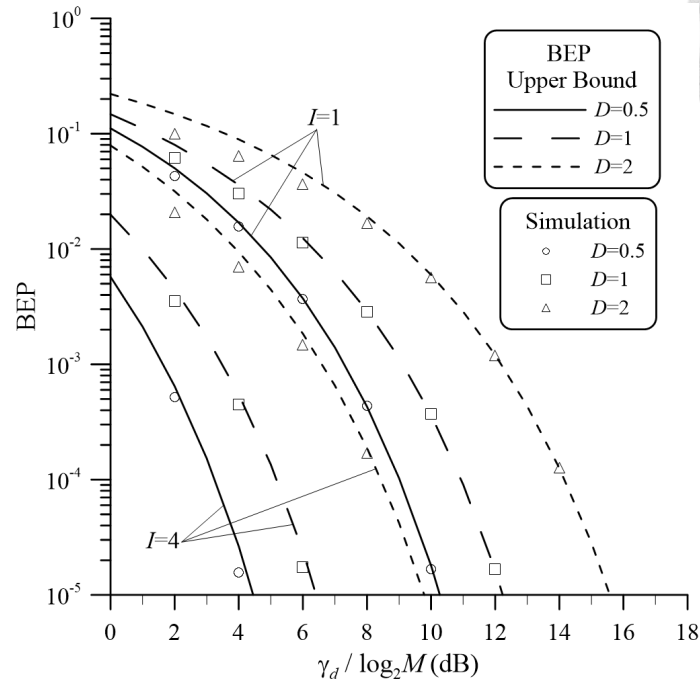


Figure 4.2: Bit error probability characteristics of the SIMO GLRT receiver for the pilot-aided OFDM with $N = 64$, $\alpha = 1/4$, $\phi = 4$, $\varphi = 1$, $\chi = 2$, QPSK component modulation, and various I antenna paths over the fixed block dispersive channel with $L = 3$ and various D factors.

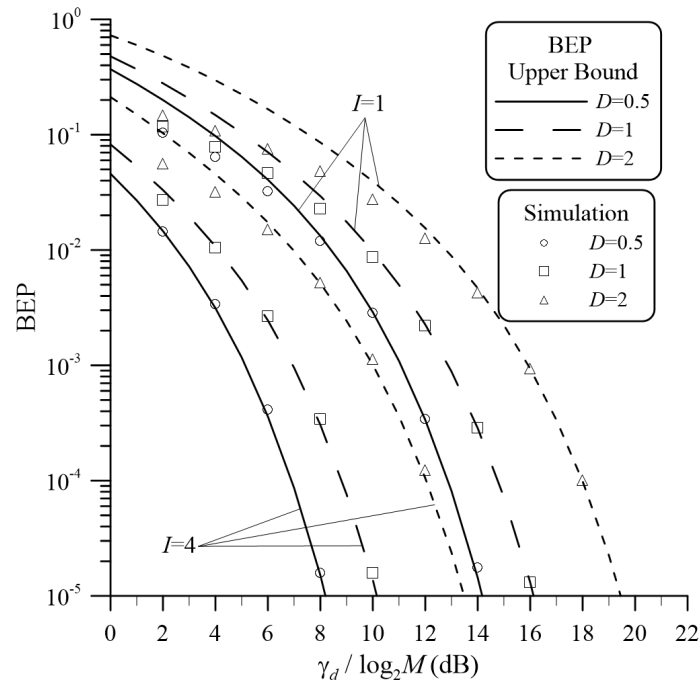


Figure 4.3: Bit error probability characteristics of the SIMO GLRT receivers for the pilot-aided OFDM with $N = 64$, $\alpha = 1/4$, $\phi = 4$, $\varphi = 1$, $\chi = 2$, 16-ary QAM component modulation, and various I antenna paths over the fixed block dispersive channel with $L = 3$ and various D factors.

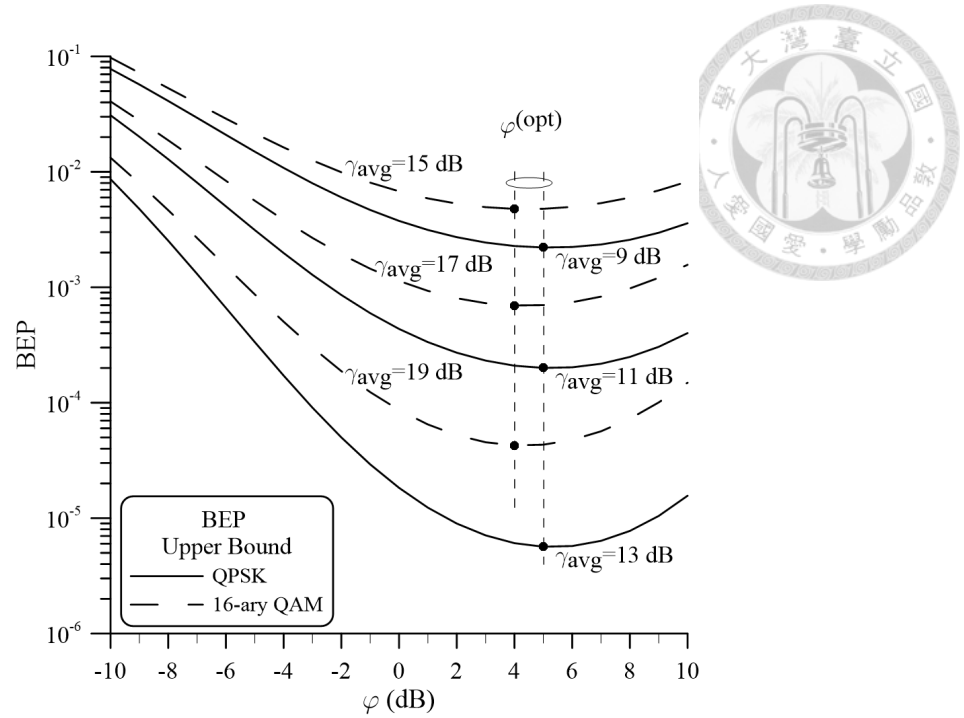


Figure 4.4: Bit error probability versus φ characteristics of the SIMO GLRT receivers for QPSK ($M = 4$) and 16-ary QAM ($M = 16$) pilot-aided OFDM with $N = 64$, $\alpha = 1/4$, $\phi = 4$, $\chi = 2$ and various γ_{avg} values over the fixed block dispersive channel with $I = 1$, $L = 3$ and $D = 0.5$. The minimum BEP upper bound versus the corresponding φ for each γ_{avg} with respective component modulation is denoted by a broken line connecting dots.

location to pilot symbols. When the larger pilot power is allocated, the better pilot-aided channel estimation is achieved and this entails the better BEP performance even for a fixed received bit DNR. Because the BEP performance improves with an increasing data power as well, there exists an optimum DPR $\varphi^{(\text{opt})}$ when the total power allocated to the entire OFDM block is fixed. This optimum $\varphi^{(\text{opt})}$ indicates the optimum power allocation to pilot symbols under a fixed block power, and it varies, however, with component modulation type, system and channel parameters.

The variation trend is illustrated in Figs. 4.8-4.13 where the BEP upper bound, computed by (3.1), are plotted versus DPR values when γ_{avg} is fixed to a certain value. In Fig. 4.4-4.9, the BEP upper bound versus DPR characteristic is illustrated for different γ_{avg} values and modulation types when the other system and channel parameters are fixed. It is shown that the optimum DPR $\varphi^{(\text{opt})}$ is relatively insensitive to γ_{avg} for the demonstrated BER range (approximately, $\varphi^{(\text{opt})} \in [3, 5]$) and close for different component modulation types (i.e., QPSK

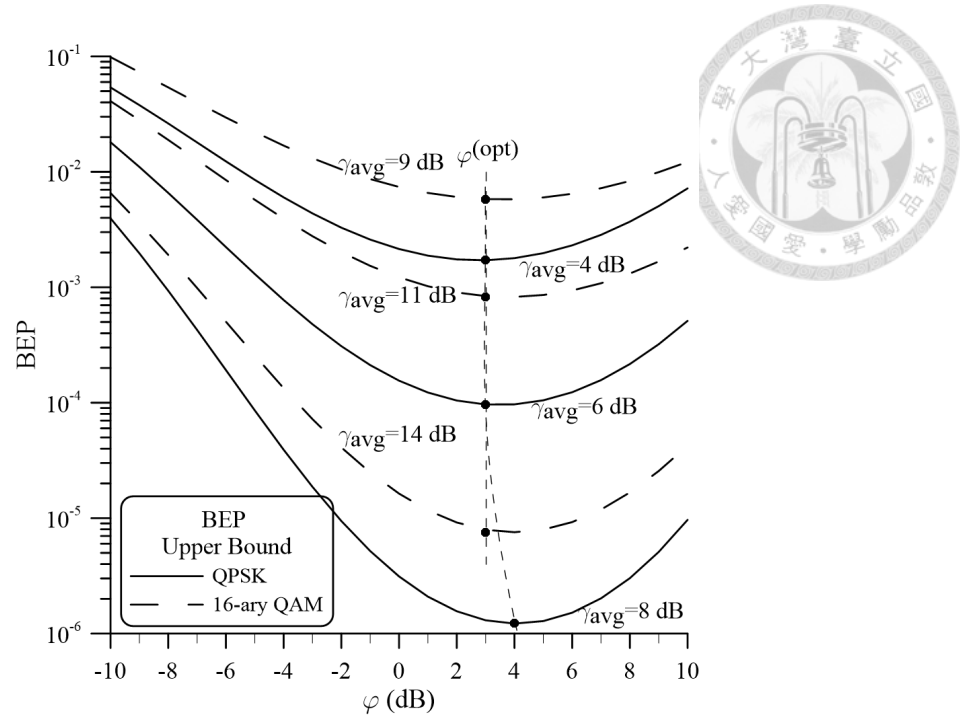


Figure 4.5: Bit error probability versus φ characteristics of the SIMO GLRT receivers for QPSK ($M = 4$) and 16-ary QAM ($M = 16$) pilot-aided OFDM with $N = 64$, $\alpha = 1/4$, $\phi = 4$, $\chi = 2$ and various γ_{avg} values over the fixed block dispersive channel with $I = 4$, $L = 3$ and $D = 0.5$. The minimum BEP upper bound versus the corresponding φ for each γ_{avg} with respective component modulation is denoted by a broken line connecting dots.

and 16-ary QAM). Although not demonstrated explicitly, the optimum $\varphi^{(\text{opt})}$ is relatively insensitive to the number of receive antennas I as well, when other system parameters and the channel type are fixed. However, the optimum $\varphi^{(\text{opt})}$ is relatively sensitive to the pilot sequence power allocated to an OFDM block, which affects directly the accuracy of embedded channel estimation in GLRT, and channel fluctuation as well. The latter trend is illustrated in Figs. 4.10-4.13 for QPSK and 16-ary QAM component modulations, respectively, where the BEP upperbound is plotted versus φ/N which indicates the ratio of data symbol power to pilot sequence power. As demonstrated, optimum $\varphi^{(\text{opt})}/N$ is relatively sensitive to channel fluctuation and sequence length, but still within a small variation.

Based on the numerically computed pairs of $\varphi^{(\text{opt})}$ and γ_{avg} obtained by searching over the BEP bound (3.1), $\varphi^{(\text{opt})}$ can be approximated as a polynomial function of γ_{avg} for a given set of system and channel parameters through the use of the curve fitting method [40].

For a specified set of system and channel parameters, the polynomial function obtained by

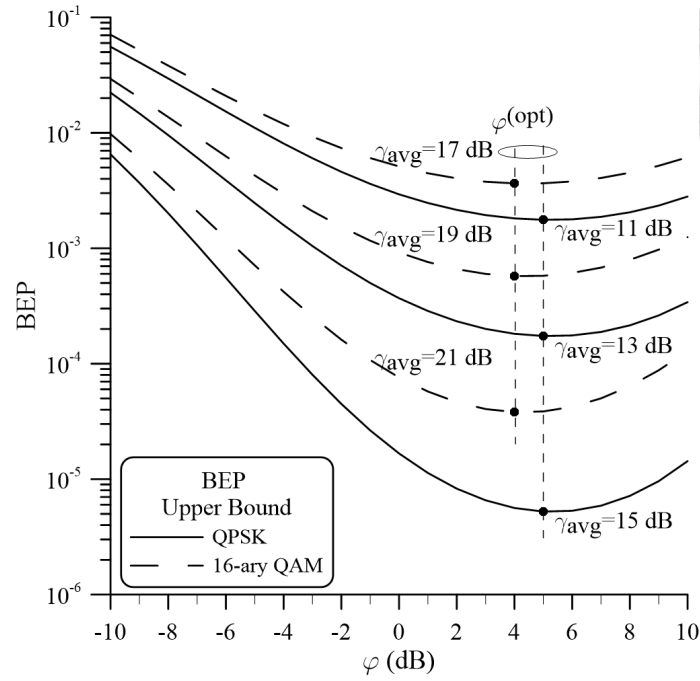


Figure 4.6: Bit error probability versus φ characteristics of the SIMO GLRT receivers for QPSK ($M = 4$) and 16-ary QAM ($M = 16$) pilot-aided OFDM with $N = 64$, $\alpha = 1/4$, $\phi = 4$, $\chi = 2$ and various γ_{avg} values over the fixed block dispersive channel with $I = 1$, $L = 3$ and $D = 1$. The minimum BEP upper bound versus the corresponding φ for each γ_{avg} with respective component modulation is denoted by a broken line connecting dots.

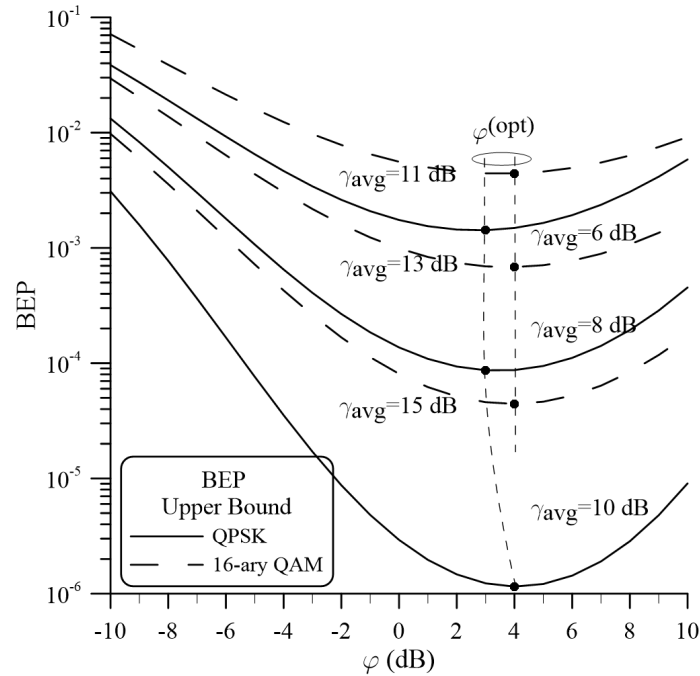


Figure 4.7: Bit error probability versus φ characteristics of the SIMO GLRT receivers for QPSK ($M = 4$) and 16-ary QAM ($M = 16$) pilot-aided OFDM with $N = 64$, $\alpha = 1/4$, $\phi = 4$, $\chi = 2$ and various γ_{avg} values over the fixed block dispersive channel with $I = 4$, $L = 3$ and $D = 1$. The minimum BEP upper bound versus the corresponding φ for each γ_{avg} with respective component modulation is denoted by a broken line connecting dots.

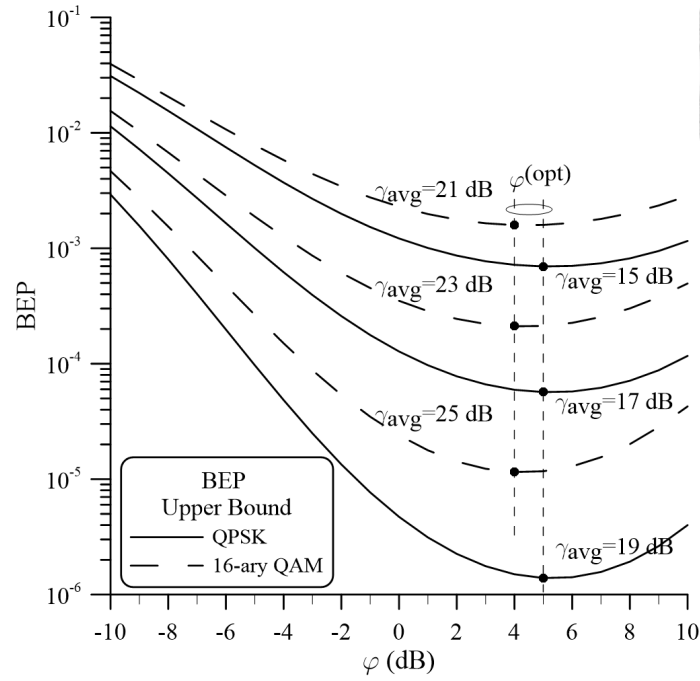


Figure 4.8: Bit error probability versus φ characteristics of the SIMO GLRT receivers for QPSK ($M = 4$) and 16-ary QAM ($M = 16$) pilot-aided OFDM with $N = 64$, $\alpha = 1/4$, $\phi = 4$, $\chi = 2$ and various γ_{avg} values over the fixed block dispersive channel with $I = 1$, $L = 3$ and $D = 2$. The minimum BEP upper bound versus the corresponding φ for each γ_{avg} with respective component modulation is denoted by a broken line connecting dots.

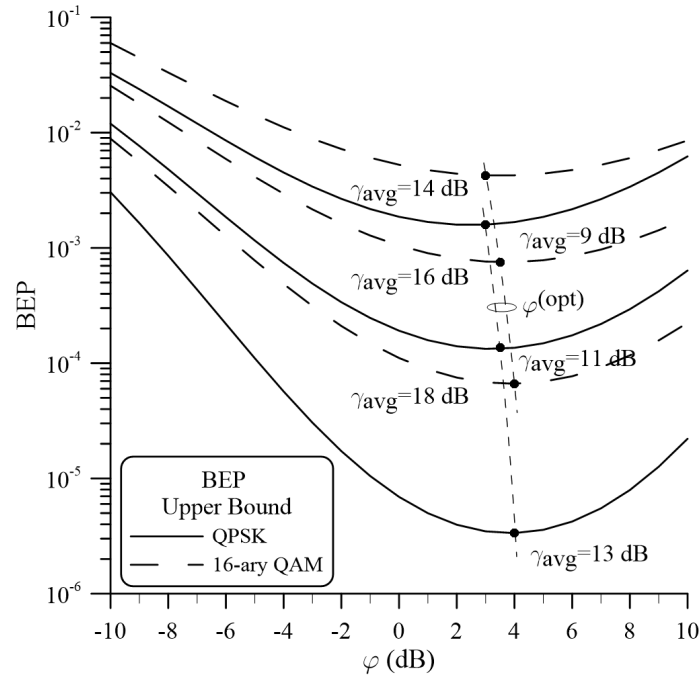


Figure 4.9: Bit error probability versus φ characteristics of the SIMO GLRT receivers for QPSK ($M = 4$) and 16-ary QAM ($M = 16$) pilot-aided OFDM with $N = 64$, $\alpha = 1/4$, $\phi = 4$, $\chi = 2$ and various γ_{avg} values over the fixed block dispersive channel with $I = 4$, $L = 3$ and $D = 2$. The minimum BEP upper bound versus the corresponding φ for each γ_{avg} with respective component modulation is denoted by a broken line connecting dots.

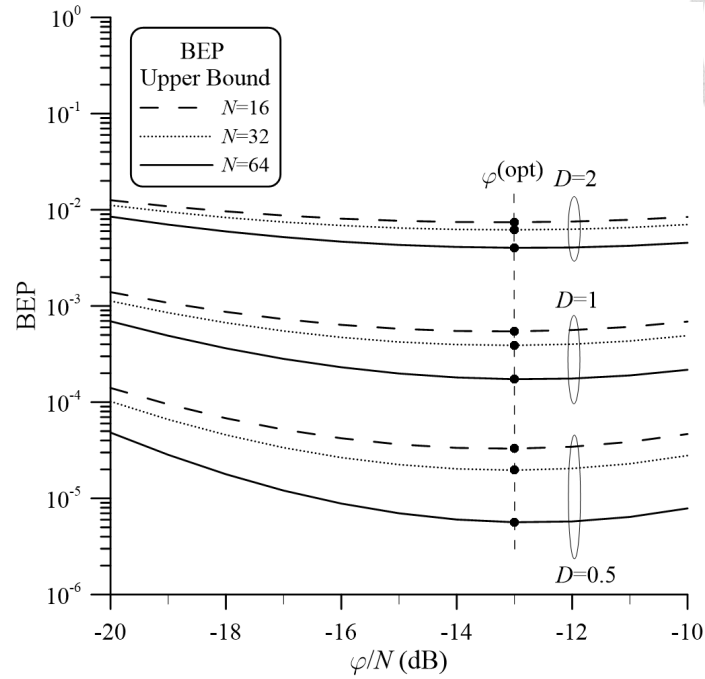


Figure 4.10: Bit error probability versus φ/N characteristics of the SIMO GLRT receivers for QPSK ($M = 4$) pilot-aided OFDM with $\alpha = 1/4$, $\phi = 4$, $\chi = 2$ and $\gamma_{\text{avg}} = 8$ dB over the fixed block dispersive channel with $I = 1$, $L = 3$ and various D . The minimum BEP upper bound versus the corresponding φ/N with respective D and N is denoted by the dot.

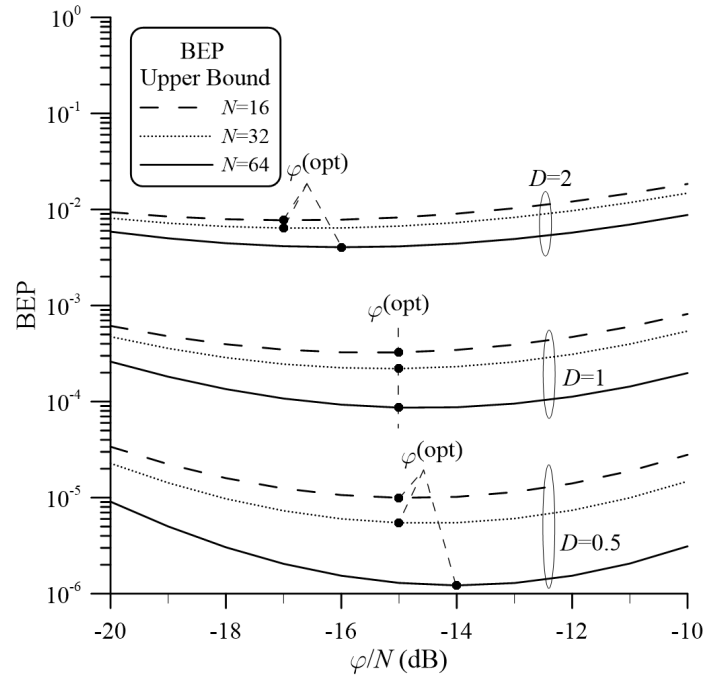


Figure 4.11: Bit error probability versus φ/N characteristics of the SIMO GLRT receivers for QPSK ($M = 4$) pilot-aided OFDM with $\alpha = 1/4$, $\phi = 4$, $\chi = 2$ and $\gamma_{\text{avg}} = 8$ dB over the fixed block dispersive channel with $I = 4$, $L = 3$ and various D . The minimum BEP upper bound versus the corresponding φ/N with respective D and N is denoted by the dot.

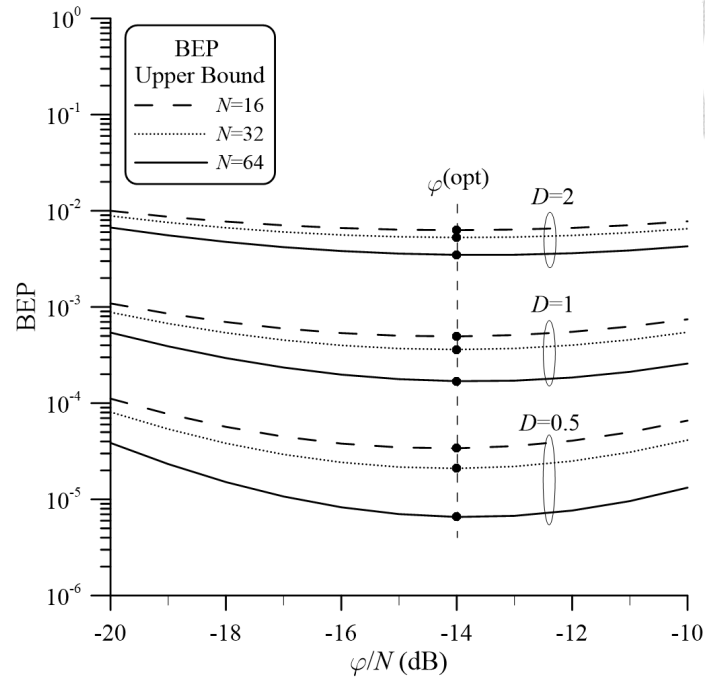


Figure 4.12: Bit error probability versus φ/N characteristics of the SIMO GLRT receivers for 16-ary QAM ($M = 16$) pilot-aided OFDM with $\alpha = 1/4$, $\phi = 4$, $\chi = 2$ and $\gamma_{\text{avg}} = 14$ dB over the fixed block dispersive channel with $I = 1$, $L = 3$ and various D . The minimum BEP upper bound versus the corresponding φ/N with respective D and N is denoted by the dot.

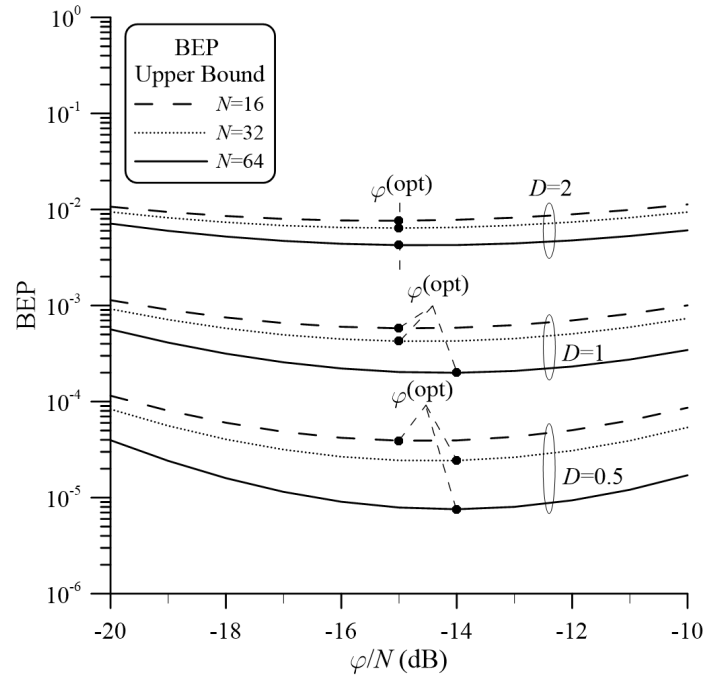


Figure 4.13: Bit error probability versus φ/N characteristics of the SIMO GLRT receivers for 16-ary QAM ($M = 16$) pilot-aided OFDM with $\alpha = 1/4$, $\phi = 4$, $\chi = 2$ and $\gamma_{\text{avg}} = 14$ dB over the fixed block dispersive channel with $I = 4$, $L = 3$ and various D . The minimum BEP upper bound versus the corresponding φ/N with respective D and N is denoted by the dot.



component modulation	I	curve-fitted polynomial function in dB
$M = 4$ (QPSK)	1	$\varphi^{(\text{opt})}(\gamma_{\text{avg}}) = 5 \text{ dB for } \gamma_{\text{avg}} \in [3, 13] \text{ dB}$
	2	$\varphi^{(\text{opt})}(\gamma_{\text{avg}}) = 0.001282\gamma_{\text{avg}}^5 - 0.0405\gamma_{\text{avg}}^4 + 0.4709\gamma_{\text{avg}}^3 - 2.451\gamma_{\text{avg}}^2 + 5.672\gamma_{\text{avg}} - 0.6667 \text{ dB for } \gamma_{\text{avg}} \in [1, 10] \text{ dB}$
	4	$\varphi^{(\text{opt})}(\gamma_{\text{avg}}) = 0.003348\gamma_{\text{avg}}^8 - 0.06295\gamma_{\text{avg}}^7 + 0.6406\gamma_{\text{avg}}^6 - 3.82\gamma_{\text{avg}}^5 + 13.48\gamma_{\text{avg}}^4 - 26.9\gamma_{\text{avg}}^3 + 26.88\gamma_{\text{avg}}^2 - 9.213\gamma_{\text{avg}} + 1 \text{ dB for } \gamma_{\text{avg}} \in [-1, 8] \text{ dB}$
$M = 16$ (16-ary QAM)	1	$\varphi^{(\text{opt})}(\gamma_{\text{avg}}) = -0.005236\gamma_{\text{avg}}^8 + 0.3137\gamma_{\text{avg}}^7 - 10.89\gamma_{\text{avg}}^6 + 241.5\gamma_{\text{avg}}^5 - 3544\gamma_{\text{avg}}^4 \text{ dB for } \gamma_{\text{avg}} \in [10, 20] \text{ dB}$
	2	$\varphi^{(\text{opt})}(\gamma_{\text{avg}}) = 4 \text{ dB for } \gamma_{\text{avg}} \in [7, 17] \text{ dB}$
	4	$\varphi^{(\text{opt})}(\gamma_{\text{avg}}) = -0.0002111\gamma_{\text{avg}}^6 + 0.01261\gamma_{\text{avg}}^5 - 0.336\gamma_{\text{avg}}^4 + 3.757\gamma_{\text{avg}}^3 - 25.1\gamma_{\text{avg}}^2 + 85.71\gamma_{\text{avg}} - 114.1 \text{ dB for } \gamma_{\text{avg}} \in [5, 14] \text{ dB}$

Table 4.1: Polynomial functions for $\varphi^{(\text{opt})}(\gamma_{\text{avg}})$ of the SIMO GLRT receivers for the pilot-aided OFDM with $N = 64$, $\alpha = 1/4$, $\phi = 4$, $\chi = 2$, various component modulations, and various I antenna paths over the fixed dispersive channel with $L = 3$ and $D = 0.5$.

component modulation	I	curve-fitted polynomial function in dB
$M = 4$ (QPSK)	1	$\varphi^{(\text{opt})}(\gamma_{\text{avg}}) = 5 \text{ dB for } \gamma_{\text{avg}} \in [5, 15] \text{ dB}$
	2	$\varphi^{(\text{opt})}(\gamma_{\text{avg}}) = -0.000196\gamma_{\text{avg}}^7 + 0.01122\gamma_{\text{avg}}^6 - 0.2712\gamma_{\text{avg}}^5 + 3.511\gamma_{\text{avg}}^4 - 26.19\gamma_{\text{avg}}^3 + 111.9\gamma_{\text{avg}}^2 - 252.2\gamma_{\text{avg}} + 233.3 \text{ dB for } \gamma_{\text{avg}} \in [3, 13] \text{ dB}$
	4	$\varphi^{(\text{opt})}(\gamma_{\text{avg}}) = 0.3909\gamma_{\text{avg}} - 0.2273 \text{ dB for } \gamma_{\text{avg}} \in [1, 10] \text{ dB}$
$M = 16$ (16-ary QAM)	1	$\varphi^{(\text{opt})}(\gamma_{\text{avg}}) = +0.000622\gamma_{\text{avg}}^7 - 0.03587\gamma_{\text{avg}}^6 + 1.167\gamma_{\text{avg}}^5 - 23.44\gamma_{\text{avg}}^4 + 297.1\gamma_{\text{avg}}^3 - 2321\gamma_{\text{avg}}^2 \text{ dB for } \gamma_{\text{avg}} \in [11, 22] \text{ dB}$
	2	$\varphi^{(\text{opt})}(\gamma_{\text{avg}}) = 4 \text{ dB for } \gamma_{\text{avg}} \in [8, 19] \text{ dB}$
	4	$\varphi^{(\text{opt})}(\gamma_{\text{avg}}) = -0.003704\gamma_{\text{avg}}^7 - 0.1068\gamma_{\text{avg}}^6 - 1.933\gamma_{\text{avg}}^5 + 22.69\gamma_{\text{avg}}^4 - 172.5\gamma_{\text{avg}}^3 + 817.9\gamma_{\text{avg}}^2 - 2189\gamma_{\text{avg}} + 2517 \text{ dB for } \gamma_{\text{avg}} \in [6, 16] \text{ dB}$

Table 4.2: Polynomial functions for $\varphi^{(\text{opt})}(\gamma_{\text{avg}})$ of the SIMO GLRT receivers for the pilot-aided OFDM with $N = 64$, $\alpha = 1/4$, $\phi = 4$, $\chi = 2$, various component modulations, and various I antenna paths over the fixed dispersive channel with $L = 3$ and $D = 1$.

component modulation	I	curve-fitted polynomial function in dB
$M = 4$ (QPSK)	1	$\varphi^{(\text{opt})}(\gamma_{\text{avg}}) = 5 \text{ dB for } \gamma_{\text{avg}} \in [6, 19] \text{ dB}$
	2	$\varphi^{(\text{opt})}(\gamma_{\text{avg}}) = 0.0001702\gamma_{\text{avg}}^6 - 0.0113\gamma_{\text{avg}}^5 + 0.3034\gamma_{\text{avg}}^4 - 4.208\gamma_{\text{avg}}^3 - 31.68\gamma_{\text{avg}}^2 - 112.2\gamma_{\text{avg}} + 190.9 \text{ dB for } \gamma_{\text{avg}} \in [5, 16] \text{ dB}$
	4	$\varphi^{(\text{opt})}(\gamma_{\text{avg}}) = -0.01506\gamma_{\text{avg}}^2 + 0.6617\gamma_{\text{avg}} - 2.099 \text{ dB for } \gamma_{\text{avg}} \in [4, 13] \text{ dB}$
$M = 16$ (16-ary QAM)	1	$\varphi^{(\text{opt})}(\gamma_{\text{avg}}) = 4 \text{ dB for } \gamma_{\text{avg}} \in [14, 26] \text{ dB}$
	2	$\varphi^{(\text{opt})}(\gamma_{\text{avg}}) = 4 \text{ dB for } \gamma_{\text{avg}} \in [11, 23] \text{ dB}$
	4	$\varphi^{(\text{opt})}(\gamma_{\text{avg}}) = -0.0006416\gamma_{\text{avg}}^6 + 0.03376\gamma_{\text{avg}}^5 - 0.9691\gamma_{\text{avg}}^4 + 16.37\gamma_{\text{avg}}^3 - 162.6\gamma_{\text{avg}}^2 + 878.5\gamma_{\text{avg}} - 1987 \text{ dB for } \gamma_{\text{avg}} \in [8, 20] \text{ dB}$

Table 4.3: Polynomial functions for $\varphi^{(\text{opt})}(\gamma_{\text{avg}})$ of the SIMO GLRT receivers for the pilot-aided OFDM with $N = 64$, $\alpha = 1/4$, $\phi = 4$, $\chi = 2$, various component modulations, and various I antenna paths over the fixed dispersive channel with $L = 3$ and $D = 2$.

curve fitting approximates the relation of $\varphi^{(\text{opt})}$ and γ_{avg} within a predetermined root-mean-square error (RMSE) of 0.3 dB by fitting several computed pair values over the range of γ_{avg} yielding the BEP from 10^{-1} to 10^{-6} . Some curve-fitted polynomial functions are illustrated in Table 4.1-4.3 for the system and channel parameters considered in Fig. 4.4-4.9. These polynomial functions are useful for the pilot power allocation in the considered GLRT-based OFDM SIMO system.

4.4 Average BEP Characteristics in Random Block Dispersive Channel

4.4.1 Random Block Dispersive Channel

The random dispersive channel can be described statistically as the particular SIMO block multipath Rician fading model in *Remark 4*, where I random SIMO channels exhibit identical power on all antenna paths for each channel path (i.e., $\sigma_{\text{direct}}^{(i)} = \sigma_{\text{direct}}$ and $\sigma_{\text{diffuse}}^{(i)}[l] = \sigma_{\text{diffuse}}[l]$ for all $l \in \mathcal{Z}_L$) and thus yield the MGF $\Phi_{\beta}(s)$ in (3.19). For illustration convenience, I normalize the sum of direct power and all diffuse powers to one, i.e., $E\{\|\mathbf{h}^{(i)}\|^2\} = \sigma_{\text{direct}}^2 + \sum_{l \in \mathcal{Z}_L} \sigma_{\text{diffuse}}^2[l] = 1$. Under this normalization, γ_d , γ_p , φ , and γ_{avg} represent the average

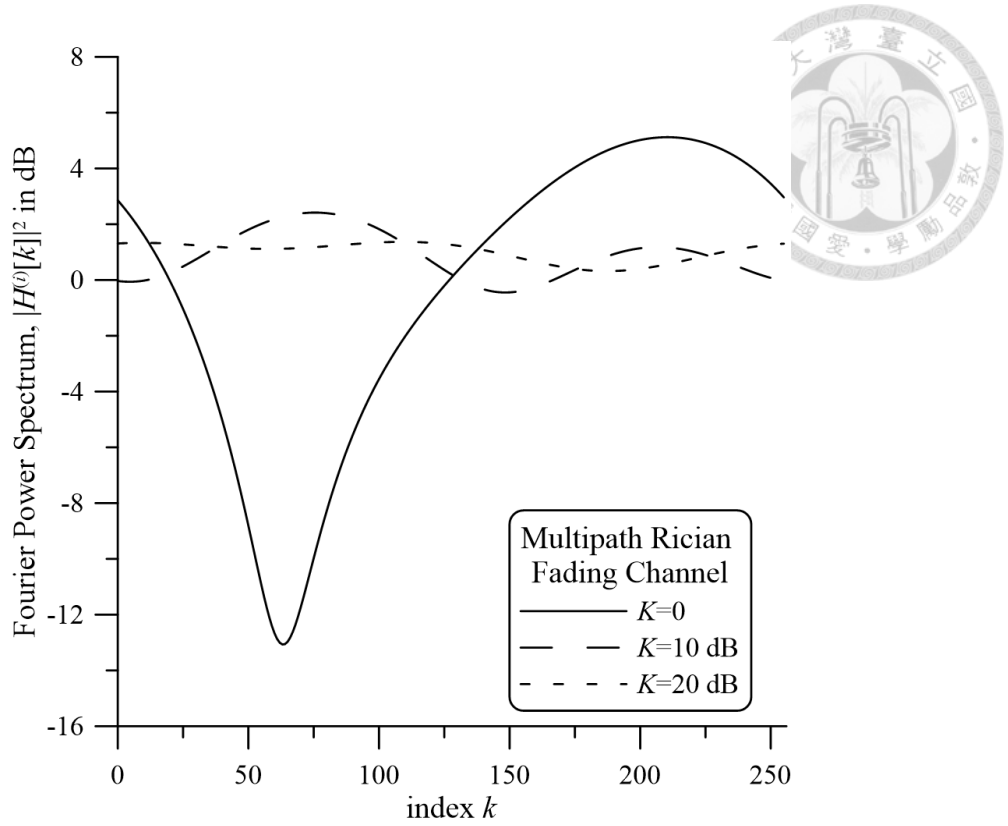


Figure 4.14: Fourier power spectrums of multipath Rician fading channel realizations with $K = 0, 10$ dB and 20 dB and $D = 2$ for the OFDM system with $i = 0, N = 64, \phi = 4$ and $L = 3$.

received symbol DNR, the average received symbol PNR, the received DPR, and the average received symbol SNR (i.e., $(1 - \frac{1}{\phi})\gamma_d + \frac{1}{\phi}\gamma_p$), respectively. Also, the multipath Rician fading channel can be further characterized by the factor K , which is defined as the ratio of direct power to diffuse power sum (i.e., $K = \sigma_{\text{direct}}^2 / \sum_{l \in \mathcal{Z}_L} \sigma_{\text{diffuse}}^2[l]$) and specifically makes $\sigma_{\text{direct}}^2 = \frac{K}{K+1}$ and $\sum_{l \in \mathcal{Z}_L} \sigma_{\text{diffuse}}^2[l] = \frac{1}{K+1}$ in (3.19). In the following results, I further fix $\sigma_{\text{diffuse}}^2[l] = C_h \exp\{-l/D\}$ for $l \in \mathcal{Z}_L$ with $C_h = \frac{1 - \exp\{-1/D\}}{(K+1)(1 - \exp\{-L/D\})}$ and $D = 2$.

The power spectrum densities for the one-time realization of different multipath Rician fading channels with various K values for antenna path i are shown in . 4.14, where $i = 0, N = 64, \phi = 4$ and $L = 3$ are fixed, to demonstrate the effect of various K on CFR. Note that the channel with $K = 0$ reduces to multipath Rayleigh channel and the channel with a very large K approaches to one-path AWGN channel. As shown, the fluctuation in CFR varies slower with subcarrier index when K is larger, and *vice versa*. However, since the fluctuation

varies randomly in different realizations, the long-term fluctuation turns to be statistically indistinguishable on all subcarriers when K is fixed. Nevertheless, the range of long-term fluctuation is wider as K is smaller. Notably, the proposed GLRT-based receiver can track the CFR fluctuation in one block and detect the data symbols appropriately with the aid of embedded channel estimation.(3.18) into (3.12)

4.4.2 Unconditional BEP Upper Bound Performance

Consider the special SIMO DAS scenario in *Remark 4* where there are Q distributed antenna ports located in different geographic locations and the q -th port consists of I_q antennas and experiences the q -th CIR vector group $\mathcal{H}^{(q)}$ for $q \in \mathcal{Z}_Q$, where all CIR vectors in each group are i.i.d. and all groups $\mathcal{H}^{(q)}$'s are i.n.i.d. with the zeroth paths being Rician distributed and all the other paths Rayleigh distributed. In this case, the MGF $\Phi_\beta(s)$ required to evaluate the average BEP upper bound in (3.12) is given by (3.19). Particularly, the considered $\Phi_\beta(s)$ can be further characterized by the factors K_q for all $q \in \mathcal{Z}_Q$, in which K_q is defined as the ratio of direct power to diffuse power sum (i.e., $K_q = \sigma_{q,\text{direct}}^2 / \sum_{l \in \mathcal{Z}_L} \sigma_{q,\text{diffuse}}^2[l]$) at the q -th port and specifically makes $\sigma_{q,\text{direct}}^2 = \frac{K_q}{K_q+1}$ and $\sum_{l \in \mathcal{Z}_L} \sigma_{q,\text{diffuse}}^2[l] = \frac{1}{K_q+1}$ in (3.19). For illustration convenience, we further fix $\sigma_{q,\text{diffuse}}^2[l] = C_{h,q} \exp\{-l/D\}$ for $l \in \mathcal{Z}_L$ and $q \in \mathcal{Z}_Q$ with $C_{h,q} = \frac{1-\exp\{-1/D\}}{(K_q+1)(1-\exp\{-L/D\})}$ and $D = 2$, and normalize the sum of direct power and all diffuse powers to one, i.e., $\sigma_{q,\text{direct}}^2 + \sum_{l \in \mathcal{Z}_L} \sigma_{q,\text{diffuse}}^2[l] = 1$ for $q \in \mathcal{Z}_Q$. With this channel setup in (3.19), average BEP upper bound is computed by (3.12) and shown in 4.15-4.19.

Two different random SIMO DAS cases are demonstrated. In Case I, two antennas are distributed with two ports (i.e., $Q = 2$), each having one antenna (i.e., $I_0 = I_1 = 1$), and the channel factors K_q 's are fixed to $K_0 = 0$ and $K_1 = 20$ dB. In Case II, four antennas are distributed with two ports (i.e., $Q = 2$), each having two antennas (i.e., $I_0 = I_1 = 2$), and channel factors K_q 's are fixed to $K_0 = K_1 = 0$ and $K_2 = K_3 = 20$ dB. Compared with

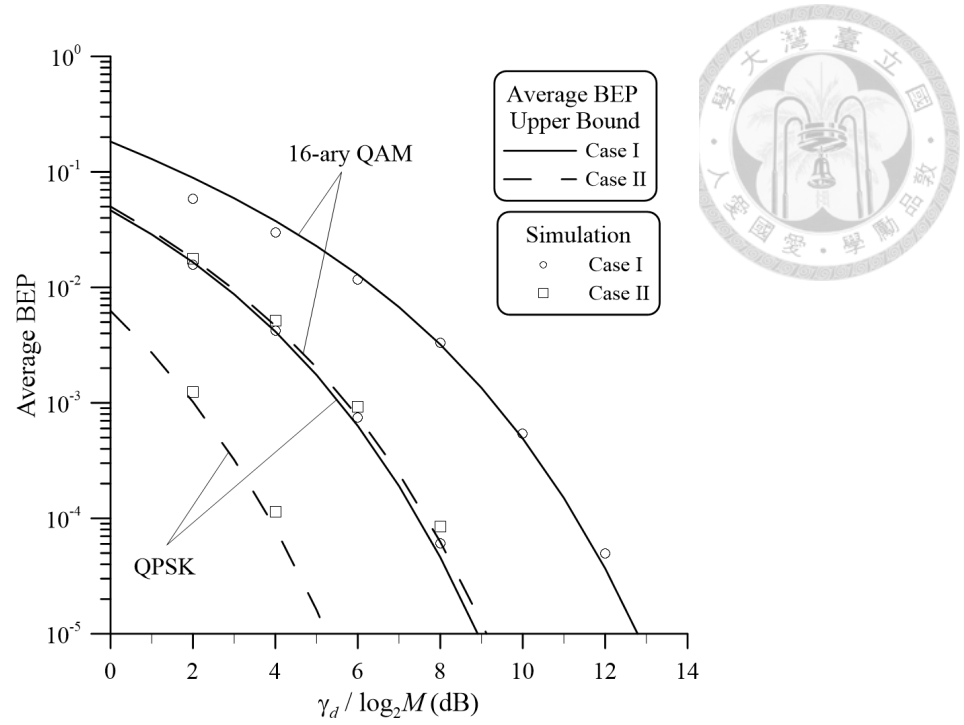


Figure 4.15: Average bit error probability characteristics of the SIMO GLRT receivers for the pilot-aided OFDM with $N = 64$, $\alpha = 1/4$, $\phi = 4$, $\varphi = 1$, and $\chi = 2$ over the i.n.i.d. random block dispersive channel with $L = 3$ and $D = 2$ under two considered cases. Both QPSK and 16-ary QAM component modulations are considered.

Case I, Case II demonstrates the SIMO system employing a larger antenna diversity order I .

Fig. 4.15 shows the average BEP versus received bit DNR characteristics of the SIMO GLRT receiver for QPSK and 16-ary QAM component modulations under two considered cases. Average BEP upper bound in (3.12) is verified for tightness by Monte Carlo simulation. The DPR is fixed to $\varphi = 1$. As shown, average BEP upper bound in (3.12) agrees very well with simulation. The system employing a larger I is shown to perform better.

When the average received symbol SNR γ_{avg} is fixed, the SIMO GLRT receiver performs sensitively to the DPR $\varphi = \gamma_d / \gamma_p$ in that more power allocated to pilot symbols results in better embedded channel estimation but simultaneously reduces power allocated to data symbols and thus degrades the data decision performance. Like fixed channel dispersion, there exists an optimum DPR $\varphi^{(\text{opt})}$ over random channel dispersion for each SIMO-OFDM system setup and preassigned channel parameters, under a fixed γ_{avg} . In Figs. 4.16 and 4.17, the average BEP upper bound versus DPR characteristic is demonstrated for different γ_{avg} values and

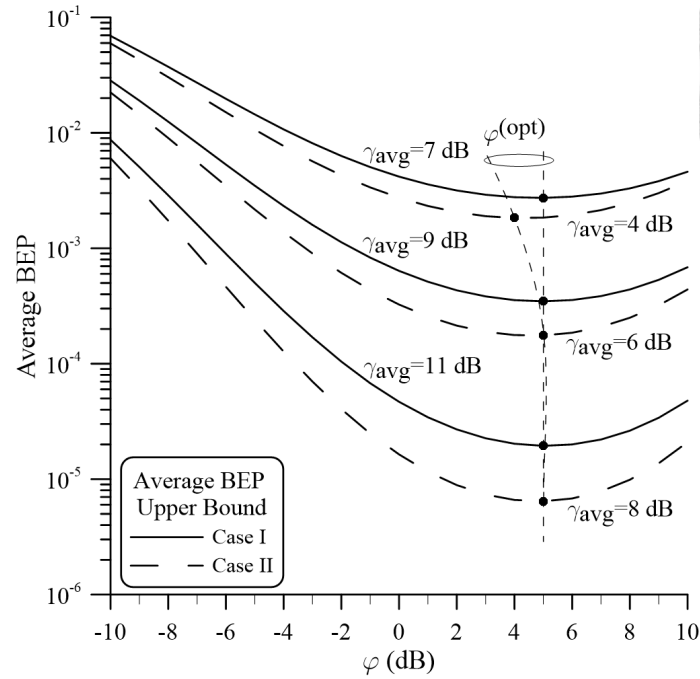


Figure 4.16: Average bit error probability versus φ characteristics of the SIMO GLRT receiver for pilot-aided OFDM with $N = 64$, $\alpha = 1/4$, $\phi = 4$, $\chi = 2$, QPSK component modulation, and various γ_{avg} values over the i.n.i.d. random block dispersive channel with $L = 3$ and $D = 2$ under two considered cases. The point φ yielding the minimum average BEP upper bound value for each SNR is denoted by a broken line connecting dots.

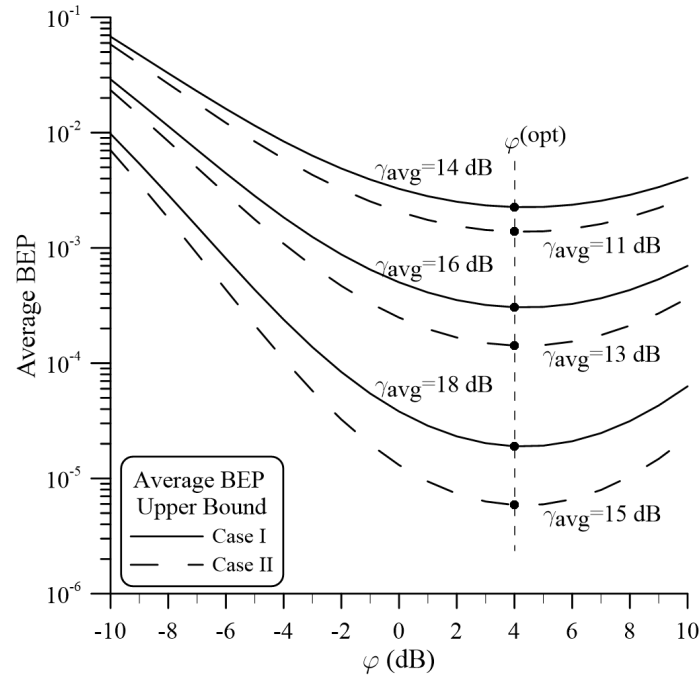


Figure 4.17: Average bit error probability versus φ characteristics of the SIMO GLRT receiver for pilot-aided OFDM with $N = 64$, $\alpha = 1/4$, $\phi = 4$, $\chi = 2$, 16-ary QAM component modulation, and various γ_{avg} values over the i.n.i.d. random block dispersive channel with $L = 3$ and $D = 2$ under two considered cases. The point φ yielding the minimum average BEP upper bound value for each SNR is denoted by a broken line connecting dots.

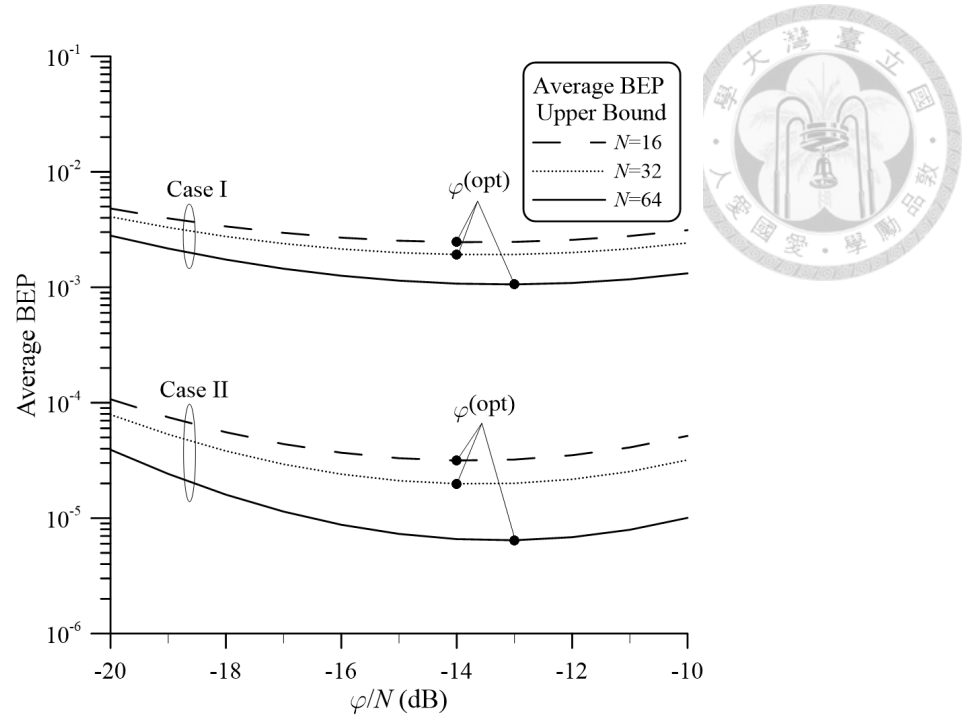


Figure 4.18: Average bit error probability versus φ/N characteristics of the SIMO GLRT receivers for pilot-aided OFDM with $\alpha = 1/4$, $\phi = 4$, $\chi = 2$, QPSK component modulation, and $\gamma_{\text{avg}} = 8$ dB over the i.n.i.d. random block dispersive channel with $L = 3$ and $D = 2$ under two considered cases. The point φ/N yielding the minimum average BEP upper bound value for respective case and N is denoted by dot.

modulation types (i.e., QPSK and 16-ary QAM) when the other system and channel parameters are fixed. As shown, the optimum $\varphi^{(\text{opt})}$ is relatively insensitive to γ_{avg} and component modulation type for a wide range of average BEP values. Table 4.4 shows the curve-fitted polynomial functions of $\varphi^{(\text{opt})}$ versus γ_{avg} for the system and channel parameters considered in Figs. 4.16 and 4.17, where each polynomial function has its own applicable range of γ_{avg} to yield the BEP from 10^{-1} to 10^{-6} . The influence of the pilot sequence power on SIMO GLRT performance is also demonstrated in Figs. 4.18 and 4.19 where the average BEP upper bound versus φ/N characteristics are shown for QPSK and 16-ary QAM component modulations, respectively. As shown, the optimum $\varphi^{(\text{opt})}/N$ (i.e., the optimum ratio of data symbol power to pilot sequence power) is more sensitive to channel fluctuation than sequence length, but still within a small variation.

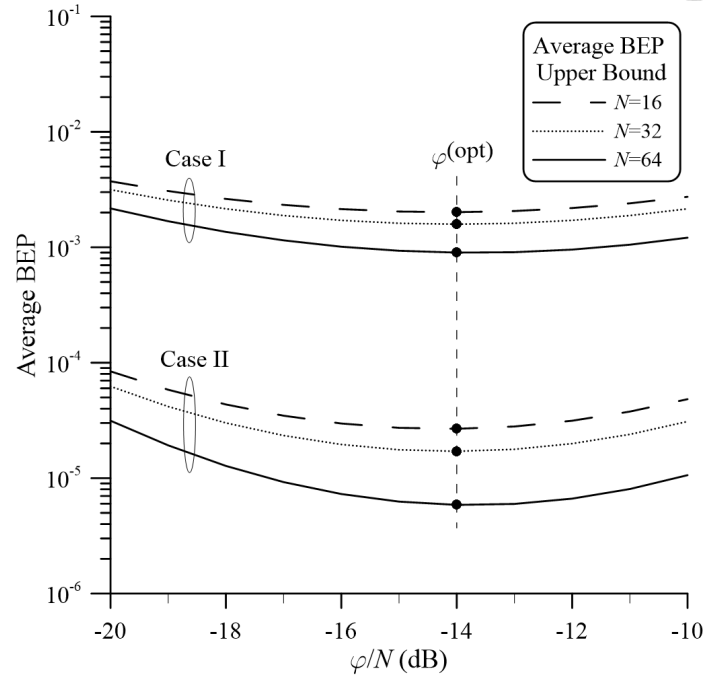


Figure 4.19: Average bit error probability versus φ/N characteristics of the SIMO GLRT receivers for pilot-aided OFDM with $\alpha = 1/4$, $\phi = 4$, $\chi = 2$, 16-ary QAM component modulation, and $\gamma_{\text{avg}} = 14$ dB over the i.n.i.d. random block dispersive channel with $L = 3$ and $D = 2$ under two considered cases. The point φ/N yielding the minimum average BEP upper bound value for respective case and N is denoted by dot.

component modulation	case	curve-fitted polynomial function in dB
QPSK	I	$\varphi^{(\text{opt})}(\gamma_{\text{avg}}) = 0.0002696\gamma_{\text{avg}}^6 - 0.0118\gamma_{\text{avg}}^5 + 0.2048\gamma_{\text{avg}}^4 - 1.78\gamma_{\text{avg}}^3 + 8.019\gamma_{\text{avg}}^2 - 17.12\gamma_{\text{avg}} + 17.47$ dB for $\gamma_{\text{avg}} \in [2, 12]$ dB
	II	$\varphi^{(\text{opt})}(\gamma_{\text{avg}}) = 0.0006987\gamma_{\text{avg}}^6 - 0.009\gamma_{\text{avg}}^5 + 0.04772\gamma_{\text{avg}}^4 - 0.049\gamma_{\text{avg}}^3 - 0.2684\gamma_{\text{avg}}^2 + 0.6053\gamma_{\text{avg}} + 3.8$ dB for $\gamma_{\text{avg}} \in [-2, 10]$ dB
16-ary QAM	I	$\varphi^{(\text{opt})}(\gamma_{\text{avg}}) = 4$ dB for $\gamma_{\text{avg}} \in [9, 19]$ dB
	II	$\varphi^{(\text{opt})}(\gamma_{\text{avg}}) = 4$ dB for $\gamma_{\text{avg}} \in [5, 15]$ dB

Table 4.4: Polynomial functions for $\varphi^{(\text{opt})}(\gamma_{\text{avg}})$ of the SIMO GLRT receivers for the pilot-aided OFDM with $N = 64$, $\alpha = 1/4$, $\phi = 4$, $\chi = 2$, various component modulations over i.n.i.d. random block dispersive channel with $L = 3$ and $D = 2$ under two considered cases.

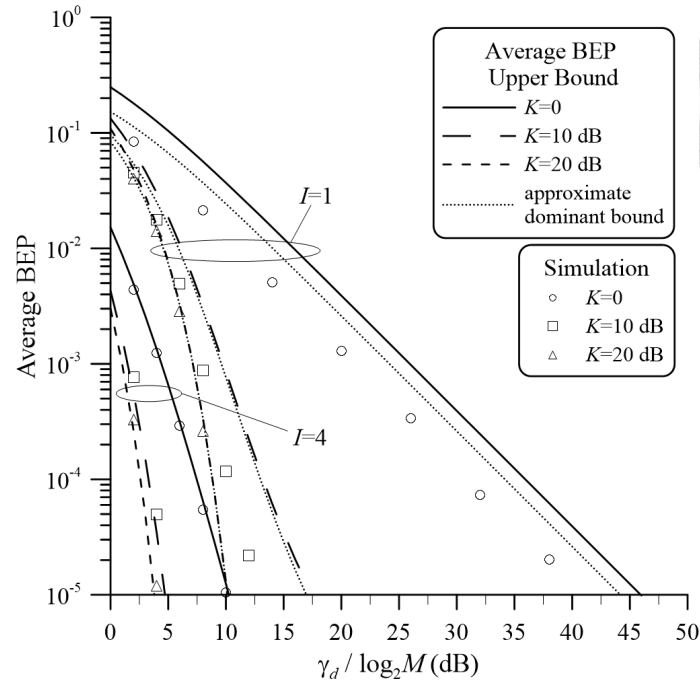


Figure 4.20: Average bit error probability characteristics of the SIMO GLRT receivers for the pilot-aided OFDM with $N = 64$, $\alpha = 1/4$, $\phi = 4$, $\varphi = 1$, $\chi = 2$, QPSK component modulation, and various I antenna paths over the random dispersive channel with $L = 3$, $D = 2$, and various K factors.

Figs. 4.20 and 4.21 show the average BEP versus received bit DNR characteristics of the SIMO GLRT receiver for QPSK and 16-ary QAM component modulations, respectively, over the i.i.d random block dispersive channel. Average BEP upper bound in (3.12) is verified for tightness by Monte Carlo simulation. The DPR is fixed to $\varphi = 1$. The results for various K factors and I antenna elements are demonstrated to show the robustness of SIMO GLRT reception over random channel dispersion. As shown, average BEP upper bound in (3.12) agrees very well with simulation when the BEP is below 10^{-2} for a larger $I \geq 4$ (i.e., more antennas) or a larger $K \geq 20$ dB (i.e., less channel fluctuation). Moreover, the average BEP performance improves when more antennas are adopted (i.e., a larger I is adopted) and when the channel is less fluctuated (i.e., K is larger).

When the channel exhibits a weak direct path or the receive diversity is not sufficiently high, the average BEP upper bound in (3.12) is not tight due to the shortage of the union bound over the union probability of highly dependent error events. To enhance the tightness,

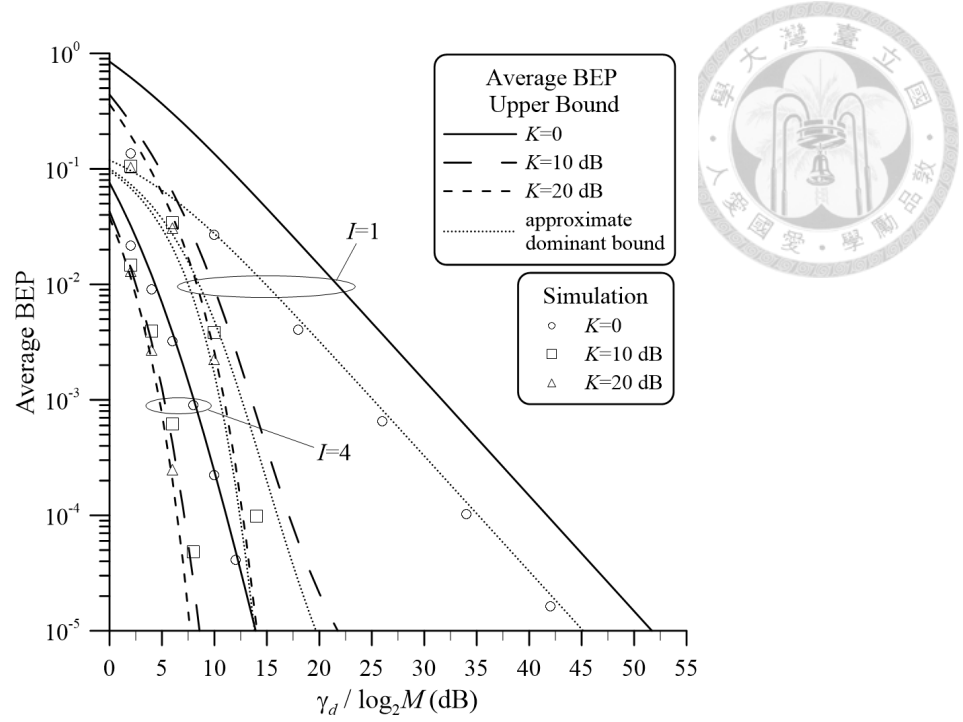


Figure 4.21: Average bit error probability characteristics of the SIMO GLRT receivers for the pilot-aided OFDM with $N = 64$, $\alpha = 1/4$, $\phi = 4$, $\varphi = 1$, $\chi = 2$, 16-ary QAM component modulation, and various I antenna paths over the random dispersive channel with $L = 3$, $D = 2$, and various K factors.

an approximate dominant bound can be used instead and approximate the true average BEP by summing up only a few dominant terms in the union sum, as in (3.12) with the innermost sum extending only over $d_k[n] \in \mathcal{S}$ and $\hat{d}_k[n] \in \mathcal{S}_{\text{near}}(d_k[n])$ where $\mathcal{S}_{\text{near}}(d_k[n])$ denotes the set of data symbols that are not $d_k[n]$ but are the nearest neighbors to $d_k[n]$.¹ As shown in Figs. 4.20 - 4.21, the approximate dominant bound agrees better with simulation than the exact upper bound when I or K is small.

When the average received symbol SNR γ_{avg} is fixed, the SIMO GLRT receiver performs sensitively to the DPR $\varphi = \gamma_d/\gamma_p$ in that more power allocation to pilot symbols results in better embedded channel estimation but simultaneously reduces power allocation to data symbols and thus degrades the data decision performance. Like fixed channel dispersion, there exists an optimum DPR $\varphi^{(\text{opt})}$ over random channel dispersion for each SIMO GLRT system

¹For examples, $\mathcal{S}_{\text{near}}(d_k[n])$ is the set $\{\frac{1}{\sqrt{2}} + j\frac{-1}{\sqrt{2}}, \frac{-1}{\sqrt{2}} + j\frac{1}{\sqrt{2}}\}$ for the QPSK symbol $d = \frac{1}{\sqrt{2}} + j\frac{1}{\sqrt{2}}$, the set $\{\frac{1}{\sqrt{10}} + j\frac{-1}{\sqrt{10}}, \frac{1}{\sqrt{10}} + j\frac{3}{\sqrt{10}}, \frac{3}{\sqrt{10}} + j\frac{1}{\sqrt{10}}, \frac{-1}{\sqrt{10}} + j\frac{1}{\sqrt{10}}\}$ for the 16-ary QAM symbol $d = \frac{1}{\sqrt{10}} + j\frac{1}{\sqrt{10}}$, and the set $\{\frac{1}{\sqrt{10}} + j\frac{1}{\sqrt{10}}, \frac{3}{\sqrt{10}} + j\frac{3}{\sqrt{10}}, \frac{3}{\sqrt{10}} + j\frac{-1}{\sqrt{10}}\}$ for the 16-ary QAM symbol $d = \frac{3}{\sqrt{10}} + j\frac{1}{\sqrt{10}}$.

setup and channel parameters, under a fixed γ_{avg} . In Fig. 4.22 - 4.27, the average BEP upper bound versus DPR characteristic is demonstrated for different γ_{avg} values and modulation types when the other system and channel parameters are fixed. Since $\varphi^{(\text{opt})}$ is found to be relatively insensitive to the number of received antennas I , I illustrate the results with $I = 4$ only. As shown in Fig. 4.22 - 4.27, the optimum $\varphi^{(\text{opt})}$ is relatively insensitive to γ_{avg} and component modulation type (i.e., QPSK and 16-ary QAM) and remains to be one, the DPR value adopted in Figs. 4.20 - 4.21, for a wide range of average BEP values. Table 4.5-4.7 shows the curve-fitted polynomial functions of $\varphi^{(\text{opt})}$ versus γ_{avg} for the system and channel parameters considered in Fig. 4.22-4.27, where each polynomial has its own applicable range of γ_{avg} to yield the BEP from 10^{-1} to 10^{-6} . The influence of the pilot sequence power on SIMO GLRT performance is also demonstrated in Figs. 4.28-4.31 where the average BEP upper bound versus φ/N characteristics are shown for QPSK and 16-ary QAM component modulations, respectively. Here, φ/N indicates the ratio of data symbol power to pilot sequence power. As shown, the sensitivity of optimum $\varphi^{(\text{opt})}/N$ is more sensitive to channel fluctuation than sequence length, but still within a small variation.

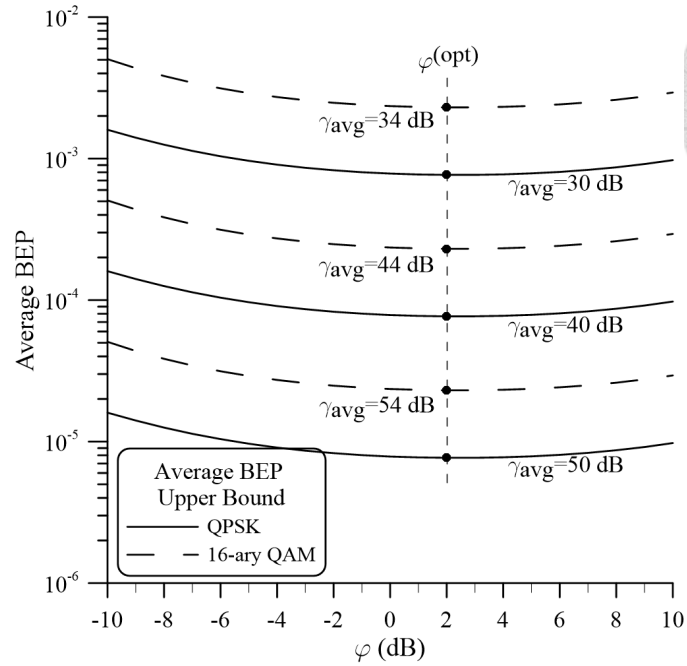


Figure 4.22: Average bit error probability versus φ characteristics of the SIMO GLRT receiver for pilot-aided OFDM with $N = 64$, $\alpha = 1/4$, $\phi = 4$, $\chi = 2$ and various γ_{avg} values over the random dispersive channel with $I = 1$, $L = 3$, $D = 2$, and $K = 0$. Both QPSK ($M = 4$) and 16-ary QAM ($M = 16$) component modulations are demonstrated. For each component modulation, the point φ yielding the minimum average BEP upper bound value for each SNR is denoted by a broken line connecting dots.

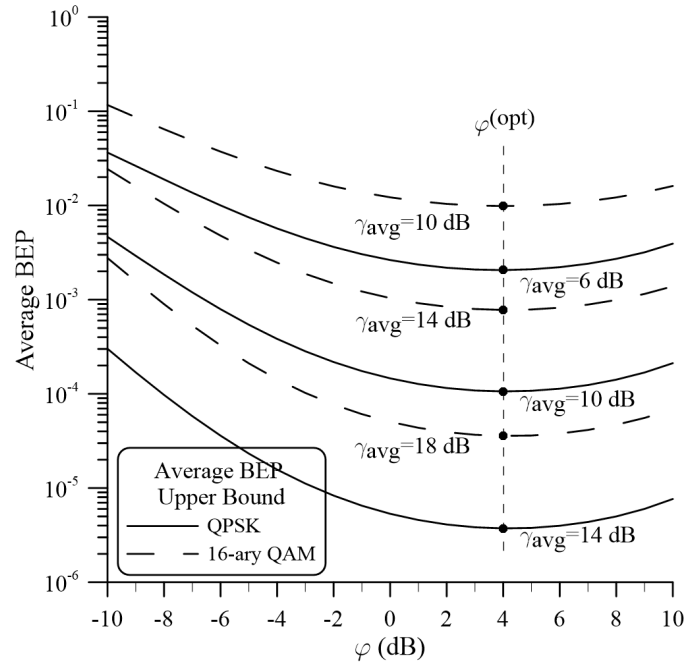


Figure 4.23: Average bit error probability versus φ characteristics of the SIMO GLRT receiver for pilot-aided OFDM with $N = 64$, $\alpha = 1/4$, $\phi = 4$, $\chi = 2$ and various γ_{avg} values over the random dispersive channel with $I = 4$, $L = 3$, $D = 2$, and $K = 0$. Both QPSK ($M = 4$) and 16-ary QAM ($M = 16$) component modulations are demonstrated. For each component modulation, the point φ yielding the minimum average BEP upper bound value for each SNR is denoted by a broken line connecting dots.

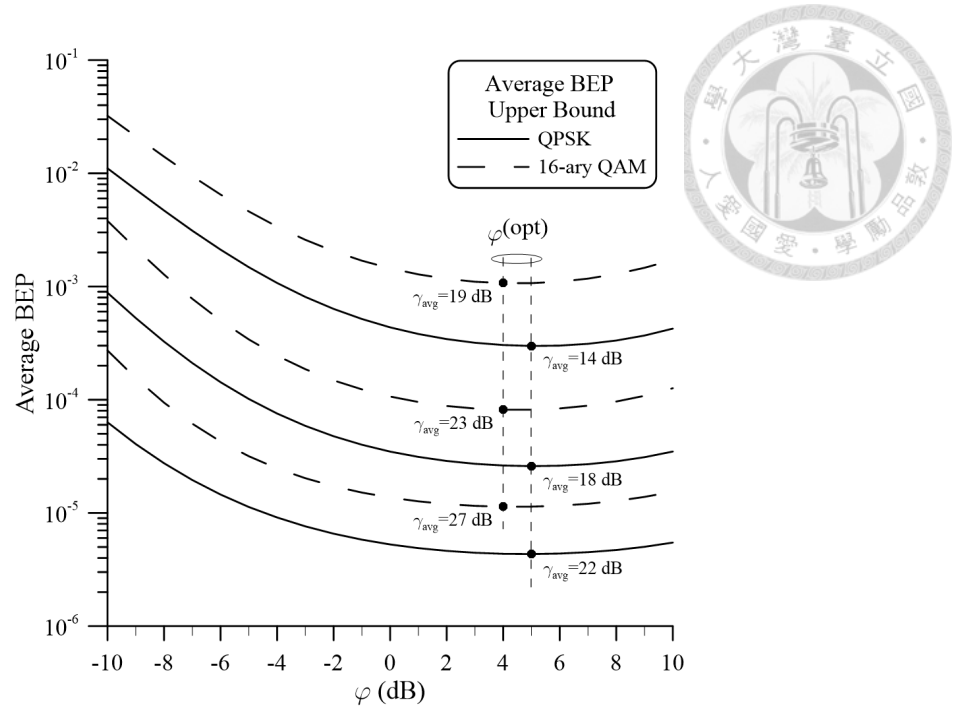


Figure 4.24: Average bit error probability versus φ characteristics of the SIMO GLRT receiver for pilot-aided OFDM with $N = 64$, $\alpha = 1/4$, $\phi = 4$, $\chi = 2$ and various γ_{avg} values over the random dispersive channel with $I = 1$, $L = 3$, $D = 2$, and $K = 10$ dB. Both QPSK ($M = 4$) and 16-ary QAM ($M = 16$) component modulations are demonstrated. For each component modulation, the point φ yielding the minimum average BEP upper bound value for each SNR is denoted by a broken line connecting dots.

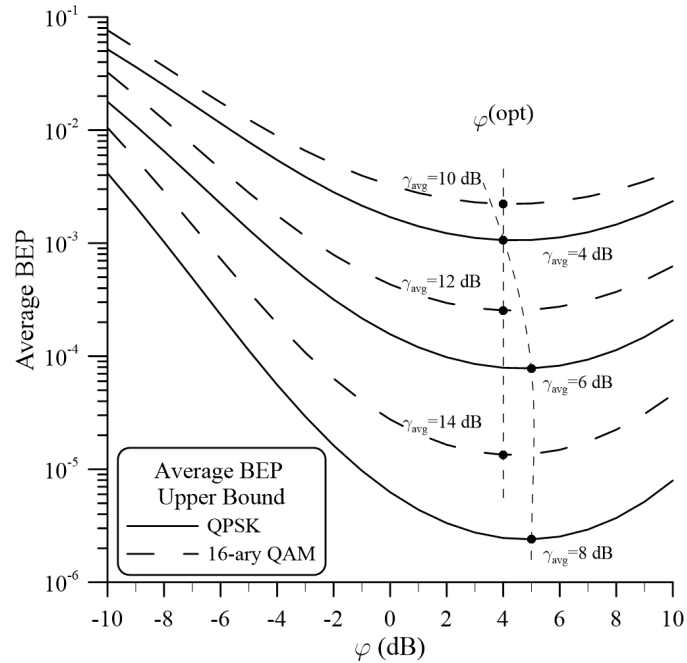


Figure 4.25: Average bit error probability versus φ characteristics of the SIMO GLRT receiver for pilot-aided OFDM with $N = 64$, $\alpha = 1/4$, $\phi = 4$, $\chi = 2$ and various γ_{avg} values over the random dispersive channel with $I = 4$, $L = 3$, $D = 2$, and $K = 10$ dB. Both QPSK ($M = 4$) and 16-ary QAM ($M = 16$) component modulations are demonstrated. For each component modulation, the point φ yielding the minimum average BEP upper bound value for each SNR is denoted by a broken line connecting dots.

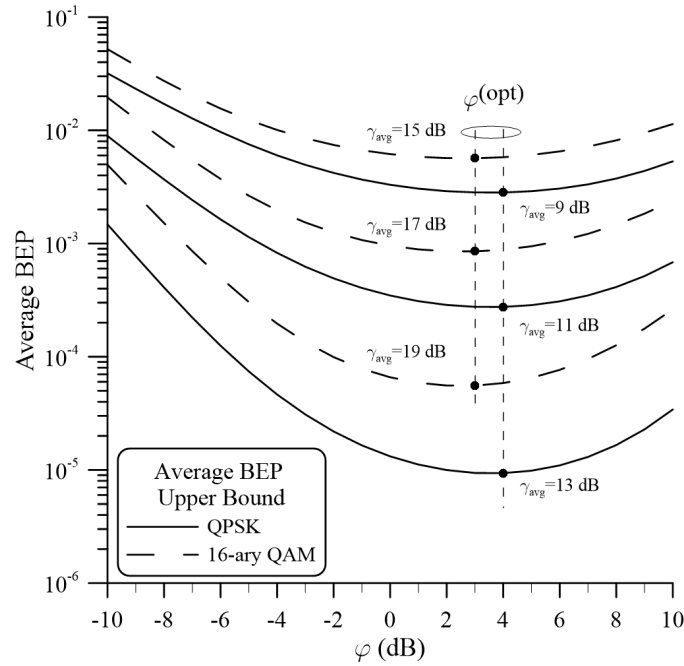


Figure 4.26: Average bit error probability versus φ characteristics of the SIMO GLRT receiver for pilot-aided OFDM with $N = 64$, $\alpha = 1/4$, $\phi = 4$, $\chi = 2$ and various γ_{avg} values over the random dispersive channel with $I = 1$, $L = 3$, $D = 2$, and $K = 20$ dB. Both QPSK ($M = 4$) and 16-ary QAM ($M = 16$) component modulations are demonstrated. For each component modulation, the point φ yielding the minimum average BEP upper bound value for each SNR is denoted by a broken line connecting dots.

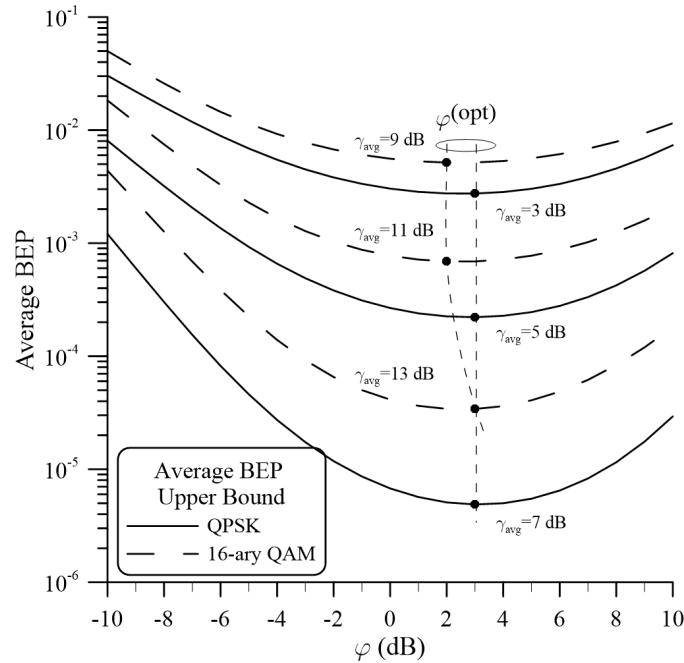


Figure 4.27: Average bit error probability versus φ characteristics of the SIMO GLRT receiver for pilot-aided OFDM with $N = 64$, $\alpha = 1/4$, $\phi = 4$, $\chi = 2$ and various γ_{avg} values over the random dispersive channel with $I = 4$, $L = 3$, $D = 2$, and $K = 10$ dB. Both QPSK ($M = 4$) and 16-ary QAM ($M = 16$) component modulations are demonstrated. For each component modulation, the point φ yielding the minimum average BEP upper bound value for each SNR is denoted by a broken line connecting dots.

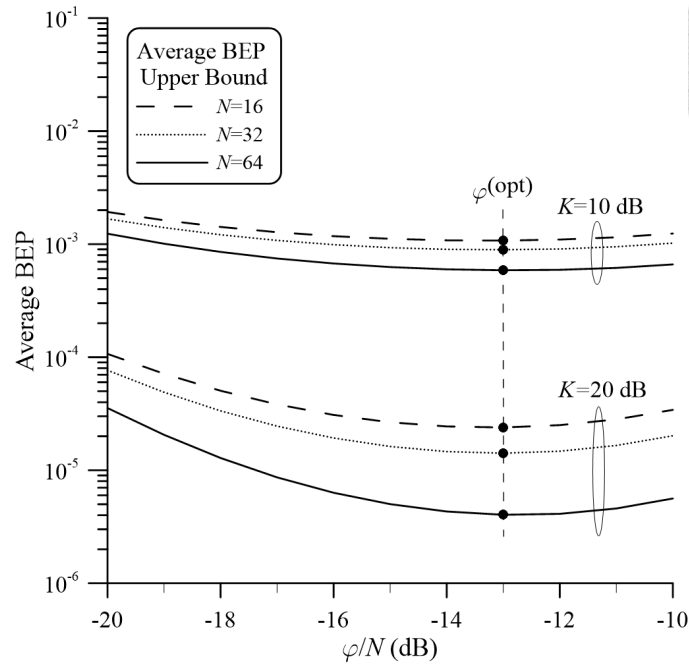


Figure 4.28: Average bit error probability versus φ/N characteristics of the SIMO GLRT receivers for pilot-aided OFDM with $\alpha = 1/4$, $\phi = 4$, $\chi = 2$, QPSK ($M = 4$) component modulation, and $\gamma_{\text{avg}} = 7$ dB over the random dispersive channel with $I = 1$, $L = 3$, $D = 2$, and various K factors. The point φ/N yielding the minimum average BEP upper bound value for respective K and N is denoted by dot.

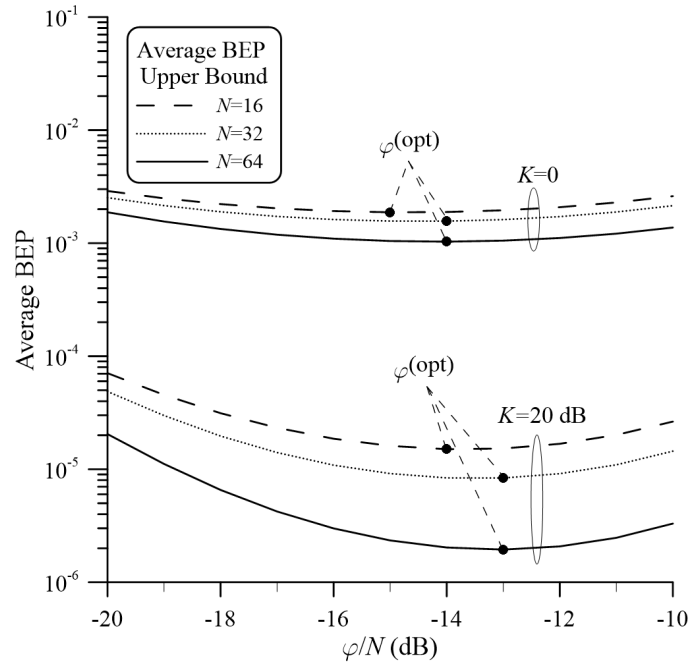


Figure 4.29: Average bit error probability versus φ/N characteristics of the SIMO GLRT receivers for pilot-aided OFDM with $\alpha = 1/4$, $\phi = 4$, $\chi = 2$, QPSK ($M = 4$) component modulation, and $\gamma_{\text{avg}} = 7$ dB over the random dispersive channel with $I = 4$, $L = 3$, $D = 2$, and various K factors. The point φ/N yielding the minimum average BEP upper bound value for respective K and N is denoted by dot.

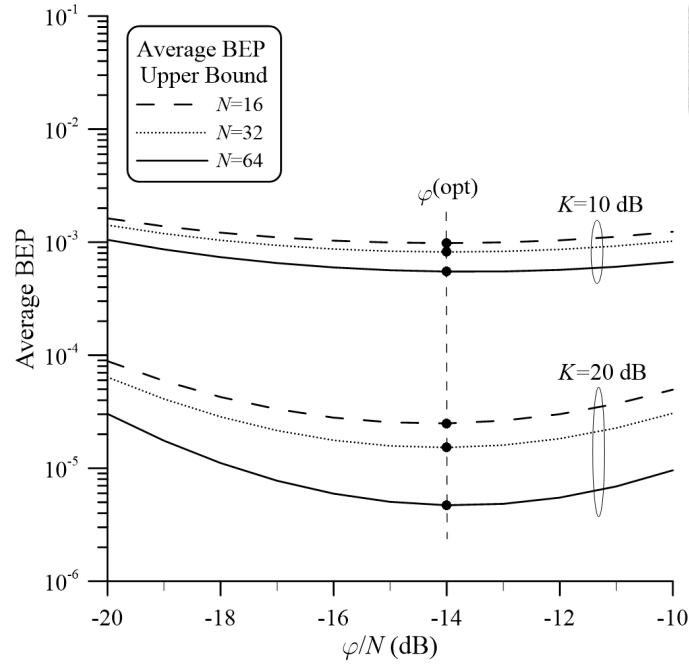


Figure 4.30: Average bit error probability versus φ/N characteristics of the SIMO GLRT receivers for pilot-aided OFDM with $\alpha = 1/4$, $\phi = 4$, $\chi = 2$, 16-ary QAM ($M = 16$) component modulation, and $\gamma_{\text{avg}} = 14$ dB over the random dispersive channel with $I = 1$, $L = 3$, $D = 2$, and various K factors. The point φ/N yielding the minimum average BEP upper bound value for respective K and N is denoted by dot.

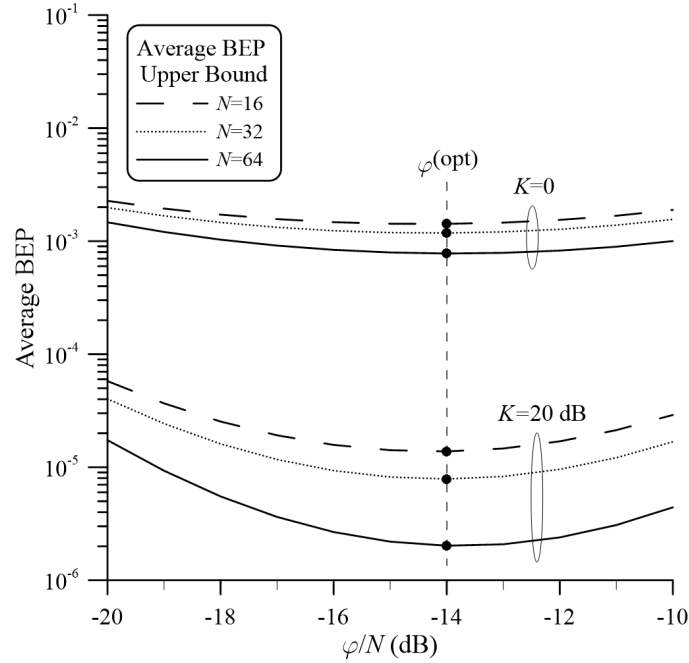


Figure 4.31: Average bit error probability versus φ/N characteristics of the SIMO GLRT receivers for pilot-aided OFDM with $\alpha = 1/4$, $\phi = 4$, $\chi = 2$, 16-ary QAM ($M = 16$) component modulation, and $\gamma_{\text{avg}} = 14$ dB over the random dispersive channel with $I = 4$, $L = 3$, $D = 2$, and various K factors. The point φ/N yielding the minimum average BEP upper bound value for respective K and N is denoted by dot.

component modulation	I	curve-fitted polynomial function in dB
$M = 4$ (QPSK)	1	$\varphi^{(\text{opt})}(\gamma_{\text{avg}}) = 4 \text{ dB for } \gamma_{\text{avg}} \in [10, 55] \text{ dB}$
	2	$\varphi^{(\text{opt})}(\gamma_{\text{avg}}) = 4 \text{ dB for } \gamma_{\text{avg}} \in [4, 30] \text{ dB}$
	4	$\varphi^{(\text{opt})}(\gamma_{\text{avg}}) = -0.0001413\gamma_{\text{avg}}^6 + 0.002935\gamma_{\text{avg}}^5 - 0.3691\gamma_{\text{avg}}^4$ $+0.2864\gamma_{\text{avg}}^3 - 1.329\gamma_{\text{avg}}^2 - 3.086\gamma_{\text{avg}} + 3 \text{ dB for } \gamma_{\text{avg}} \in [0, 18] \text{ dB}$
$M = 16$ (16-ary QAM)	1	$\varphi^{(\text{opt})}(\gamma_{\text{avg}}) = 4 \text{ dB for } \gamma_{\text{avg}} \in [5, 66] \text{ dB}$
	2	$\varphi^{(\text{opt})}(\gamma_{\text{avg}}) = 4 \text{ dB for } \gamma_{\text{avg}} \in [10, 36] \text{ dB}$
	4	$\varphi^{(\text{opt})}(\gamma_{\text{avg}}) = 4 \text{ dB for } \gamma_{\text{avg}} \in [7, 23] \text{ dB}$

Table 4.5: Polynomial functions for $\varphi^{(\text{opt})}(\gamma_{\text{avg}})$ of the SIMO GLRT receivers for the pilot-aided OFDM with $N = 64$, $\alpha = 1/4$, $\phi = 4$, $\chi = 2$, various component modulations, and various I antenna paths over random dispersive channel with $L = 3$, $D = 2$ and $K = 0$.

component modulation	I	curve-fitted polynomial function in dB
$M = 4$ (QPSK)	1	$\varphi^{(\text{opt})}(\gamma_{\text{avg}}) = 5 \text{ dB for } \gamma_{\text{avg}} \in [4, 26] \text{ dB}$
	2	$\varphi^{(\text{opt})}(\gamma_{\text{avg}}) = -0.0001037\gamma_{\text{avg}}^5 + 0.003447\gamma_{\text{avg}}^4 - 0.03502\gamma_{\text{avg}}^3$ $+0.1007\gamma_{\text{avg}}^2 + 0.3315\gamma_{\text{avg}} + 3.5 \text{ dB for } \gamma_{\text{avg}} \in [1, 13] \text{ dB}$
	4	$\varphi^{(\text{opt})}(\gamma_{\text{avg}}) = 0.000641\gamma_{\text{avg}}^5 - 0.1515\gamma_{\text{avg}}^4 + 0.1157\gamma_{\text{avg}}^3$ $-0.2914\gamma_{\text{avg}}^2 + 0.1902\gamma_{\text{avg}} + 4.007 \text{ dB for } \gamma_{\text{avg}} \in [-4, 9] \text{ dB}$
$M = 16$ (16-ary QAM)	1	$\varphi^{(\text{opt})}(\gamma_{\text{avg}}) = 0.0007896\gamma_{\text{avg}}^8 - 0.06672\gamma_{\text{avg}}^7 + 3.273\gamma_{\text{avg}}^6$ $-102.7\gamma_{\text{avg}}^5 + 2137\gamma_{\text{avg}}^4 \text{ dB for } \gamma_{\text{avg}} \in [15, 27] \text{ dB}$
	2	$\varphi^{(\text{opt})}(\gamma_{\text{avg}}) = 4 \text{ dB for } \gamma_{\text{avg}} \in [8, 20] \text{ dB}$
	4	$\varphi^{(\text{opt})}(\gamma_{\text{avg}}) = 4 \text{ dB for } \gamma_{\text{avg}} \in [7, 17] \text{ dB}$

Table 4.6: Polynomial functions for $\varphi^{(\text{opt})}(\gamma_{\text{avg}})$ of the SIMO GLRT receivers for the pilot-aided OFDM with $N = 64$, $\alpha = 1/4$, $\phi = 4$, $\chi = 2$, various component modulations, and various I antenna paths over random dispersive channel with $L = 3$, $D = 2$ and $K = 10$ dB.

component modulation	I	curve-fitted polynomial function in dB
$M = 4$ (QPSK)	1	$\varphi^{(\text{opt})}(\gamma_{\text{avg}}) = 5 \text{ dB for } \gamma_{\text{avg}} \in [3, 16] \text{ dB}$
	2	$\varphi^{(\text{opt})}(\gamma_{\text{avg}}) = -0.000105\gamma_{\text{avg}}^7 + 0.039646\gamma_{\text{avg}}^6 - 0.05919\gamma_{\text{avg}}^5$ $+0.4494\gamma_{\text{avg}}^4 - 1.791\gamma_{\text{avg}}^3 - 3.416\gamma_{\text{avg}}^2 - 1.977\gamma_{\text{avg}} + 3.994 \text{ dB}$ for $\gamma_{\text{avg}} \in [0, 10] \text{ dB}$
	4	$\varphi^{(\text{opt})}(\gamma_{\text{avg}}) = 0.000531\gamma_{\text{avg}}^6 - 0.006853\gamma_{\text{avg}}^5 + 0.0146\gamma_{\text{avg}}^4$ $+0.08221\gamma_{\text{avg}}^3 - 0.2342\gamma_{\text{avg}}^2 - 0.03549\gamma_{\text{avg}} + 4.139 \text{ dB}$ for $\gamma_{\text{avg}} \in [-3, 7] \text{ dB}$
$M = 16$ (16-ary QAM)	1	$\varphi^{(\text{opt})}(\gamma_{\text{avg}}) = 0.0001362\gamma_{\text{avg}}^6 - 0.01211\gamma_{\text{avg}}^5 + 0.4413\gamma_{\text{avg}}^4$ $-8.424\gamma_{\text{avg}}^3 + 88.69\gamma_{\text{avg}}^2 - 488.1\gamma_{\text{avg}} - 1102 \text{ dB for } \gamma_{\text{avg}} \in [10, 21] \text{ dB}$
	2	$\varphi^{(\text{opt})}(\gamma_{\text{avg}}) = 4 \text{ dB for } \gamma_{\text{avg}} \in [5, 17] \text{ dB}$
	4	$\varphi^{(\text{opt})}(\gamma_{\text{avg}}) = 4 \text{ dB for } \gamma_{\text{avg}} \in [4, 14] \text{ dB}$

Table 4.7: Polynomial functions for $\varphi^{(\text{opt})}(\gamma_{\text{avg}})$ of the SIMO GLRT receivers for the pilot-aided OFDM with $N = 64$, $\alpha = 1/4$, $\phi = 4$, $\chi = 2$, various component modulations, and various I antenna paths over random dispersive channel with $L = 3$, $D = 2$ and $K = 20$ dB.



Chapter 5

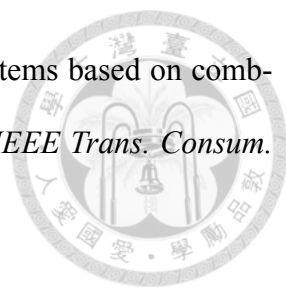
Conclusion

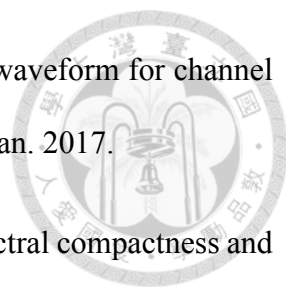
In this paper, general bit-error-probability upper bounds are derived for the pilot-aided GLRT-based SIMO-OFDM demodulation system employing an arbitrary two-dimensional component modulation over both deterministic and random block dispersive channels. For random block dispersive channel, the derived upper bound is applicable to any independent but not necessarily identical distributed channel paths over various antenna elements as long as the marginal statistic of the channel frequency response magnitudes is available. These upper bounds are verified by simulation to be tight when the block dispersive channel is less fluctuated or when the SIMO diversity is sufficiently high. Error performance characteristics are also illustrated for both QPSK and 16-ary QAM component modulations. It is shown that the derived upper bounds are useful to characterize the GLRT-based SIMO-OFDM system performance with respect to data-to-noise power ratio, data-to-pilot power ratio, channel condition, and antenna diversity.





Bibliography

- [1] L. J. Cimini, Jr., "Analysis and simulation of a digital mobile channel using orthogonal frequency division multiplexing," *IEEE Trans. Commun.*, vol. COM-33, no.7, pp. 665-75, July 1985.
- [2] R. V. Nee and R. Prasad, *OFDM for Wireless Multimedia Communications*. Artech House, 2000.
- [3] A. R. S. Bahai and B. R. Saltzberg, *Multi-Carrier Digital Communications: Theory and Applications of OFDM*. Kluwer Academic/Plenum Publishers, 1999.
- [4] B. Muquet, M. de courville, and P. Duhamel, "Subspace-based blind and semi-blind channel estimation for OFDM systems," *IEEE Trans. Signal Process.*, vol. 50, no. 7, pp. 1699-1712, Jul. 2002.
- [5] S. Zhou and G. B. Giannakis, "Subspace-based blind and semi-blind channel estimation for OFDM systems," *IEEE Trans Commun.*, vol. 49, no. 8, pp. 1402-1414, Aug. 2001.
- [6] M.-X. Chang and Y. T. Su, "Model-based channel estimation for OFDM signals in Rayleigh fading," *IEEE Trans. Commun.*, vol. 50, no. 4, pp. 540-544, Apr. 2002.
- [7] K. Hung and D. W. Lin, "Pilot-based LMMSE channel estimation for OFDM systems with power-delay profile approximation," *IEEE Trans. Veh. Technol.*, vol. 59, no. 1, pp. 150-159, Jan. 2010.

- 
- [8] M.-H. Hsieh and C.-H. Wei, "Channel estimation for OFDM systems based on comb-type pilot arrangement in frequency selective fading channels," *IEEE Trans. Consum. Electron.*, vol. 44, no. 1, pp. 217-225, Feb. 1998.
- [9] J. W. Choi and Y. H. Lee, "Design of 2-D channel estimation filters for OFDM systems," *Proc. IEEE Intl. Conf. on Commun.*, vol. 4, pp. 2568—2572, May 2005.
- [10] K. J. Kim, H. G. Hwang, K. J. Choi, and K. S. Kim, "Low-complexity DFT-based channel estimation with leakage nulling for OFDM systems," *IEEE Commun. Lett.*, vol. 18, no. 3, pp. 415-418, Mar. 2014.
- [11] F. Gu, Y. Fan, L. Wang, X. Tan, and J. Wei, "A universal channel estimation algorithm based on DFT smoothing filtering," *IEEE Access*, vol. 7, pp. 129883-129891, 2019.
- [12] J. Seo, S. Jang, J. Yang, W. Jeon and D. K. Kim, "Analysis of pilot-aided channel estimation with optimal leakage suppression for OFDM systems," *IEEE Commun. Lett.*, vol. 14, no. 9, pp. 809-811, Sep. 2010.
- [13] M. Morelli and U. Mengali, "A comparison of pilot-aided channel estimation methods for OFDM systems," *IEEE Trans. Sig. Process.*, vol. 49, no. 12, pp. 3065-3073, Dec. 2001
- [14] J.-W. Choi and Y.-H. Lee, "Optimum pilot pattern for channel estimation in OFDM systems," *IEEE Trans. Wireless Commun.*, vol. 4, no. 5, pp. 2083-2088, Sep. 2005.
- [15] S. Tong, B. M. Sadler, and M. Dong, "Optimal training and redundant precoding for block transmissions with application to wireless OFDM," *IEEE Trans. Commun.*, vol. 50, no. 12, pp. 2113-2123, Dec. 2002.
- [16] R. Negi and J. Cioffi, "Pilot tone selection for channel estimation in a mobile OFDM system," *IEEE Trans. Consumer Electron.*, vol. 44, no. 3, pp. 1122-1128, Aug. 1998.

- 
- [17] W.-C. Chen and C.-D. Chung, "Spectrally efficient OFDM pilot waveform for channel estimation," *IEEE Trans. Commun.*, vol. 65, no. 1, pp. 387-402, Jan. 2017.
- [18] C.-D. Chung and W.-C. Chen, "Preamble sequence design for spectral compactness and initial synchronization in OFDM," *IEEE Trans. Veh. Technol.*, vol. 67, no. 2, pp. 1428-1443, Feb. 2018.
- [19] C.-D. Chung, W.-C. Chen, and C.-K. Yang, "Constant-amplitude sequences for spectrally compact OFDM training waveforms," *IEEE Trans. Veh. Technol.*, vol. 69, no. 11, pp. 12974-12991, Nov. 2020.
- [20] S. Adireddy, L. Tong, and H. Viswanathan, "Optimal placement of training for frequency-selective block-fading channels," *IEEE Trans. Inform. Theory*, vol. 48, no. 8, pp. 2338-2353, Aug. 2002.
- [21] M.-X. Chang and Y. T. Su, "Performance analysis of equalized OFDM systems in Rayleigh fading," *IEEE Trans. Wireless Commun.*, vol. 1, no. 4, pp. 721-732, Oct. 2002.
- [22] W. Zhang, X. Xia, and P.-C. Ching, "Optimal training and pilot pattern design for OFDM systems in Rayleigh fading," *IEEE Trans. Broadcast.*, vol. 52, no. 4, pp. 505-514, Dec. 2006.
- [23] X. Cai and G. B. Giannakis, "Error probability minimizing pilots for OFDM with M-PSK modulation over Rayleigh-fading channels," *IEEE Trans. Veh. Technol.*, vol. 53, no. 1, pp. 146-155, Jan. 2004.
- [24] P. Tan and N. C. Beaulieu, "Effect of channel estimation error on bit error probability in OFDM systems over Rayleigh and Rician fading channels," *IEEE Trans. Commun.*, vol. 56, no. 4, pp. 675-685, Apr. 2008.

- 
- [25] 3GPP TS 36.211 V12.3.0, *LTE; Evolved universal terrestrial radio access (E-UTRA): Physical channels and modulation*, Oct. 2014.
- [26] IEEE Standard 802.22-2011, *Part 22: Cognitive wireless RAN medium access control (MAC) and physical layer (PHY) specifications: Policies and procedures for operation in the TV bands*, Jul. 2011.
- [27] 3GPP TS 38.211 V15.4, *5G NR: Physical channels and modulation*, Dec. 2018.
- [28] M. K. Simon and M.-S. Alouini, *Digital Communication over Fading Channels*, John Wiley & Sons, Inc., 2005.
- [29] M. K. Simon and M. Alouini, "A unified approach to the probability of error for noncoherent and differentially coherent modulations over generalized fading channels," *IEEE Trans. Commun.*, vol. 46, no. 12, pp. 1625-1638, Dec. 1998.
- [30] R. A. Horn and C. R. Johnson, *Matrix Analysis*. Cambridge Univ. Press, 1985.
- [31] J. G. Proakis and M. Salehi, *Digital Communications, 5th ed.* New York: McGraw-Hill, 2008.
- [32] M. Schwartz, W. R. Bennett, and S. Stein, *Communication Systems and Techniques*. New York: McGraw-Hill, 1966.
- [33] M. K. Simon, S. M. Hinedi, and W. C. Lindsey, *Digital Communication Techniques: Signal Design and Detection*. Englewood Cliffs, N.J.: Prentice Hall, 1995.
- [34] H. L. Van Trees, *Detection, Estimation, and Modulation Theory*. John Wiley & Sons Inc., 1968.

- 
- [35] R.-Y. Yen, H. Liu and W.-K. Tsai, "QAM symbol error rate in OFDM systems over frequency-selective fast Ricean-fading channels," *IEEE Trans. Veh. Technol.*, vol. 57, no. 2, pp. 1322-1325, Mar. 2008.
- [36] R. J. Muirhead, *Aspects of Multivariate Statical Theory*. John Wiley & Sons Inc., 2005.
- [37] A. A. M. Saleh, A. J. Rustako, and R. S. Roman, "Distributed antennas for indoor radio communications," *IEEE Trans. Commun.*, vol. 35, no. 12, pp. 1245-1251, Dec. 1987.
- [38] L. Arevalo, R. C. de Lamare, M. Haardt, and R. Sampaio-Neto, "Uplink block diagonalization for massive MIMO-OFDM systems with distributed antennas," in *Proc. IEEE Int. Workshop on Computational Advances in Multi-Sensor Adaptive Process.*, pp. 389-392, Dec. 2015.
- [39] H. Arslan and T. Yucek, "Delay spread estimation for wireless communication systems," in *Proc. IEEE 8th Int. Symp. Comput. and Commun.*, pp. 282-287, Kemer-Antalya, Turkey, Jul. 2003.
- [40] J.H. Mathews and K.K. Fink, *Numerical Methods Using Matlab, 4th edition*. Prentice Hall Inc. New Jersey, USA, 2004.
- [41] T. M. Cover and J. A. Thomas, *Elements of Information Theory*. New York: Wiley, 1991.



Appendix A

Derivation of (3.2)

Here, I denote $d_k[n] = d$ and $\hat{d}_k[n] = \hat{d}$ for notational simplicity and derive the pairwise error probability $\Pr\{\sum_{i=0}^{I-1} F_{k,n}^{(i)}(\hat{d}) < \sum_{i=0}^{I-1} F_{k,n}^{(i)}(d) | d, \{\mathbf{h}^{(i)}\}\}$ for given k and n . For notational convenience, I denote $F_{k,n}^{(i)}(\hat{d}) = |X^{(i)}|^2$ and $F_{k,n}^{(i)}(d) = |Y^{(i)}|^2$ where

$$X^{(i)} \triangleq \tilde{r}^{(i)}[n\phi + k] - \varphi^{1/2} \hat{\mathbf{d}}_n^t \mathbf{V}_k \tilde{\mathbf{r}}_\chi^{(i)} \quad (\text{A.1})$$

$$Y^{(i)} \triangleq \tilde{r}^{(i)}[n\phi + k] - \varphi^{1/2} \mathbf{d}_n^t \mathbf{V}_k \tilde{\mathbf{r}}_\chi^{(i)}. \quad (\text{A.2})$$

Given $d_k[n] = d$ and $\{\mathbf{h}^{(i)}\}$, $X^{(i)}$ and $Y^{(i)}$ are conditionally CSCG random variables with means

$$\overline{X}^{(i)} = (\rho^{(d)})^{1/2} \mathbf{d}_n^t \mathbf{W}_L \boldsymbol{\Omega}_k \mathbf{h}^{(i)} - (\rho^{(d)})^{1/2} \hat{\mathbf{d}}_n^t \mathbf{V}_k \mathbf{D}_\chi \mathbf{W}_L \boldsymbol{\Omega}_\chi \mathbf{h}^{(i)} \quad (\text{A.3})$$

$$\overline{Y}^{(i)} = (\rho^{(d)})^{1/2} \mathbf{d}_n^t \mathbf{W}_L \boldsymbol{\Omega}_k \mathbf{h}^{(i)} - (\rho^{(d)})^{1/2} \mathbf{d}_n^t \mathbf{V}_k \mathbf{D}_\chi \mathbf{W}_L \boldsymbol{\Omega}_\chi \mathbf{h}^{(i)} \quad (\text{A.4})$$

, respectively, and variances and covariance can also be derived as

$$\mu_{XX}^{(i)} = \sigma^2(1 + \varphi|\hat{d}|^2\psi_{k,n}) \quad (\text{A.5})$$

$$\mu_{YY}^{(i)} = \sigma^2(1 + \varphi|d|^2\psi_{k,n}) \quad (\text{A.6})$$

$$\mu_{XY}^{(i)} = (\mu_{YX}^{(i)})^* = \sigma^2(1 + \varphi\hat{d}d^*\psi_{k,n}) \quad (\text{A.7})$$

, where $\psi_{k,n} \triangleq \mathbf{1}_n^t \mathbf{V}_k \mathbf{V}_k^h \mathbf{1}_n$.¹ Obviously, $X^{(i)}$ and $Y^{(i)}$ are correlated. However, $\{X^{(i)}, Y^{(i)}\}$ are independent of $\{X^{(l)}, Y^{(l)}\}$ for $i \neq l$ due to the independence among receive antenna paths, In this case, $\sum_{i=0}^{I-1} (|X^{(i)}|^2 - |Y^{(i)}|^2)$ is a special case of quadratic sum in complex Gaussian random variable in [31, Appendix B, eq. (B-1)]. Thus, $\Pr\{\sum_{i=0}^{I-1} F_{k,n}^{(i)}(\hat{d}) < \sum_{i=0}^{I-1} F_{k,n}^{(i)}(d) | d, \{\mathbf{h}^{(i)}\}\}$ in (3.1) can be derived by using [31, Appendix B, eq. (B-21)] as²

$$\begin{aligned} & \Pr\left\{\sum_{i \in \mathcal{Z}_I} F_{k,n}^{(i)}(\hat{d}) < \sum_{i \in \mathcal{Z}_I} F_{k,n}^{(i)}(d) | d, \{\mathbf{h}^{(i)}\}\right\} \\ &= Q_1(\eta_1, \eta_2) - I_0(\eta_1 \eta_2) \exp\left\{-\frac{1}{2}(\eta_1^2 + \eta_2^2)\right\} \\ &+ \frac{I_0(\eta_1 \eta_2) \exp\left\{-\frac{1}{2}(\eta_1^2 + \eta_2^2)\right\}}{(1 + \nu_2/\nu_1)^{2I-1}} \times \sum_{a=0}^{I-1} \binom{2I-1}{a} \left(\frac{\nu_2}{\nu_1}\right)^a \\ &+ \frac{\exp\left\{-\frac{1}{2}(\eta_1^2 + \eta_2^2)\right\}}{(1 + \nu_2/\nu_1)^{2I-1}} \sum_{b=1}^{I-1} I_b(\eta_1 \eta_2) \sum_{a=0}^{I-1-b} \binom{2I-1}{a} \left[\left(\frac{\eta_2}{\eta_1}\right)^b \left(\frac{\nu_2}{\nu_1}\right)^a \right. \\ &\left. - \left(\frac{\eta_1}{\eta_2}\right)^b \left(\frac{\nu_2}{\nu_1}\right)^{2I-1-a}\right] \end{aligned} \quad (\text{A.8})$$

where η_1 and η_2 are given by [31, Appendix B, eq. (B-22)]

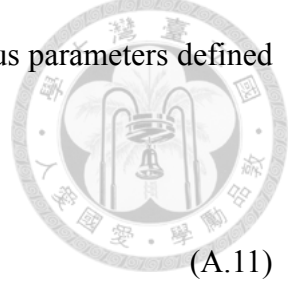
$$\eta_1 = \left[\frac{1 - \lambda^2}{2} (\beta_1 \zeta - \beta_2 \nu_1) \right]^{\frac{1}{2}} \quad (\text{A.9})$$

$$\eta_2 = \left[\frac{1 - \lambda^2}{2} (\beta_1 \zeta + \beta_2 \nu_2) \right]^{\frac{1}{2}}. \quad (\text{A.10})$$

¹Here, I have defined $\mu_{XX}^{(i)} = E\{|X^{(i)} - \bar{X}^{(i)}|^2\}$, $\mu_{YY}^{(i)} = E\{|Y^{(i)} - \bar{Y}^{(i)}|^2\}$, and $\mu_{XY}^{(i)} = E\{(X^{(i)} - \bar{X}^{(i)})(Y^{(i)} - \bar{Y}^{(i)})^*\}$.

²For notational simplicity, I do not show the dependence of all parameters on indices n and k herein. It should be cautious to evaluate the performance results based on the formulae obtained in *Appendices A* and *B*.

Here, I have defined $\beta_1 = \sum_{i \in \mathcal{Z}_I} \beta_1^{(i)}$ and $\beta_2 = \sum_{i \in \mathcal{Z}_I} \beta_2^{(i)}$ with various parameters defined as



$$\nu_1 = (\xi^2 + \zeta)^{\frac{1}{2}} - \xi, \quad \nu_2 = (\xi^2 + \zeta)^{\frac{1}{2}} + \xi \quad (\text{A.11})$$

$$\beta_1^{(i)} = \frac{|\overline{X}^{(i)}|^2}{\sigma^2} (1 + \varphi |d|^2 \psi_{k,n}) + \frac{|\overline{Y}^{(i)}|^2}{\sigma^2} (1 + \varphi |\hat{d}|^2 \psi_{k,n}) - 2 \text{Re} \left\{ \frac{\overline{X}^{(i)*} \overline{Y}^{(i)}}{\sigma^2} (1 + \varphi \hat{d} d^* \psi_{k,n}) \right\} \quad (\text{A.12})$$

$$\beta_2^{(i)} = \frac{|\overline{X}^{(i)}|^2}{\sigma^2} - \frac{|\overline{Y}^{(i)}|^2}{\sigma^2} \quad (\text{A.13})$$

$$\zeta = \psi_{k,n}^{-1} \varphi^{-1} |\hat{d} - d|^{-2} \quad (\text{A.14})$$

$$\xi = \frac{|\hat{d}|^2 - |d|^2}{2|\hat{d} - d|^2} \quad (\text{A.15})$$

$$\lambda = \frac{|\hat{d}|^2 - |d|^2}{[(|\hat{d}|^2 - |d|^2)^2 + 4\varphi^{-1} \psi_{k,n}^{-1} |\hat{d} - d|^2]^{\frac{1}{2}}}. \quad (\text{A.16})$$

Notably, $\frac{\overline{X}^{(i)}}{\sigma}$ and $\frac{\overline{Y}^{(i)}}{\sigma}$ are the only expressions in (A.11)-(A.16) that rely on the data SNR γ_d and can be rewritten as

$$\frac{\overline{X}^{(i)}}{\sigma} = \gamma_d^{\frac{1}{2}} d \mathbf{1}_n^t \mathbf{W}_L \mathbf{\Omega}_k \mathbf{h}^{(i)} - \gamma_d^{\frac{1}{2}} \hat{d} \mathbf{1}_n^t \mathbf{V}_k \mathbf{D}_\chi \mathbf{W}_L \mathbf{\Omega}_\chi \mathbf{h}^{(i)} \quad (\text{A.17})$$

$$\frac{\overline{Y}^{(i)}}{\sigma} = \gamma_d^{\frac{1}{2}} d \mathbf{1}_n^t \mathbf{W}_L \mathbf{\Omega}_k \mathbf{h}^{(i)} - \gamma_d^{\frac{1}{2}} d \mathbf{1}_n^t \mathbf{V}_k \mathbf{D}_\chi \mathbf{W}_L \mathbf{\Omega}_\chi \mathbf{h}^{(i)}. \quad (\text{A.18})$$

For CA pilot sequence \mathbf{p} with $|p[n]| = 1$ for all $n \in \mathcal{Z}_N$, $\mathbf{D}_\chi^h \mathbf{D}_\chi = \mathbf{I}_N$, \mathbf{V}_k simplifies to $\mathbf{V}_k|_{\text{CA pilot}}$ and $\mathbf{V}_k|_{\text{CA pilot}} \mathbf{V}_k^h|_{\text{CA pilot}} = N^{-1} \mathbf{W}_L \mathbf{W}_L^h$ is the same for all $k \in \mathcal{Z}_\phi$. This $\mathbf{V}_k|_{\text{CA pilot}}$ thereby simplifies $\psi_{k,n} = \mathbf{1}_n^t \mathbf{V}_k \mathbf{V}_k^h \mathbf{1}_n$ to a constant $\psi_{k,n}|_{\text{CA pilot}} = N^{-1} \|\mathbf{1}_n^t \mathbf{W}_L\|^2 = \frac{L}{N}$, $\frac{\overline{X}^{(i)}}{\sigma}$ in (A.17) to $\sum_{i=0}^{I-1} \gamma_d^{1/2} (d - \hat{d}) \mathbf{1}_n^t \mathbf{W}_L \mathbf{\Omega}_k \mathbf{h}^{(i)}$, $\frac{\overline{Y}^{(i)}}{\sigma}$ in (A.18) to 0, and thus the parameters $\beta_1^{(i)}$,

$\beta_2^{(i)}$, ζ , and λ in (A.12)-(A.16) to

$$\beta_1^{(i)} = \beta_2^{(i)} \vartheta \quad (\text{A.19})$$

$$\beta_2^{(i)} = \gamma_d |d - \hat{d}|^2 |\mathbf{1}_n^t \mathbf{W}_L \mathbf{\Omega}_k \mathbf{h}^{(i)}|^2 \quad (\text{A.20})$$

$$\zeta = \frac{N}{L\varphi} |\hat{d} - d|^{-2} \quad (\text{A.21})$$

$$\lambda = \frac{|\hat{d}|^2 - |d|^2}{[(|\hat{d}|^2 - |d|^2)^2 + \frac{4N}{L\varphi} |\hat{d} - d|^2]^{\frac{1}{2}}}. \quad (\text{A.22})$$

$$\vartheta = (1 + \frac{L\varphi}{N} |d|^2) \quad (\text{A.23})$$

(A.19) yields the relationship $\beta_1 = \beta_2 \vartheta$, which further simplifies η_1 and η_2 in (A.9)-(A.13) to $\eta_1 = \beta^{1/2} \varepsilon_1$ and $\eta_2 = \beta^{1/2} \varepsilon_2$ with ε_1 , ε_2 , and β defined as in (3.3)-(3.5). Using (3.3)-(3.4), I can further simplify (A.8) to (3.2), with the aid of [32, Appendix A, eq. A-3-1] and [31, eqs. (2.3-36)], i.e., $Q_1(\eta_1, \eta_2) + Q_1(\eta_2, \eta_1) = 1 + I_0(\eta_1 \eta_2) \exp\{-\frac{1}{2}(\eta_1^2 + \eta_2^2)\}$ and $Q_a(\eta_1, \eta_2) = Q_1(\eta_1, \eta_2) + \exp\{-\frac{1}{2}(\eta_1^2 + \eta_2^2)\} \sum_{b=1}^{a-1} \left(\frac{\eta_2}{\eta_1}\right)^b I_b(\eta_1 \eta_2)$.



Appendix B

Derivation of (3.10)

First, introduce a new parameter $\varrho \triangleq \nu_2/\nu_1$ in order to simplify the derivation, then add back the $a = 1$ term in last tow sums in (3.2) since they have zero value

$$\begin{aligned}
 & \Pr\left\{\sum_{i \in \mathcal{Z}_I} F_{k,n}^{(i)}(\widehat{d}) < \sum_{i \in \mathcal{Z}_I} F_{k,n}^{(i)}(d) \mid d, \{\mathbf{h}^{(i)}\}\right\} \\
 &= [1 - Q_1(\beta^{1/2}\varepsilon_2, \beta^{1/2}\varepsilon_1)] \left[1 - \frac{\sum_{a=0}^{I-1} \binom{2I-1}{a} \varrho^a}{(1 + \varrho)^{2I-1}}\right] \\
 &+ Q_1(\beta^{1/2}\varepsilon_1, \beta^{1/2}\varepsilon_2) \frac{\sum_{a=0}^{I-1} \binom{2I-1}{a} \varrho^a}{(1 + \varrho)^{2I-1}} \\
 &+ \frac{\sum_{a=1}^I \binom{2I-1}{I-a} \varrho^{I-a}}{(1 + \varrho)^{2I-1}} \times [Q_a(\beta^{1/2}\varepsilon_1, \beta^{1/2}\varepsilon_2) - Q_1(\beta^{1/2}\varepsilon_1, \beta^{1/2}\varepsilon_2)] \\
 &- \frac{\sum_{a=1}^I \binom{2I-1}{I-a} \varrho^{I-1+a}}{(1 + \varrho)^{2I-1}} \times [Q_a(\beta^{1/2}\varepsilon_2, \beta^{1/2}\varepsilon_1) - Q_1(\beta^{1/2}\varepsilon_2, \beta^{1/2}\varepsilon_1)].
 \end{aligned} \tag{B.1}$$

With the aid of the identity $\sum_{a=0}^{I-1} \binom{2I-1}{a} = \sum_{a=1}^I \binom{2I-1}{I-a}$, the first two sums in PEP are rewritten as

$$\begin{aligned}
 & \Pr\left\{\sum_{i \in \mathcal{Z}_I} F_{k,n}^{(i)}(\hat{d}) < \sum_{i \in \mathcal{Z}_I} F_{k,n}^{(i)}(d) \mid d, \{\mathbf{h}^{(i)}\}\right\} \\
 &= [1 - Q_1(\beta^{1/2}\varepsilon_2, \beta^{1/2}\varepsilon_1)] \left[1 - \frac{\sum_{a=1}^I \binom{2I-1}{I-a} \varrho^{I-a}}{(1+\varrho)^{2I-1}}\right] \\
 &+ Q_1(\beta^{1/2}\varepsilon_1, \beta^{1/2}\varepsilon_2) \frac{\sum_{a=1}^I \binom{2I-1}{I-a} \varrho^{I-a}}{(1+\varrho)^{2I-1}} \\
 &+ \frac{\sum_{a=1}^I \binom{2I-1}{I-a} \varrho^{I-a}}{(1+\varrho)^{2I-1}} \times [Q_a(\beta^{1/2}\varepsilon_1, \beta^{1/2}\varepsilon_2) - Q_1(\beta^{1/2}\varepsilon_1, \beta^{1/2}\varepsilon_2)] \\
 &- \frac{\sum_{a=1}^I \binom{2I-1}{I-a} \varrho^{I-1+a}}{(1+\varrho)^{2I-1}} \times [Q_a(\beta^{1/2}\varepsilon_2, \beta^{1/2}\varepsilon_1) - Q_1(\beta^{1/2}\varepsilon_2, \beta^{1/2}\varepsilon_1)].
 \end{aligned} \tag{B.2}$$

Next, rearrange the PEP into three parts, the part without Marcum's Q -function, the part with $Q_1(\beta^{1/2}\varepsilon_1, \beta^{1/2}\varepsilon_2)$ and $Q_a(\beta^{1/2}\varepsilon_1, \beta^{1/2}\varepsilon_2)$, and the part with $Q_1(\beta^{1/2}\varepsilon_2, \beta^{1/2}\varepsilon_1)$ and

$$Q_a(\beta^{1/2}\varepsilon_2, \beta^{1/2}\varepsilon_1)$$

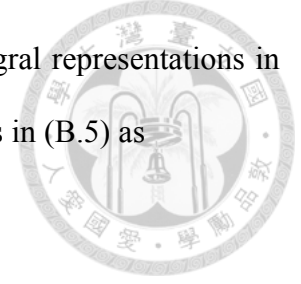


$$\begin{aligned} & \Pr\left\{\sum_{i \in \mathcal{Z}_I} F_{k,n}^{(i)}(\hat{d}) < \sum_{i \in \mathcal{Z}_I} F_{k,n}^{(i)}(d) | d, \{\mathbf{h}^{(i)}\}\right\} \\ &= 1 - \frac{\sum_{a=1}^I \binom{2I-1}{I-a} \varrho^{I-a}}{(1+\varrho)^{2I-1}} \\ & \quad \frac{\sum_{a=1}^I \binom{2I-1}{I-a} \varrho^{I-a}}{(1+\varrho)^{2I-1}} Q_1(\beta^{1/2}\varepsilon_1, \beta^{1/2}\varepsilon_2) \end{aligned} \quad (\text{B.3})$$

$$\begin{aligned} & + \frac{\sum_{a=1}^I \binom{2I-1}{I-a} \varrho^{I-a}}{(1+\varrho)^{2I-1}} \times [Q_a(\beta^{1/2}\varepsilon_1, \beta^{1/2}\varepsilon_2) - Q_1(\beta^{1/2}\varepsilon_1, \beta^{1/2}\varepsilon_2)] \\ & - [1 - \frac{\sum_{a=1}^I \binom{2I-1}{I-a} \varrho^{I-a}}{(1+\varrho)^{2I-1}}] Q_1(\beta^{1/2}\varepsilon_2, \beta^{1/2}\varepsilon_1) \\ & - \frac{\sum_{a=1}^I \binom{2I-1}{I-a} \varrho^{I-1+a}}{(1+\varrho)^{2I-1}} \times [Q_a(\beta^{1/2}\varepsilon_2, \beta^{1/2}\varepsilon_1) - Q_1(\beta^{1/2}\varepsilon_2, \beta^{1/2}\varepsilon_1)] \\ &= 1 - \frac{\sum_{a=1}^I \binom{2I-1}{I-a} \varrho^{I-a}}{(1+\varrho)^{2I-1}} \\ & + \frac{\sum_{a=1}^I \binom{2I-1}{I-a} \varrho^{I-a}}{(1+\varrho)^{2I-1}} Q_1(\beta^{1/2}\varepsilon_1, \beta^{1/2}\varepsilon_2) \end{aligned} \quad (\text{B.4})$$

$$\begin{aligned} & + \frac{\sum_{a=1}^I \binom{2I-1}{I-a} \varrho^{I-a}}{(1+\varrho)^{2I-1}} Q_a(\beta^{1/2}\varepsilon_1, \beta^{1/2}\varepsilon_2) - \frac{\sum_{a=1}^I \binom{2I-1}{I-a} \varrho^{I-a}}{(1+\varrho)^{2I-1}} Q_1(\beta^{1/2}\varepsilon_1, \beta^{1/2}\varepsilon_2) \\ & - [1 - \frac{\sum_{a=1}^I \binom{2I-1}{I-a} \varrho^{I-a}}{(1+\varrho)^{2I-1}}] Q_1(\beta^{1/2}\varepsilon_2, \beta^{1/2}\varepsilon_1) \\ & - \frac{\sum_{a=1}^I \binom{2I-1}{I-a} \varrho^{I-1+a}}{(1+\varrho)^{2I-1}} Q_a(\beta^{1/2}\varepsilon_2, \beta^{1/2}\varepsilon_1) + \frac{\sum_{a=1}^I \binom{2I-1}{I-a} \varrho^{I-1+a}}{(1+\varrho)^{2I-1}} Q_1(\beta^{1/2}\varepsilon_2, \beta^{1/2}\varepsilon_1) \\ &= 1 - \frac{\sum_{a=1}^I \binom{2I-1}{I-a} \varrho^{I-a}}{(1+\varrho)^{2I-1}} \\ & + \frac{\sum_{a=1}^I \binom{2I-1}{I-a} \varrho^{I-a}}{(1+\varrho)^{2I-1}} Q_a(\beta^{1/2}\varepsilon_1, \beta^{1/2}\varepsilon_2) \end{aligned} \quad (\text{B.5})$$

Adopting a new parameter $\tau \triangleq \varepsilon_1/\varepsilon_2$ and the alternative single-integral representations in [29, eqs. (22) and (61)], I rewrite the generalized Marcum Q -functions in (B.5) as



$$Q_a(\beta^{1/2}\varepsilon_1, \beta^{1/2}\varepsilon_2) = \frac{1}{2\pi} \int_{-\pi}^{\pi} \exp\left\{-\frac{\beta\varepsilon_2^2}{2}(1 + 2\tau \sin \theta + \tau^2)\right\} \times \frac{\tau^{1-a}[\cos((a-1)(\theta + \pi/2)) - \tau \cos(a(\theta + \pi/2))]}{1 + 2\tau \sin \theta + \tau^2} d\theta \quad (\text{B.6})$$

$$Q_a(\beta^{1/2}\varepsilon_2, \beta^{1/2}\varepsilon_1) = 1 - \frac{1}{2\pi} \int_{-\pi}^{\pi} \exp\left\{-\frac{\beta\varepsilon_2^2}{2}(1 + 2\tau \sin \theta + \tau^2)\right\} \times \frac{\tau^a[\cos(a(\theta + \pi/2)) - \tau \cos((a-1)(\theta + \pi/2))]}{1 + 2\tau \sin \theta + \tau^2} d\theta \quad (\text{B.7})$$

for $a \geq 1$ and both hold good for $0 \leq \tau < 1$.¹ Further, define two new parameters $\mathbf{X} = 1 + 2\tau \sin \theta + \tau^2$ and $\mathbf{Y} = \exp\left\{-\frac{\beta\varepsilon_2^2}{2}(1 + 2\tau \sin \theta + \tau^2)\right\}$, and substituting (B.6)-(B.7) into (B.5) as

$$\begin{aligned} & \Pr\left\{\sum_{i=0}^{I-1} F_{k,n}^{(i)}(\hat{d}) < \sum_{i=0}^{I-1} F_{k,n}^{(i)}(d)\right\} \\ &= \frac{\varrho^I}{2\pi(1 + \varrho)^{2I-1}} \\ & \times \int_{-\pi}^{\pi} \frac{\sum_{a=1}^I \binom{2I-1}{I-a} \varrho^{-a} [\tau^{-a+1} \{\cos((a-1)(\theta + \frac{\pi}{2})) - \tau \cos(a(\theta + \frac{\pi}{2}))\}]}{\mathbf{X}} \times \mathbf{Y} d\theta \\ & - \frac{\varrho^I}{2\pi(1 + \varrho)^{2I-1}} \int_{-\pi}^{\pi} \frac{\binom{(1+\varrho)^{2I-1}}{\varrho^I} (\tau^2 + \tau \sin \theta)}{\mathbf{X}} \times \mathbf{Y} d\theta \\ & + \frac{\varrho^I}{2\pi(1 + \varrho)^{2I-1}} \int_{-\pi}^{\pi} \frac{\sum_{a=1}^I \binom{2I-1}{I-a} [\varrho^{-a} + \varrho^{a-1}] (\tau^2 + \tau \sin \theta)}{\mathbf{X}} \times \mathbf{Y} d\theta \\ & + \frac{\varrho^I}{(1 + \varrho)^{2I-1}} \\ & \times \frac{1}{2\pi} \int_{-\pi}^{\pi} \frac{\sum_{a=1}^I \binom{2I-1}{I-a} (\varrho^{a-1} [\tau^a \{\cos(a(\theta + \frac{\pi}{2})) - \tau \cos((a-1)(\theta + \frac{\pi}{2}))\}]}{\mathbf{X}} \times \mathbf{Y} d\theta. \end{aligned} \quad (\text{B.8})$$

¹Notably, $0 \leq \tau < 1$ is guaranteed due to (3.3) and (3.4)

Combining all single-integrals into one such as

$$\Pr\left\{\sum_{i=0}^{I-1} F_{k,n}^{(i)}(\hat{d}) < \sum_{i=0}^{I-1} F_{k,n}^{(i)}(d)\right\} = \frac{\varrho^I}{2\pi(1+\varrho)^{2I-1}} \int_{-\pi}^{\pi} \frac{\Psi(\theta; I, \tau, \varrho)}{\mathbf{X}} \times \mathbf{Y} d\theta \quad (\text{B.9})$$

where

$$\begin{aligned} \Psi(\theta; I, \tau, \varrho) = & \left(-\frac{(1+\varrho)^{2I-1}}{\varrho^I}\right)(\tau^2 + \tau \sin \theta) \\ & + \sum_{a=1}^I \binom{2I-1}{I-a} [\varrho^{-a} + \varrho^{a-1}](\tau^2 + \tau \sin \theta) \\ & + \sum_{a=1}^I \binom{2I-1}{I-a} \varrho^{-a} \tau^{-a+1} \cos((a-1)(\theta + \frac{\pi}{2})) \end{aligned} \quad (\text{B.10})$$

$$\begin{aligned} & - \sum_{a=1}^I \binom{2I-1}{I-a} \varrho^{-a} \tau^{-a+2} \cos(a(\theta + \frac{\pi}{2})) \\ & + \sum_{a=1}^I \binom{2I-1}{I-a} \varrho^{a-1} \tau^a \cos(a(\theta + \frac{\pi}{2})) \\ & - \sum_{a=1}^I \binom{2I-1}{I-a} \varrho^{a-1} \tau^{a+1} \cos((a-1)(\theta + \frac{\pi}{2})) \\ = & (\tau^2 + \tau \sin \theta) \left\{ \left(-\frac{(1+\varrho)^{2I-1}}{\varrho^I}\right) + \sum_{a=1}^I \binom{2I-1}{I-1} [\varrho^{-a} + \varrho^{a-1}] \right\} \\ & + \sum_{a=1}^I \binom{2I-1}{I-1} \cos((a-1)(\theta + \frac{\pi}{2})) [\varrho^{-a} \tau^{-a+1} - \varrho^{a-1} \tau^{a+1}] \end{aligned} \quad (\text{B.11})$$

$$\begin{aligned} & - \sum_{a=1}^I \binom{2I-1}{I-1} \cos(a(\theta + \frac{\pi}{2})) [\varrho^{-a} \tau^{-a+2} - \varrho^{a-1} \tau^a] \\ = & (\tau^2 + \tau \sin \theta) \left\{ \left(-\frac{(1+\varrho)^{2I-1}}{\varrho^I}\right) + \sum_{a=1}^I \binom{2I-1}{I-a} [\varrho^{-a} + \varrho^{a-1}] \right\} \\ & + \sum_{a=1}^I \binom{2I-1}{I-a} \left\{ \cos((a-1)(\theta + \frac{\pi}{2})) [\varrho^{-a} \tau^{-a+1} - \varrho^{a-1} \tau^{a+1}] \right. \\ & \left. - \cos(a(\theta + \frac{\pi}{2})) [\varrho^{-a} \tau^{-a+2} - \varrho^{a-1} \tau^a] \right\}. \end{aligned} \quad (\text{B.12})$$

Therefore, by substituting \mathbf{X} and \mathbf{Y} in (B.9), the PEP can be rewritten into a single-integral

representation as

$$\begin{aligned} \Pr\left\{\sum_{i \in \mathcal{Z}_I} F_{k,n}^{(i)}(\hat{d}) < \sum_{i \in \mathcal{Z}_I} F_{k,n}^{(i)}(d) | d, \{\mathbf{h}^{(i)}\}\right\} \\ = \frac{\varrho^I}{2\pi(1+\varrho)^{2I-1}} \int_{-\pi}^{\pi} \frac{\Psi(\theta; I, \tau, \varrho)}{1+2\tau \sin \theta + \tau^2} \times \exp\left\{-\frac{\beta \varepsilon_2^2}{2}(1+2\tau \sin \theta + \tau^2)\right\} d\theta \end{aligned} \quad (\text{B.13})$$

where

$$\begin{aligned} \Psi(\theta; I, \tau, \varrho) = (\tau^2 + \tau \sin \theta) \left\{ -\frac{(1+\varrho)^{2I-1}}{\varrho^I} + \sum_{a=1}^I \binom{2I-1}{I-a} [\varrho^{-a} + \varrho^{a-1}] \right\} \\ + \sum_{a=1}^I \binom{2I-1}{I-a} \{ \cos((a-1)(\theta + \pi/2)) \times [\varrho^{-a} \tau^{-a+1} - \varrho^{a-1} \tau^{a+1}] \\ - \cos(a(\theta + \pi/2)) \times [\varrho^{-a} \tau^{-a+2} - \varrho^{a-1} \tau^a] \}. \end{aligned} \quad (\text{B.14})$$